uOttawa

L'Université canadienne
Canada's university

FACULTÉ DES ÉTUDES SUPÉRIEURES ET POSTOCTORALES

uOttawa

L'Université canadienne
Canada's university

FACULTY OF GRADUATE AND POSDOCTORAL STUDIES

Qingsheng Zeng
AUTEUR DE LA THÈSE / AUTHOR OF THESIS

Ph.D. (Electrical Engineering)
GRADE / DEGREE

School of Information Technology and Engineering
FACULTÉ, ÉCOLE, DÉPARTEMENT / FACULTY, SCHOOL, DEPARTMENT

Transient Analysis of Electromagnetic Waves Based on Numerical Inversion of Laplace Transform

TITRE DE LA THÈSE / TITLE OF THESIS

Gilles Delisle
DIRECTEUR (DIRECTRICE) DE LA THÈSE / THESIS SUPERVISOR

CO-DIRECTEUR (CO-DIRECTRICE) DE LA THÈSE / THESIS CO-SUPERVISOR

Derek McNamara

Mustapha Yagoub

Thomas Wong
Illinois Institute of Technology

Qi-jun Zhang

Gary W. Slater
Le Doyen de la Faculte des études superieures et postdoctorales / Dean of the Faculty of Graduate and Postdoctoral Studies

TRANSIENT ANALYSIS OF ELECTROMAGNETIC WAVES BASED ON NUMERICAL INVERSION OF LAPLACE TRANSFORM

Qingsheng Zeng

Thesis submitted to the
Faculty of Graduate and Postdoctoral Studies
In partial fulfillment of the requirements for the degree of
DOCTOR OF PHILOSOPHY
in Electrical and Computer Engineering

Ottawa-Carleton Institute for Electrical and Computer Engineering
School of Information Technology and Engineering
Faculty of Engineering
University of Ottawa

Copyright © Qingsheng Zeng, Ottawa, Canada, 2010

Library and Archives Canada

Published Heritage Branch

395 Wellington Street
Ottawa ON K1A 0N4
Canada

Bibliothèque et Archives Canada

Direction du Patrimoine de l'édition

395, rue Wellington
Ottawa ON K1A 0N4
Canada

Your file Votre référence
ISBN: 978-0-494-73918-1
Our file Notre référence
ISBN: 978-0-494-73918-1

NOTICE:

The author has granted a non-exclusive license allowing Library and Archives Canada to reproduce, publish, archive, preserve, conserve, communicate to the public by telecommunication or on the Internet, loan, distribute and sell theses worldwide, for commercial or non-commercial purposes, in microform, paper, electronic and/or any other formats.

The author retains copyright ownership and moral rights in this thesis. Neither the thesis nor substantial extracts from it may be printed or otherwise reproduced without the author's permission.

AVIS:

L'auteur a accordé une licence non exclusive permettant à la Bibliothèque et Archives Canada de reproduire, publier, archiver, sauvegarder, conserver, transmettre au public par télécommunication ou par l'Internet, prêter, distribuer et vendre des thèses partout dans le monde, à des fins commerciales ou autres, sur support microforme, papier, électronique et/ou autres formats.

L'auteur conserve la propriété du droit d'auteur et des droits moraux qui protège cette thèse. Ni la thèse ni des extraits substantiels de celle-ci ne doivent être imprimés ou autrement reproduits sans son autorisation.

In compliance with the Canadian Privacy Act some supporting forms may have been removed from this thesis.

While these forms may be included in the document page count, their removal does not represent any loss of content from the thesis.

Conformément à la loi canadienne sur la protection de la vie privée, quelques formulaires secondaires ont été enlevés de cette thèse.

Bien que ces formulaires aient inclus dans la pagination, il n'y aura aucun contenu manquant.

Canada

ABSTRACT

The advancement of electromagnetic engineering has been driving the need to develop efficient techniques for the transient analysis of transmission, propagation and reception of electromagnetic waves in different media. This thesis addresses a new method based on the numerical inversion of Laplace transform (NILT), which overcomes the restrictions in previous approaches, leads to good accuracy in both late and early time, and has simple algorithms, short calculation time and small required memory sizes. To our knowledge, this would be the first time that systematically treats the theory of NILT and its application in the transient analysis of electromagnetic waves. In this thesis, firstly a literature survey is carried out and the weaknesses and limitations of some current time domain techniques are identified. Then Hosono's algorithm for the NILT is treated and developed under a strict theoretical framework. Next, this new technique based on NILT is employed to model the transient reflection of horizontally and vertically polarized waves from a conductive interface with exponentially decaying incident signals. After that, this technique is combined with Prony's method and applied to modeling the transient reflection from a conductive interface and propagation through a lossy dielectric slab with an arbitrary incident signal for both polarizations. Furthermore, this technique is used for the transient analysis of exponentially decaying pulses propagating in plasma with a zero and nonzero electron collision frequency for both polarizations. The technique is extended and applied to the transient anlysis of horizontally and vertically polarized waves reflected from Lorentz, Debye and Cole–Cole half spaces with an arbitrary incident pulse, using the convolution of a time domain reflection coefficients and an incident signal. Finally, based on the transient anlysis of pulses reflected from a dispersive medium half space, the relationships between the waveform parameters of reflected pulses and the properties of dispersive materials as well as the incident angles are discussed, and the application of these results to material characterization and diagnosis is explored. This thesis highlights how to overcome the restriction that numerical inversion of Laplace transform has high demands on image functions, and places the emphasis on how to

extend and apply this method to a variety of cases. The correctness and effectiveness of this thesis work are validated through the comparisons between our results and those published in the literature. Meanwhile, the results that cannot be achieved with the previous approaches are also provided. Moreover, this thesis presents some applications of the new technique in diverse engineering fields, including ultra wideband technology and material science.

ACKNOWLEDGEMENTS

My deepest gratitude for this thesis goes to my supervisor, Prof. Gilles Y. Delisle, Director of Technology Integration Centre, Technopôle Defense & Security, and the former Director of School of Information Technology and Engineering, University of Ottawa, for accepting me as his PhD student, for his continuous guidance, assistance and encouragement. He has been supporting me to attend a number of conferences and symposia for discussing and interchanging the related ideas, which has been very helpful to crystallize some parts of my thesis work. Without his every endeavor in assisting me, I would not be able to pursue my PhD studies at University of Ottawa.

I am indebted to Professors. Derek McNamara and Mustapha Yagoub from University of Ottawa, Professor Qijun Zhang from Carleton University, Professor Thomas Wong from Illinois Institute of Technology for helpful suggestions and valuable comments on my thesis.

The author would like to thank the National Science and Engineering Research Council of Canada for its partial support through my supervisor's discovery grant.

PUBLICATIONS

[1] Q. Zeng and G. Y. Delisle, "Transient analysis of electromagnetic wave reflection from a stratified medium," in *Proceedings of 2010 Asia-Pacific Symposium on Electromagnetic Compatibility (2010 APEMC)*, Beijing, China, pp. 892-895, April 12 – 16, 2010.

[2] Q. Zeng and G. Y. Delisle, "Time domain analysis of ultra wideband pulses reflected from a conductive interface," submitted to *Journal of Electromagnetic Waves and Applications*, March 2010.

[3] Q. Zeng and G. Y. Delisle, "Waveform parameter estimation and material characterization," *PIERS Online*, Vol. 5, No. 3, pp. 241-247, 2009.

[4] Q. Zeng and G. Y. Delisle, "Waveform parameter estimation and dispersive material characterization", in *Proceedings of the 25th Progress In Electromagnetics Research Symposium (PIERS 2009)*, Beijing, China, pp. 169-175, March 23 – 27, 2009.

[5] Q. Zeng and G. Y. Delisle, "Transient analysis of plane wave reflection from a Debye half space," in *Proceedings of 1st Microsystems and Nanoelectronics Research Conference (MNRC 2008)*, Ottawa, Ontario, Canada, pp. 217-220, October 15, 2008.

[6] Q. Zeng and G. Y. Delisle, "Time domain analysis of electromagnetic pulse propagating in plasma," in *Proceedings of 2008 IEEE International Symposium on Antennas and Propagation and USNC/URSI National Radio Science Meeting*, San Diego, California, USA, July 5-12, 2008.

[7] Q. Zeng and G. Y. Delisle, "Time domain analysis of ultra wideband pulse reflection from a lossy interface," *International URSI Commission B – Electromagnetic Theory Symposium (EMTS 2007)*, Ottawa, Ontario, Canada, July 26 – 28, 2007.

[8] Q. Zeng and G. Y. Delisle, "Characterization for ultra wideband pulses transmitting through a lossy dielectric slab," *2006 IEEE International Conference on Ultra-Wideband (ICUWB 2006)*, pp. 213-218, Waltham, Massachusetts, USA, September 24-27, 2006.

[9] Q. Zeng and G. Y. Delisle, "Path loss model for ultra wideband signal propagation," *ANTEM / URSI 2006: 12th International Symposium on Antenna Technology and Applied Electromagnetics [ANTEM] and Canadian Radio Sciences [URSI/CNC]*, pp. 415-419, Montreal, Quebec, Canada, July 16-19, 2006.

[10] Q. Zeng and G. Y. Delisle, "Time-domain analysis for electromagnetic pulses reflected from a conductive half space," in *Proceedings of 2006 IEEE Canadian Conference on Electrical and Computer Engineering (CCECE2006)*, pp. 92-95, Ottawa, Ontario, Canada, May 7-10, 2006.

[11] Q. Zeng and G. Y. Delisle, "Parameter estimation of ultra wideband (UWB) electromagnetic pulses reflected from a lossy half space," *GESTS International Transactions on Computer Science and Engineering*, Vol. 18, No. 1, October 2005, pp. 161-171.

[12] Q. Zeng and G. Y. Delisle, "Characterization of discontinuities and propagation in waveguides using simplified finite element schemes," *AP-RASC 2004: 2nd Asia-Pacific Radio Science Conference*, pp. 84-87, Qingdao, China, Aug. 24-27, 2004.

[13] Q. Zeng and G. Y. Delisle, "Characterization of a transient wave reflected from a lossy half space using numerical inversion of Laplace transform," *Antem 2004/URSI: 10th International Symposium on Antenna Technology and Applied Electromagnetics and URSI Conference*, pp. 87-90, Ottawa, ON, July 20-23, 2004.

CONTENTS

CHAPTER 1: INTRODUCTION

The transient analysis of short duration electromagnetic pulses propagating through a variety of media is of interest in diverse technological applications, e.g., wireless communications, geophysical probing, material science and biomedical engineering. When an appropriate model has been adopted for the medium, one can manage to work out the frequency-domain solution for wave propagation in this medium. The main difficulties are encountered when trying to transform from the frequency-domain to the time-domain. An inverse fast Fourier transform (IFFT) can be employed to yield the desired transient result. However, several investigations have shown that a large number of sample points are required if one desires to reduce aliasing so that an accurate characterization can be obtained. Besides, when a frequency-domain solution has singular behaviors at some frequencies, direct use of IFFT is inappropriate and some preprocessing must be done for removing these singularities. Furthermore, it is preferable to solve the problems directly in the time-domain under certain circumstances, in which time-varying media or nonlinear systems are involved, or a time-domain response persists very long time.

Other techniques have their own inherent problems. Numerical integration algorithms are free from the problem of aliasing, but the highly oscillatory integrands that are encountered mandate a large number of sample points for the integration and correspondingly a relatively large amount of computation time. Asymptotic techniques are computationally efficient and provide valuable insight into the physical mechanism. However, an asymptotic analysis can be quite cumbersome and the resulting asymptotic expressions can be applied only to parameter values that fall within the range of applicability for the asymptotic expansion. The finite-difference time-domain (FDTD) technique has the advantage that it can be applied to relatively complex, inhomogeneous media, but it also has the following disadvantages. Firstly, the FDTD method does not accurately fulfill the boundary conditions at material interfaces posed by Maxwell's equations, and can cause high calculation costs even in combination with surface impedance boundary conditions for achieving high accuracy under

some circumstances. Secondly, when the widths of signal pulses are very narrow and the calculation time domain is large, FDTD solutions may become computationally intractable. Thirdly, the standard FDTD approach cannot handle simulations of long propagation distances because of finite computer memory resources and accumulation of phase errors associated with numerical dispersion. Another common drawback of the FDTD technique, fast Fourier transform (FFT) and numerical integration is that all the three techniques are purely numerical, and therefore it is difficult to extract the physical phenomenology from the numerical data.

The advancement in various engineering fields has been driving the need to develop efficient techniques for transient analyses of electromagnetic pulses. The objective of this thesis research is to develop some new technique that is based on the numerical inversion of Laplace transform (NILT) for the analysis of transient electromagnetic fields in a variety of media. In this chapter, first of all, the previous related investigations, majority of which are not based either on FFT, or on FDTD, or on other purely numerical methods, are overviewed, and some limitations of these methods are discussed. Then our research aims are addressed. Next, the contributions of this thesis to the development of efficient time-domain methods are presented. Lastly, the thesis outline is given.

1.1 Overview of Previous Investigations

Theoretical investigations of pulse propagation through different media and interaction with objects have been performed since the days of Sommerfeld during the early last century [1]. These investigations involved the calculations of the reflected and/or transmitted fields at the interface between two different media. The problem involving a time-harmonic plane wave obliquely incident on a finite conductive half-space is a classic boundary value problem in electromagnetic theory that is thoroughly treated in standard textbooks, for instance, those by Stratton [2] and by Balanis [3]. However, due to the mathematical complexity, it is not easy to analytically integrate the required inverse Laplace transform. Dudley et al. [4] undertook a thorough investigation of transverse electric (TE) and transverse magnetic (TM) reflected waves associated with a double decaying exponential,

obliquely incident plane wave. They utilized contour integration techniques to rewrite the inverse Fourier transform representation for the reflected fields in terms of a residue term and an integral around the branch cut. The contribution of this branch cut was calculated using numerical integration. Papazoglou [5] extended the analysis to the treatment of TE and TM transmitted waves. He also studied a Debye model which accounted for the frequency dependence in the electrical properties of the conductive media. Klaasen [6] showed that the TE transmitted and reflected fields associated with a unit-step, obliquely incident plane wave can be represented in terms of convolution integrals involving exponential functions and modified Bessel functions. Klassen employed a time marching procedure to evaluate the required convolution integrals. The FDTD technique was applied to this problem [7-9], but computation costs are high even in combination with surface impedance boundary conditions [9]. The approximate form of a frequency-domain reflection coefficient permits one analytical expression for the impulse response of a lossy half space [10], but makes the solutions inaccurate or even invalid in some cases, e.g., for large incident angles relative to the normal to the interface and/or for relative dielectric constants below the order of 10. Pao et al [11] [12] developed a method for the analytical evaluation of the inverse Laplace transform representations for transient TE and TM plane waves, obliquely incident on a conductive half space. They assumed that the permittivity and conductivity of the dispersive half space are independent of frequency. The time-domain expressions for the reflected and transmitted waves are first represented as inverse Laplace transforms. The transient fields are then shown to consist of two canonical integrals that in turn are solved analytically, thus leading to the solutions involving incomplete Lipschitz-Hankel integrals (ILHI's). Rothwell and Suk introduced a rapidly converging series of the time-domain reflection coefficient into the analysis of the transient reflection from a lossy half space, which is valid for all the incident angles for the horizontal polarization [13], and for the incident angles less than the Brewster angle for the vertical polarization [14]. Few terms provide good accuracy for late time, while many more terms may be required to approach acceptable accuracy for early time. Pantoja et al [15] compared the method in [13] [14] with that in [10] by changing angles of incidence and

constitutive parameters of half-spaces, and presented the accuracy and errors for the direct computation of the time-domain plane wave reflection coefficients for TE and TM plane waves incident on a lossy half-space.

Electromagnetic wave propagation through dispersive media has been a subject of interest to researchers for many years. The advent of ultra wideband (UWB), short pulse sources has recently attracted renewed interest in this aspect. Accurate modeling and improved physical understanding of pulse propagation in and scattering from dispersive media is crucial in a number of applications, including optical waveguides, UWB radar, ground penetrating radar, UWB biological effects, propagation through the ionosphere, stealth technology and remote sensing. Numerous researchers have demonstrated that plasma, Lorentz, Debye and Cole-Cole models can be used to accurately predict dispersive properties of many media.

If a simple homogeneous, collisionless, cold plasma model is utilized for the ionosphere, i.e., the plasma is characterized by a plasma cutoff frequency and losses are ignored, then the dispersion is analogous to that exhibited in a single mode, homogeneously filled waveguide. It has been demonstrated that the impulse response for this problem can be expressed in a closed form in terms of Bessel functions of the first kind [16-18]. In 1948, Cerillo showed that the transient waveguide fields, corresponding to a number of typical source typical source excitations, can be expressed as Neumann series expansions which were in the form of Lommel functions of two variables [19]. Cerillo noted that the usefulness of the closed form expressions, in terms of Lommel functions of two variables, is limited by the slow convergence properties of the Neumann series expansions. He also found it difficult to extract the physics from the closed form solutions because of the highly oscillatory behavior of the Lommel functions of two variables. Thus he resorted to asymptotic techniques to achieve the approximate expressions for the response. Knop [20] used the Neumann series expansions to numerically calculate the transient waveguide response of a step modulated carrier signal. He noted that the result is also applicable to a lossless, unbound, isotropic plasma excited by a pulsed electromagnetic wave. Wait and Spies [21] used the exact Neumann series

expansions to numerically validate an approximate transient result involving Fresnel integrals that was applied to the earth-ionosphere waveguide. Vogler [22] further extended the analysis by achieving Neumann series expansions for arbitrary source distributions. He demonstrated the extension through the investigation of the propagation of a double exponential signal in a waveguide. Vaisleib and Gan [23] noticed that, in addition to being able to represent the Neumann series expansions for waveguide transients in terms of Lommel functions of two variables, it is also possible to relate them to incomplete Weber integrals and incomplete Lipschitz-Hankel integrals (ILHI's) of the first kind [24]. They used these relationships to directly obtain approximate expressions for the early and late time responses. Mohammadian [25] represented the time dependent dyadic waveguide Green's function in terms of Lommel functions of two variables, but did not perform any numerical calculations. Dvorak [26] employed the contour integration techniques to analytically evaluate the inverse Fourier transform representation for the potential associated with a continuous wave transient pulse propagating in a waveguide. The obtained closed form expression for the potential has the same form as the results of Vaisleib and Gan [23], and involves ILHI's of the first kind. With a differential-equation-based technique, Dvorak and Dudley [27] derived a closed form expression for a double decaying exponential pulse propagating in a homogeneous, collisionless, cold plasma in terms of ILHI's, and evaluated the ILHI's using efficient convergent and asymptotic series expansions. Dvorak, Ziolkowski and Dudley [28] also investigated the propagation of a double decaying exponential signal through homogeneous, cold plasma that is characterized by a nonzero electron collision frequency. Because the high-frequency behavior does not depend on the electron collision frequency, an analytical frequency-domain expression, which is similar in form to the one encountered for the collisionless, cold plasma and encompasses this high-frequency behavior, can be subtracted from the exact expression for the plasma with nonzero collision frequency. In their treatment, the extracted term was evaluated analytically, and the remaining expression was transformed to the time domain through FFT with a modest number of sample points.

In the seminal work of Sommerfeld [1] and in the subsequent refinements of Oughstun and Sherman [29-32], the investigations have focused on the Lorentz material, which is a good model for many materials encountered in optics and engineering. The reflection of a short pulse by a Lorentz medium has been considered for TE polarization by Gray [33] and for TM polarization by Stanic et al [34]. In each of these studies, the authors find the impulse response of the reflected field by calculating the inverse transform of the frequency-domain reflection coefficient as an infinite series of fractional order Bessel functions. Although this gives a convenient analytical result, the series form provides little insight into the behavior of the reflected field waveform. Cossman et al have presented a compact form for both TE [35] and TM [36] reflection coefficients, which provide useful intuition about the response of a Lorentz medium half space, involve exponential and modified Bessel functions and require convolution operation to evaluate.

The use of short pulses to probe materials has prompted the study of the reflection of transient waves from material half space of other types. The Debye model [37] is utilized to describe the frequency behavior of the permittivity of many type materials, especially polar liquids. This model has been extended to include conductivity [38] and several relaxation components [39], and has been used to describe the behavior of such diverse materials as biological tissues [40], building materials [41], circuit boards [42] and ceramics [43]. A standard technique for the measurement of material parameters is to interrogate the material, either in free space [44] or in a waveguide system [45] with an electromagnetic pulse. It is therefore important to have an efficient method analyzing the time-domain reflection properties of a Debye material. Rothwell [46] worked out the time domain reflection coefficients of a Debye half space for both horizontal and vertical polarizations that involve exponential and modified Bessel functions and require convolution operations to evaluate. Another model commonly used to capture the relaxation-based dispersive properties is the Cole–Cole model [47] that is more general than the Debye model. For many types of materials including biological tissues, the Cole–Cole models provided an excellent fit to experimental data over the entire measurement frequency range. However, to our knowledge, the time-domain reflection

coefficient of a Cole–Cole half space for any polarization has been not available so far, perhaps due to the computational complexity of embedding a Cole–Cole dispersion model into numerical methods.

The reflection of electromagnetic waves from a layered medium is of interest in diverse technological applications, e.g., electromagnetic compatibility, geophysical probing, material science and biomedical engineering. Based on the results achieved from the studies of pulse propagation in a single medium and pulse reflection from a single medium half space, some time-domain analyses of wave scattering in a layered, lossy or dispersive material have been pursued. Suk and Rothwell analyzed both TE [48] and TM [49] transient reflection from a layered, lossy medium. Oh et al presented the natural resonance representations of the transient fields reflected by a conductor-backed lossy layer [50] and by a conductor-backed layer of Debye material [51]. Perry and Rothwell [52] investigated the transient wave reflections from layered, dispersive media. In contrast, a large number of achievements have been made in FDTD and other pure numerical modeling of lossy and dispersive media, for instance, FDTD analysis of lossy dielectrics [53], FDTD formulation for a plasma slab [54], 2-Debye-pole FDTD model [55], FDTD modeling of biological tissue Cole–Cole dispersion [56], FDTD and FETD algorithms for modeling complex media [57].

1.2 Our Research Aims

There are four major goals in this thesis work.

1. Conduct a literature survey and identify the weaknesses and limitations of some current time domain techniques, including both purely and non-purely numerical ones.
2. Discuss and further develop the algorithm for the numerical inversion of Laplace transform under a strict theoretical framework.
3. Extend and apply the approach for the numerical inversion of Laplace transform to transient analysis of electromagnetic pulses and other topics of the time domain electromagnetic fields.

4. Combine other numerical methods with the numerical inversion of Laplace transform to develop some hybrid techniques and find the applications of these hybrid techniques in electromagnetics.

1.3 THESIS CONTRIBUTIONS

The contribution of this thesis is listed as follows.

1. Hosono's algorithm for the numerical inversion of Laplace transform is treated and developed under a strict theoretical framework.
2. The numerical inversion of Laplace transform is employed to model transient reflection of TE- and TM-polarized waves from a conductive interface with an exponentially decaying incident signal.
3. The technique based on the numerical inversion of Laplace transform is combined with Prony's method and then is applied to modeling transient reflection of TE- and TM-polarized waves from a conductive interface with an arbitrary incident signal.
4. The technique combining the numerical inversion of Laplace transform and Prony's method is extended and applied to the characterization of horizontally and vertically polarized waves transmitting through a lossy dielectric slab with an arbitrary incident pulse.
5. The technique based on the numerical inversion of Laplace transform is used for the transient analysis of exponentially decaying pulses propagating in plasma with a zero and nonzero electron collision frequency for horizontally and vertically polarizations.
6. The technique based on the numerical inversion of Laplace transform is extended and applied to transient analysis of TE- and TM-polarized waves reflected from Lorentz, Debye and Cole–Cole half spaces with an arbitrary incident pulse, using the convolution of a time domain reflection coefficients and an incident signal.
7. Based on the transient anlysis of pulses reflected from a dispersive medium half space, the relationships between the waveform parameters of reflected pulses and the properties of

dispersive material as well as incident angles are discussed, and the application of these results to material characterization and diagnosis is explored. Furthermore, using the reduced time domain reflection coefficients brings more physical insights and leads to an efficient algorithm and a robust scheme for dispersive material diagnosis.

1.4 THESIS ORGANIZATION

This thesis consists of this introductory chapter, a literature review chapter, three fundamental chapters and a concluding chapter. Each of the three fundamental chapters deals with a topic of this thesis research. Following this introductory chapter, our work is presented in the order below.

Chapter 2 reviews four major analytical methods to model the transient reflection of horizontally and vertically polarized wave reflected from lossy and dispersive medium half spaces, summarizes the merits and limitations of these methods, and lays a base for this thesis work.

Chapter 3 treats and develops the algorithm for the numerical inversion of Laplace transform under a strict theoretical framework.

Chapter 4 covers the transient reflection of exponentially decaying and arbitrary signals from a conductive interface and propagation of arbitrary signals through a lossy dielectric slab for TE- and TM-polarizations.

Chapter 5 handles transient analysis of exponential pulses propagating in plasma and arbitrary pulses reflected from Lorentz, Debye and Cole–Cole half spaces for horizontally and vertically polarizations, presents the waveform estimation of reflected pulses, and shows the application of transient analysis to material characterization and diagnosis.

Finally, chapter 6 summaries this thesis research and achievements and proposes the future work in this orientation.

CHAPTER 2: REVIEW OF MAJOR ANALYTICAL METHODS FOR TRANSIENT REFLECTION AND TRANSMISSION

2.1 BARNES AND TESCHE'S METHOD

Barnes and Tesche [10] discussed an approach for calculating the electromagnetic field reflected from a lossy half space directly in time domain. This approach requires first evaluating the impulse response of the half space and then convolving it with the specified incident field waveform. To obtain the impulsive reflected field, either for vertical or horizontal polarization, approximations to the reflection coefficients in frequency domain are made, thus permitting an analytical expression in time domain.

The reflected electric field spectrum excited by an incident plane wave $E^{inc}(s)$ impinging on a lossy half space is given as

$$E^{ref}(s) = R(\theta, s)\, E^{inc}(s). \tag{2.1-1}$$

In this expression, s is the complex frequency Laplace variable, θ is the incidence angle relative to the normal to the interface, and $R(\theta, s)$ is the Fresnel reflection coefficient, and is denoted by R_v and R_h below for vertical and horizontal polarization, respectively. The frequency domain reflection coefficients for a lossy half space with a conductivity σ and a relative dielectric constant ε_r are

$$R_v(\theta, s) = \frac{\left(\varepsilon_r + \dfrac{\sigma}{s\varepsilon_0}\right)\cos\theta - \sqrt{\varepsilon_r + \dfrac{\sigma}{s\varepsilon_0} - \sin^2\theta}}{\left(\varepsilon_r + \dfrac{\sigma}{s\varepsilon_0}\right)\cos\theta + \sqrt{\varepsilon_r + \dfrac{\sigma}{s\varepsilon_0} - \sin^2\theta}} \tag{2.1-2}$$

and

$$R_h(\theta, s) = \frac{\cos\theta - \sqrt{\varepsilon_r + \dfrac{\sigma}{s\varepsilon_0} - \sin^2\theta}}{\cos\theta + \sqrt{\varepsilon_r + \dfrac{\sigma}{s\varepsilon_0} - \sin^2\theta}}, \tag{2.1-3}$$

where ε_0 is the permittivity of free space.

The transient counterpart of (2.1-1) for the reflected field is given as the convolution of the incident field and the inverse Laplace transform of the reflection coefficient $R(t)$ as

$$E^{ref}(t) = R(t) * E^{inc}(t). \tag{2.1-4}$$

In this way, the transient quantity $R(t)$ is viewed as the impulse response of the lossy half space. The evaluation of $R(t)$ directly in time domain requires the analytical inverse Laplace transform of the Fresnel reflection coefficient. This is difficult to do without making some approximations. It is found that (2.1-2) can be written as

$$R_v(\theta,s) = \frac{s+\tau-\beta\sqrt{s(s+\gamma)}}{s+\tau+\beta\sqrt{s(s+\gamma)}} \tag{2.1-5}$$

where $\tau = \frac{\sigma}{\varepsilon}$, $\beta = \frac{\sqrt{\varepsilon_r - \sin^2\theta}}{\varepsilon_r \cos\theta}$, and $\gamma = \tau\left(1 - \frac{\sin^2\theta}{\varepsilon_r}\right)^{-1}$. For the cases where ε_r is on the order of 10 or more and the angle θ is small so that $\frac{\sin^2\theta}{\varepsilon_r} << 1$ and then $\gamma \approx \tau$. This allows (2.1-5) to be approximated as

$$R_v(\theta,s) = \frac{\sqrt{s+\tau}-\beta\sqrt{s}}{\sqrt{s+\tau}+\beta\sqrt{s}}. \tag{2.1-6}$$

It is noted that this approximation will limit the applicability of the solution to non-grazing angles of incidence. The horizontally polarized reflection coefficient of (2.1-3) has the form

$$R_h(\theta,s) = \frac{\sqrt{s}-\varepsilon_r\beta\sqrt{s+\gamma}}{\sqrt{s}+\varepsilon_r\beta\sqrt{s+\gamma}}. \tag{2.1-7}$$

It is noted again that $\gamma \approx \tau$ for a large relative dielectric constant and non-grazing angles of incidence, so that (2.1-7) can be approximated as

$$R_h(\theta,s) = -\frac{\sqrt{s+\tau}-(\varepsilon_r\beta)^{-1}\sqrt{s}}{\sqrt{s+\tau}+(\varepsilon_r\beta)^{-1}\sqrt{s}}. \tag{2.1-8}$$

Both the vertical and horizontal reflection coefficients now have the form

$$R(\theta,s)=\pm\frac{\sqrt{s+2a}-\kappa\sqrt{s}}{\sqrt{s+2a}+\kappa\sqrt{s}}. \tag{2.1-9}$$

where $a=\frac{\tau}{2}$ and $\kappa=\beta$ for vertical polarization, and $\kappa=(\varepsilon_r\,\beta)^{-1}$ for horizontal polarization. The leading + and − signs are used for vertical and horizontal polarizations, respectively. Thus, the same inverse Laplace transform can be utilized to determine the transient reflected field for either polarization.

In order to invert (2.1-9) into the time domain, the Laplace transform pair

$$L^{-1}\left[F(s-a)\right]=e^{at}f(t) \tag{2.1-10}$$

can be used. Equation (2.1-9) can be written as a function of $(s-a)$ as

$$R(s-a)=\pm\frac{\sqrt{s+a}-\kappa\sqrt{s-a}}{\sqrt{s+a}+\kappa\sqrt{s-a}} \tag{2.1-11}$$

which can be expanded to give

$$R(s-a)=\pm\left[\frac{1-\kappa}{1+\kappa}+\frac{4\kappa}{(1+\kappa)^2}\frac{a}{s+\sqrt{s^2-a^2}+a\frac{1-\kappa}{1+\kappa}}\right]. \tag{2.1-12}$$

Defining $K=\frac{1-\kappa}{1+\kappa}$ and $S=s+\sqrt{s^2-a^2}$, (2.1-12) can be written as

$$R(s-a)=\pm\left[K+\frac{4\kappa}{1-\kappa^2}\sum_{n=1}^{\infty}(-1)^{n+1}(Ka)^n S^{-n}\right]. \tag{2.1-13}$$

The inverse Laplace transform of (2.13) is given as

$$L^{-1}\left[R(s-a)\right]=\pm\left[K\delta(t)+\frac{4\kappa t^{-1}}{1-\kappa^2}\sum_{n=1}^{\infty}(-1)^n n K^n I_n(at)\right] \tag{2.1-14}$$

where $\delta(t)$ is the Dirac function and $I_n(\cdot)$ is the modified Bessel function of order n. Using (2.1-10), the impulse response of the lossy half space is then given by

$$R(t) = \pm\left[K\,\delta(t) + \frac{4\kappa}{1-\kappa^2}\,\frac{e^{-at}}{t}\sum_{n=1}^{\infty}(-1)^n\, n\, K^n\, I_n(at)\right]. \qquad (2.1\text{-}15)$$

This expression is valid for both vertical and horizontal polarization, depending on the values of κ and K and the ± sign, and contains two terms, with the first being an impulse that is independent of the material conductivity and the second being a response term persisting in time. With (2.1-15), the transient reflected field can be calculated through (2.1-4).

2.2 PAO, DVORAK AND DUDLEY'S METHOD

Pao, Dvorak and Dudley presented a method that allows for the analytical evaluation of the inverse Laplace transform representations for transient TE [11] and TM [12] plane waves, obliquely incident on a conductive half space. They assumed that the permittivity, permeability and conductivity of the lossy half space are independent of frequency, but did not make any approximation to the reflection coefficients in frequency domain. The time domain expressions for the reflected and transmitted waves are first represented as inverse Laplace transforms. The transient fields are then shown to consist of two canonical integrals. The canonical integrals are solved analytically in turn, thereby yielding closed form solutions involving incomplete Lipschitz-Hankel integrals (ILHI's). The ILHI's are calculated numerically using the algorithms developed by Dvorak and Kuester [58]. Only the transmitted fields are discussed for the TE case, while both the transmitted and reflected fields are discussed for the TM case, which is more complex than the TE case since the TM transmission and reflection coefficients contain second-order poles.

As shown in Figure 2.2-1, consider a uniform TM plane wave that is obliquely incident with angle of incidence θ_i on a conductive half space (medium II), and assume that the source of the plane wave resides in the air, that the half space is homogeneous and that μ, ε and σ are independent of frequency.

The wave equation in the lossy medium is given by

$$\nabla^2 H_y(t) - \varepsilon\,\mu \frac{\partial^2 H_y(t)}{\partial t^2} = \sigma\,\mu \frac{\partial H_y(t)}{\partial t}. \tag{2.2-1}$$

After defining the Laplace transform pair as

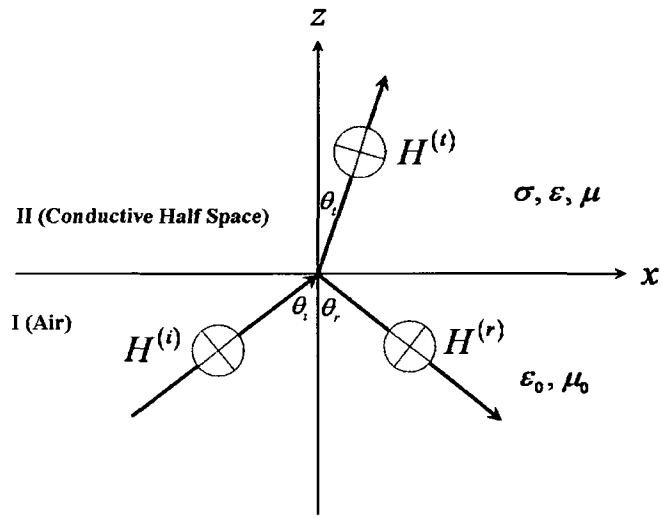

Figure 2.2-1: Geometry and coordinate system for a transverse magnetic (TM) plane wave incident onto a conductive half space.

$$\bar{H}_y(s) = \int_0^\infty e^{-s\,t} H_y(t)\,dt \tag{2.2-2}$$

and

$$H_y(t) = \frac{1}{2\pi j} \int_{\xi-J\infty}^{\xi+J\infty} e^{s\,t} \bar{H}_y(s)\,ds, \tag{2.2-3}$$

it is found that the wave equation reduce to

$$\left(\nabla^2 - \gamma^2\right)\bar{H}_y(x,z,s) = 0 \tag{2.2-4}$$

in the Laplace transform domain. In the above equation

$$\gamma = \sqrt{s\left(s\,\mu\,\varepsilon + \mu\,\sigma\right)} = \frac{1}{\tilde{v}}\sqrt{s\left(s + \frac{\sigma}{\varepsilon}\right)}; \qquad \mathrm{Re}(\gamma) > 0 \tag{2.2-5}$$

is the complx propagation constant and

$$\tilde{v} = \frac{1}{\sqrt{\mu \varepsilon}} \tag{2.2-6}$$

is the phase velocity of light in a lossless medium modeled by μ and ε.

The general solution for (2.2-4), under the constraint $\frac{\partial}{\partial y} = 0$, can be written as

$$\bar{H}_y(x,z,s) = \bar{H}_0(s) \exp(\mp \vec{\gamma} \cdot \vec{r}) \tag{2.2-7}$$

where

$$\vec{\gamma} = \gamma_x \vec{x} + \gamma_y \vec{y} \tag{2.2-8}$$

and

$$\vec{r} = x\vec{x} + y\vec{y} + z\vec{z} \tag{2.2-9}$$

The incident magnetic field can be written as

$$\bar{H}_y^{(i)}(x,z,s) = \bar{H}_0(s) \exp\left(-\frac{s}{c}(x \sin\theta_i + z \cos\theta_i)\right) \tag{2.2-10}$$

where $\bar{H}_0(s)$ is the spectrum of the incident waveform and c is the speed of light in free space. Likewise, the reflected and transmitted fields are given by

$$\bar{H}_y^{(r)}(x,z,s) = \bar{H}_0(s) R \exp\left(-\frac{s}{c}(x \sin\theta_r - z \cos\theta_r)\right) \tag{2.2-11}$$

and

$$\bar{H}_y^{(t)}(x,z,s) = \bar{H}_0(s) T \exp\left(-(\gamma_x x + \gamma_z z)\right) \tag{2.2-12}$$

where R and T are the reflection and transmission coefficients, respectively.

After defining the constant

$$a = \frac{\sigma}{2\varepsilon \cos^2 \tilde{\theta}_t} \tag{2.2-13}$$

and the lossless refraction angle

$$\cos\tilde{\theta}_t = \sqrt{1 - \frac{\tilde{v}^2}{c^2}\sin^2\theta_i}\,, \tag{2.2-14}$$

use the phase matching condition along x at $z = 0$ to show that

$$\gamma_x = \frac{s}{c}\sin\theta_i = \frac{s}{\tilde{v}}\sin\tilde{\theta}_t \tag{2.2-15}$$

and

$$\gamma_z = \frac{\cos\tilde{\theta}_t}{\tilde{v}}\sqrt{s^2 + 2as} \tag{2.2-16}$$

The corresponding electric fields are given by

$$\bar{E}_x^{(i)}(x,z,s) = \frac{1}{c\varepsilon_0}\cos\theta_i\,\bar{H}_0(s)\exp\left(-\frac{s}{c}(x\sin\theta_i + z\cos\theta_i)\right), \tag{2.2-17}$$

$$\bar{E}_z^{(i)}(x,z,s) = \frac{-1}{c\varepsilon_0}\sin\theta_i\,\bar{H}_0(s)\exp\left(-\frac{s}{c}(x\sin\theta_i + z\cos\theta_i)\right), \tag{2.2-18}$$

$$\bar{E}_x^{(r)}(x,z,s) = \frac{-R}{c\varepsilon_0}\cos\theta_i\,\bar{H}_0(s)\exp\left(-\frac{s}{c}(x\sin\theta_i - z\cos\theta_i)\right), \tag{2.2-19}$$

$$\bar{E}_z^{(r)}(x,z,s) = \frac{-R}{c\varepsilon_0}\sin\theta_i\,\bar{H}_0(s)\exp\left(-\frac{s}{c}(x\sin\theta_i - z\cos\theta_i)\right), \tag{2.2-20}$$

$$\bar{E}_x^{(t)}(x,z,s) = \frac{T}{\sigma + s\varepsilon}\frac{\cos\tilde{\theta}_t}{\tilde{v}}\sqrt{s^2 + 2as}\;\bar{H}_0(s)\exp\left(-\left(\frac{x}{\tilde{v}}s\sin\tilde{\theta}_t + \frac{z}{\tilde{v}}\cos\tilde{\theta}_t\sqrt{s^2 + 2as}\right)\right), \tag{2.2-21}$$

$$\bar{E}_z^{(t)}(x,z,s) = \frac{-Ts}{\sigma + s\varepsilon}\frac{\sin\theta_i}{c}\bar{H}_0(s)\exp\left(-\left(\frac{x}{\tilde{v}}s\sin\tilde{\theta}_t + \frac{z}{\tilde{v}}\cos\tilde{\theta}_t\sqrt{s^2 + 2as}\right)\right). \tag{2.2-22}$$

After enforcing the boundary conditions (i.e., $\bar{H}_y$ and $\bar{E}_x$ are continuous at $z = 0$), it is found that

$$R = \frac{(s+\rho) - b\sqrt{s^2 + 2as}}{(s+\rho) + b\sqrt{s^2 + 2as}} \tag{2.2-23}$$

and

$$T = \frac{2(s+\rho)}{(s+\rho) + b\sqrt{s^2 + 2as}} \tag{2.2-24}$$

where

$$b=\sqrt{\frac{\varepsilon\,\mu_0}{\mu\,\varepsilon_0}}\,\frac{\cos\tilde{\theta}_t}{\cos\theta_i} \tag{2.2-25}$$

and

$$\rho=\frac{\sigma}{\varepsilon}. \tag{2.2-26}$$

Starting with (2.2-12) and (2.2-24), the transmitted magnetic field is given by

$$\bar{H}_y^{(t)}(x,z,s)=\frac{2(s+\rho)}{(s+\rho)+b\sqrt{s^2+2as}}\,\bar{H}_0(s)\exp\left(-\left(\frac{x}{\tilde{v}}\,s\sin\tilde{\theta}_t+\frac{z}{\tilde{v}}\cos\tilde{\theta}_t\sqrt{s^2+2as}\right)\right). \tag{2.2-27}$$

Multiply the denominator as well as numerator of (2.2-27) by $-(s+\rho)+b\sqrt{s^2+2as}$ so that

$$\bar{H}_y^{(t)}(x,z,s)=\frac{2(s+\rho)\left(b\sqrt{s^2+2as}-(s+\rho)\right)}{(b^2-1)s^2+(ab^2-\rho)s-\rho^2}\,\bar{H}_0(s)\exp\left(-\left(\frac{x}{\tilde{v}}\,s\sin\tilde{\theta}_t+\frac{z}{\tilde{v}}\cos\tilde{\theta}_t\sqrt{s^2+2as}\right)\right). \tag{2.2-28}$$

The poles of the transmitted magnetic field, which are the roots of the polynomial

$$(b^2-1)s^2+(ab^2-\rho)s-\rho^2=0. \tag{2.2-29}$$

are given by

$$\left.\begin{aligned}s_1&=-\frac{a}{b^2-1}\left(b^2-2\cos^2\tilde{\theta}_t-b\sqrt{b^2-\sin^2 2\tilde{\theta}_t}\right)\\ s_2&=-\frac{a}{b^2-1}\left(b^2-2\cos^2\tilde{\theta}_t+b\sqrt{b^2-\sin^2 2\tilde{\theta}_t}\right)\end{aligned}\right\};\qquad b\neq 1. \tag{2.2-30}$$

Applying the polynomial factorization technique, the transmitted magnetic field can be rewritten as

$$\bar{H}_y^{(t)}(x,z,s)=\frac{\bar{H}_0(s)}{b^2-1}\,\frac{2(s+\rho)\,b\sqrt{s^2+2as}-2(s+\rho)^2}{(s-s_1)(s-s_2)}\exp\left(-\left(\frac{x}{\tilde{v}}\,s\sin\tilde{\theta}_t+\frac{z}{\tilde{v}}\cos\tilde{\theta}_t\sqrt{s^2+2as}\right)\right). \tag{2.2-31}$$

It can be shown that the term under the square root in s_1 and s_2 is always larger than or equal to zero. Hence, s_1 and s_2 are always real valued. The special case $b=1$ needs to be handled separately but is not included in [12].

Consider the transient transmitted fields associated with a double decaying exponential pulse excitation,

$$H_0(t) = A\left(e^{-\alpha_1 t} - e^{-\alpha_2 t}\right) u(t) \tag{2.2-32}$$

where A is chosen so that the peak value of the pulse is unity and $\alpha_1, \alpha_2 > 0$. Because the pulse reaches a maximum at

$$t_m = \frac{\ln\left(\frac{\alpha_1}{\alpha_2}\right)}{\alpha_1 - \alpha_2} \tag{2.2-33}$$

it is found that

$$A = \left(e^{-\alpha_1 t_m} - e^{-\alpha_2 t_m}\right)^{-1}. \tag{2.2-34}$$

The spectral representation of the double exponential pulse is

$$\bar{H}_0(s) = A\left(\frac{1}{s+\alpha_1} - \frac{1}{s+\alpha_2}\right). \tag{2.2-35}$$

Reference to (2.2-31) shows that the time domain transmitted field is given by the inverse Laplace transform representation below

$$H_y^{(t)}(x,z,t) = \frac{A}{\pi j\left(b^2-1\right)}\left\{\int_{\xi-j\infty}^{\xi+j\infty} \frac{2(s+\rho)\, b\sqrt{s^2+2as} - 2(s+\rho)^2}{(s-s_1)(s-s_2)}\right.$$

$$\left.\left(\frac{1}{s+\alpha_1} - \frac{1}{s+\alpha_2}\right) \exp\left(s\,t - \frac{x}{\tilde{v}}\, s \sin\tilde{\theta}_t - \frac{z}{\tilde{v}} \cos\tilde{\theta}_t \sqrt{s^2+2as}\right) ds\right\}. \tag{2.2-36}$$

Use the partial fraction expansion technique to express the time domain transmitted field in the following canonical form

$$H_y^{(t)}(x,z,t)=\frac{2Ae^{-at'}}{b^2-1}\Big[(B_{21}-B_{11})\,b\,f(\beta_1)+(B_{12}-B_{22})\,b\,f(\beta_2)-C_1\,b\,f(\beta_3)+C_2\,b\,f(\beta_4)$$

$$+(D_{21}-D_{11})\,e(\beta_1)+(D_{12}-D_{22})\,e(\beta_2)-E_1\,e(\beta_3)+E_2\,e(\beta_4)\Big]. \tag{2.2-37}$$

The canonical integrals are defined as

$$f(\beta)=\frac{1}{2\pi j}\int_{\xi-j\infty}^{\xi+j\infty}\frac{\exp\left(u\,t'-\frac{z}{\tilde{v}}\cos\tilde{\theta}_t\sqrt{u^2+\omega_p{}^2}\right)}{\sqrt{u^2+\omega_p{}^2}\,(u+\beta)}\,du \tag{2.2-38}$$

$$e(\beta)=\frac{1}{2\pi j}\int_{\xi-j\infty}^{\xi+j\infty}\frac{\exp\left(u\,t'-\frac{z}{\tilde{v}}\cos\tilde{\theta}_t\sqrt{u^2+\omega_p{}^2}\right)}{u+\beta}\,du \tag{2.2-39}$$

The constants in the above expressions are defined by

$$\left.\begin{aligned}\omega_p&=ja\\ t'&=t-\frac{x}{\tilde{v}}\sin\tilde{\theta}_t\\ \beta_1&=-s_1-a\\ \beta_2&=-s_2-a\\ \beta_3&=-\alpha_1-a\\ \beta_4&=-\alpha_2-a\end{aligned}\right\} \tag{2.2-40}$$

and

$$\left.\begin{aligned}B_{mn}&=\frac{(2a+\rho-\alpha_m+s_1+s_2)\,s_n{}^2+(2a\rho-s_1s_2+\alpha_m s_n)\,s_n}{(s_1-s_2)(s_n+\alpha_m)}\\ C_m&=\frac{(2a+\rho-\alpha_m+s_1+s_2)\,\alpha_m{}^2+(2a\rho+s_1\alpha_m+s_2\alpha_m)\,\alpha_m}{(s_1+\alpha_m)(s_2+\alpha_m)}\\ D_{mn}&=\frac{(s_n+\rho)^2}{(s_1-s_2)(s_n+\alpha_m)}\\ E_m&=\frac{(\alpha_m-\rho)^2}{(s_1+\alpha_m)(s_2+\alpha_m)}\end{aligned}\right\}\quad m,n=1,2. \tag{2.2-41}$$

To calculate the transient fields, an efficient method for calculating the canonical integrals needs to be found. FFT techniques can be used to evaluate $f(\beta)$ and $e(\beta)$ numerically, however, a large number of points are required in the FFT to minimize aliasing and truncation errors. To achieve high

accuracy, the analytical evaluations of $f(\beta)$ and $e(\beta)$ are desirable but difficult because of the presence of the branch cut. $f(\beta)$ and $e(\beta)$ can be expressed as

$$f(\beta)=\frac{u\left(t'-\frac{z}{\tilde{v}}\cos\tilde{\theta}_t\right)}{\sqrt{\beta^2+\omega_p{}^2}}\left\{e^{-\beta t'}\sinh\left(\frac{z}{\tilde{v}}\cos\tilde{\theta}_t\sqrt{\beta^2+\omega_p{}^2}\right)+\frac{1}{2\zeta}\left[\left(\frac{\beta z}{\tilde{v}}\cos\tilde{\theta}_t-t'\sqrt{\beta^2+\omega_p{}^2}\right)e^{a_+\zeta}Je_0(a_+,\zeta)\right.\right.$$

$$\left.\left.-\left(\frac{\beta z}{\tilde{v}}\cos\tilde{\theta}_t+t'\sqrt{\beta^2+\omega_p{}^2}\right)e^{a_-\zeta}Je_0(a_-,\zeta)\right]\right\} \tag{2.2-42}$$

$$e(\beta)=u\left(t'-\frac{z}{\tilde{v}}\cos\tilde{\theta}_t\right)\left\{e^{-\beta t'}\cosh\left(\frac{z}{\tilde{v}}\cos\tilde{\theta}_t\sqrt{\beta^2+\omega_p{}^2}\right)+\frac{1}{2\zeta}\left[\left(\frac{\beta z}{\tilde{v}}\cos\tilde{\theta}_t-t'\sqrt{\beta^2+\omega_p{}^2}\right)e^{a_+\zeta}Je_0(a_+,\zeta)\right.\right.$$

$$\left.\left.+\left(\frac{\beta z}{\tilde{v}}\cos\tilde{\theta}_t+t'\sqrt{\beta^2+\omega_p{}^2}\right)e^{a_-\zeta}Je_0(a_-,\zeta)\right]\right\} \tag{2.2-43}$$

where

$$a_\pm=\frac{-\beta t'\pm\frac{z}{\tilde{v}}\cos\tilde{\theta}_t\sqrt{\beta^2+\omega_p{}^2}}{\zeta} \tag{2.2-44}$$

and

$$\zeta=\omega_p\sqrt{t'^2-\frac{z^2}{\tilde{v}^2}\cos^2\tilde{\theta}}\,. \tag{2.2-45}$$

These expressions involve ILHI's of the first kind

$$Je_n(a_\pm,\zeta)=\int_0^\zeta e^{-a_\pm\tau}\,\tau^n\,J_n(\tau)\,d\tau\,, \tag{2.2-46}$$

which is numerically calculated using the algorithms Dvorak and Kuester developed [58].

The transient transmitted electric field components are given by

$$E_x^{(t)}(x,z,t)=\frac{2A\eta\cos\tilde{\theta}\,e^{-at'}}{b^2-1}\left[(G_{11}-G_{21})\,be(\beta_1)+(G_{22}-G_{12})\,be(\beta_2)+H_1\,be(\beta_3)-H_2\,be(\beta_4)\right.$$

$$\left.+(B_{11}-B_{21})\,f(\beta_1)+(B_{22}-B_{12})\,f(\beta_2)+C_1\,f(\beta_3)-C_2\,f(\beta_4)\right] \tag{2.2-47}$$

and

$$E_Z^{(t)}(x,z,t)=\frac{2A\sin\theta_t e^{-at'}}{c\,\varepsilon\left(b^2-1\right)}\left[\left(F_{11}-F_{21}\right)e(\beta_1)+\left(F_{22}-F_{12}\right)be(\beta_2)+I_1\,e(\beta_3)-I_2\,e(\beta_4)\right.$$

$$\left.+\left(G_{11}-G_{21}\right)s_1 bf(\beta_1)+\left(G_{12}-G_{22}\right)s_2 bf(\beta_2)+\alpha_1 H_1 bf(\beta_3)-\alpha_2 H_2 bf(\beta_4)\right] \qquad (2.2\text{-}48)$$

where η is the intrinsic impedance of the medium and the constants are defined as

$$\left.\begin{aligned} F_{mn}&=\frac{s_n^{\,2}+\rho\, s_n}{(s_1-s_2)(s_n+\alpha_m)}\\ G_{mn}&=\frac{(2a+s_n)s_n}{(s_1-s_2)(s_n+\alpha_m)}\\ D_{mn}&=\frac{(\alpha_m-2a)}{(s_1+\alpha_m)(s_2+\alpha_m)}\\ E_m&=\frac{\alpha_m^{\,2}+\rho\,\alpha_m}{(s_1+\alpha_m)(s_2+\alpha_m)} \end{aligned}\right\} \quad m,n=1,2. \qquad (2.2\text{-}49)$$

Using the usual relationship between the transmission and reflection coefficients

$$R=T-1, \qquad (2.2\text{-}50)$$

the following expressions for the transient reflected fields are obtained

$$H_y^{(r)}(x,z,t)=H_y^{(t)}\left(0,0,t-\frac{x}{c}\sin\theta_t+\frac{z}{c}\cos\theta_t\right)-\exp\left(-\alpha_1\left(t-\frac{x}{c}\sin\theta_t+\frac{z}{c}\cos\theta_t\right)\right)$$

$$+\exp\left(-\alpha_2\left(t-\frac{x}{c}\sin\theta_t+\frac{z}{c}\cos\theta_t\right)\right), \qquad (2.2\text{-}51)$$

$$E_x^{(r)}(x,z,t)=-\frac{\cos\theta_t}{c\,\varepsilon_0}H_y^{(t)}(x,z,t), \qquad (2.2\text{-}52)$$

$$E_z^{(r)}(x,z,t)=-\frac{\sin\theta_t}{c\,\varepsilon_0}H_y^{(t)}(x,z,t). \qquad (2.2\text{-}53)$$

The expression $t-\frac{x}{c}\sin\theta_t+\frac{z}{c}\cos\theta_t$ denotes the retarded time in the free space.

As shown in Figure 2.2-2, consider a uniform TE plane wave that is obliquely incident with angle of incidence θ_t on a conductive half space (medium II), and assume again that the source of the plane wave resides in the air, that the half space is homogeneous and that μ, ε and σ are

independent of frequency. Following the above procedure, only the transmitted fields for the TE case are discussed below. The obliquely incident electric field is defined as

$$\bar{E}_y^{(i)}(x,z,s) = \bar{E}_0 \exp\left(-\frac{s}{c}(x\sin\theta_i + z\cos\theta_i)\right) \tag{2.2-54}$$

and the boundary conditions are used to show that the transmitted field is given by

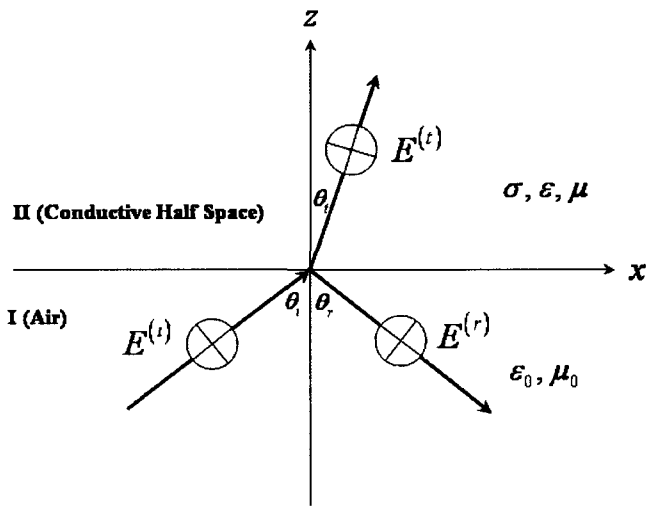

Figure 2.2-2: Geometry and coordinate system for a transverse electric (TE) plane wave incident onto a conductive half space.

$$\bar{E}_y^{(t)}(x,z,s) = \bar{E}_0 T \exp\left(-\frac{1}{\tilde{v}}\left(x\,s\sin\tilde{\theta}_t + z\cos\tilde{\theta}_t\sqrt{s^2+2as}\right)\right) \tag{2.2-55}$$

where the transmission coefficient is given by

$$T = \frac{2s}{s + b\sqrt{s^2+2as}}, \tag{2.2-56}$$

s, c, $\tilde{v}$, a and b are the same as those in TM case. The phase velocity for the wave propagating in medium II is frequency dependent and is given by

$$v=\frac{\omega}{\gamma}=\frac{1}{\sqrt{\frac{\mu\varepsilon}{2}\left(\sqrt{1+\frac{\sigma^2}{\omega^2\varepsilon^2}}+1\right)}}. \tag{2.2-57}$$

The corresponding magnetic fields are given by

$$\bar{H}_y^{(t)}(x,z,s)=-\bar{E}_0\frac{T}{s\mu}\frac{\cos\tilde{\theta}_t}{\tilde{v}}\exp\left(-\frac{1}{\tilde{v}}\left(x\,s\sin\tilde{\theta}_t+z\cos\tilde{\theta}_t\sqrt{s^2+2as}\right)\right) \tag{2.2-58}$$

$$\bar{H}_y^{(t)}(x,z,s)=\bar{E}_0\frac{T}{c\mu}\sin\theta_i\exp\left(-\frac{1}{\tilde{v}}\left(x\,s\sin\tilde{\theta}_t+z\cos\tilde{\theta}_t\sqrt{s^2+2as}\right)\right). \tag{2.2-59}$$

Consider the transient transmitted fields associated with a double decaying exponential pulse excitation, i.e., $E_0(t)$ has the same waveform as $H_0(t)$ in (2.2-32), the transmitted fields in terms of the canonical integrals are given as

$$E_y^{(t)}(x,z,t)=\frac{2Ae^{-at'}}{b^2-1}\left\{\frac{\alpha_0(\alpha_1-\alpha_2)}{(\alpha_0-\alpha_1)(\alpha_0-\alpha_2)}\left[(\beta_0-a)bf(\beta_0)-e(\beta_0)\right]\right.$$

$$\left.+\frac{\alpha_1}{(\alpha_1-\alpha_0)}\left[(\beta_1-a)bf(\beta_1)-e(\beta_1)\right]-\frac{\alpha_2}{(\alpha_2-\alpha_0)}\left[(\beta_2-a)bf(\beta_2)-e(\beta_2)\right]\right\} \tag{2.2-60}$$

$$H_x^{(t)}(x,z,t)=\frac{2A\cos\tilde{\theta}_t e^{-at'}}{(b^2-1)\mu\tilde{v}}\left\{\frac{(\alpha_2-\alpha_1)(2a-\alpha_0)}{(\alpha_1-\alpha_0)(\alpha_2-\alpha_0)}\left[be(\beta_0)-\alpha_0 f(\beta_0)\right]\right.$$

$$\left.+\frac{(2a-\alpha_1)}{\alpha_0-\alpha_1}\left[be(\beta_1)-\alpha_1 f(\beta_1)\right]-\frac{(2a-\alpha_2)}{\alpha_0-\alpha_2}\left[be(\beta_2)-\alpha_2 f(\beta_2)\right]\right\} \tag{2.2-61}$$

and

$$H_z^{(t)}(x,z,t)=\frac{\sin\theta_i}{\mu c}E_y^{(t)}(x,z,t) \tag{2.2-62}$$

where $\beta_i=\alpha_i-a$ for $i=1,2$, and all the rest parameters are the same as those in TM case.

2.3 ROTHWELL AND SUK'S METHOD

Rothwell and Suk introduced the converging series representations of the time domain TE [13] and TM [14] plane wave reflection coefficients. They also assumed that material parameters are

frequency independent but did not use any approximation to the reflection coefficients in frequency domain. Their analytical expressions of the transient reflection coefficients have the forms similar to that in [10]. The first term involves a Dirac δ function and is the specular reflection coefficient identical to the lossless case, while the remainder involves modified Bessel functions and the integral of modified Bessel functions and results from the dispersive nature of the conducting medium. Since the integral of modified Bessel functions hindered efficiency of computation, it was replaced with an infinite sum of modified Bessel functions through mathematical manipulations. Then the infinite sum was truncated, resulting in an approximation for the reflection coefficient.

Consider a plane wave incident from free space onto an interface between free space and a conducting material with frequency independent material parameters $\varepsilon = \varepsilon_r \varepsilon_0$, μ_0 and σ. If the electric field is polarized parallel to the interface (TE polarization) and the incident wave vector makes an angle θ_0 with the normal to the interface, then the frequency domain reflection coefficient is

$$\Gamma(\omega) = \frac{\cos\theta_0 - \sqrt{\varepsilon_r - \sin^2\theta_0 - j\dfrac{\sigma}{\omega\varepsilon_0}}}{\cos\theta_0 + \sqrt{\varepsilon_r - \sin^2\theta_0 - j\dfrac{\sigma}{\omega\varepsilon_0}}}.$$

The inverse Fourier transform of this expression is the time domain reflection coefficient given by

$$\Gamma(t) = \frac{1-\sqrt{D}}{1+\sqrt{D}}\delta(t) + \frac{Be^{-\frac{Bt}{2D}}}{\sqrt{D}(D-1)}\left[I_0\left(\frac{Bt}{2D}\right) + I_1\left(\frac{Bt}{2D}\right)\right]u(t)$$

$$-\frac{2Be^{-\frac{Bt}{D-1}}}{(D-1)\left(1+\sqrt{D}\right)}u(t) - \frac{B^2 e^{-\frac{Bt}{D-1}}u(t)}{\sqrt{D}(D-1)^2}\int_0^{\frac{B(1+D)x}{2D(D-1)}} e^{\left[I_0\left(\frac{Bt}{2D}\right) + I_1\left(\frac{Bt}{2D}\right)\right]dx} \quad (2.3\text{-}1)$$

where $u(x)$ is the unit step function, $I_n(x)$ is the modified Bessel function of the first kind, and

$$D = \frac{\varepsilon_r - \sin^2\theta_0}{\cos^2\theta_0} \qquad B = \frac{\sigma}{\varepsilon_0\cos^2\theta_0}.$$

The first term in (2.3-1) is the specular reflection coefficient identical to the lossless case, while the remainder, designated $R(t)$, results from the dispersive nature of the conducting medium.

Writing the integral in (2.3-1) as

$$\int_0(\cdot)dx=\int_{-\infty}(\cdot)dx-\int_{-\infty}^{0}(\cdot)dx. \tag{2.3-2}$$

With the help of the integral [59]

$$\int_0^{\infty}e^{-\alpha x}I_n(\beta x)dx=\frac{\beta^n}{\sqrt{\alpha^2-\beta^2}\left(\alpha+\sqrt{\alpha^2-\beta^2}\right)^n}, \tag{2.3-3}$$

it is found that the integral over $[-\infty,0]$ exactly cancels the third term in (2.3-1), leading to

$$R(t)=-\frac{B^2u(t)}{\sqrt{D}(D-1)^2}\int_0^{\frac{B(t-x)}{D-1}}\left[f_0\left(\frac{Bx}{2D}\right)+f_1\left(\frac{Bx}{2D}\right)\right]dx+\frac{Bu(t)}{\sqrt{D}(D-1)}\left[f_0\left(\frac{Bt}{2D}\right)+f_1\left(\frac{Bt}{2D}\right)\right] \tag{2.3-4}$$

where $f_n(x)=e^{-x}I_n(x)$, and polynomial approximations for $f_0(x)$ and $f_1(x)$ may be found in [60]. Using the change of variables $u=\frac{B(t-x)}{D-1}$ and defining $Q(x)=f_0(x)+f_1(x)$, (2.3-4) can be written as

$$R(t)=-\frac{Bu(t)}{\sqrt{D}(D-1)}\int_0^{\infty}e^{-u}\left[Q\left(\frac{Bt}{2D}-\frac{D-1}{2D}u\right)-Q\left(\frac{Bt}{2D}\right)\right]du, \tag{2.3-5}$$

which is conducive to numerical calculation due to the presence of the decaying exponential in the integrand. It is also noted that when t is large the term in brackets is a good approximation to the derivative of $Q(x)$, and thus $R(t)$ should be proportional to $Q'\left(\frac{Bt}{2D}\right)$. However, for small t this approximation is poor and the integral must be calculated with more accuracy.

If the magnetic field is polarized parallel to the interface (TM polarization) and the incident wave vector makes an angle θ_0 with the normal to the interface, then the frequency domain reflection coefficient is

$$\Gamma(\omega)=\frac{\sqrt{\varepsilon_r-\sin^2\theta_0-j\frac{\sigma}{\omega\varepsilon_0}}-\cos\theta_0\left(\varepsilon_r-j\frac{\sigma}{\omega\varepsilon_0}\right)}{\sqrt{\varepsilon_r-\sin^2\theta_0-j\frac{\sigma}{\omega\varepsilon_0}}+\cos\theta_0\left(\varepsilon_r-j\frac{\sigma}{\omega\varepsilon_0}\right)}.$$

Here Γ is defined as the ratio of the tangential component of the reflected electric field to the tangential component of the incident electric field. The inverse Fourier transform of this expression is the time domain reflection coefficient given by

$$\Gamma(t)=\frac{1-\sqrt{D}}{1+\sqrt{D}}\delta(t)+\frac{2\beta\sqrt{D}}{D-1}(K_3+K_4)e^{-\beta t}I(\beta t)u(t)-\frac{2\sqrt{D}}{(D-1)(1+\sqrt{D})}\left(K_1e^{P_1t}+K_2e^{P_2t}\right)u(t)$$

$$+\frac{2K_3P_1\beta\sqrt{D}\,e^{P_1t}}{D-1}u(t)\int_0^t e^{-(P_1+\beta)x}I(\beta x)dx+\frac{2K_4P_2\beta\sqrt{D}\,e^{P_2t}}{D-1}u(t)\int_0^t e^{-(P_2+\beta)x}I(\beta x)dx \qquad (2.3\text{-}6)$$

where $u(x)$ is the unit step function and $I(x)=I_0(x)+I_1(x)$ with $I_n(x)$ the modified Bessel function of the first kind. Additional quantities are given by

$$D=\frac{\varepsilon_r^2\cos^2\theta_0}{\varepsilon_r-\sin^2\theta_0} \qquad B=\frac{\frac{\sigma}{\varepsilon_0}}{\varepsilon_r-\sin^2\theta_0}$$

$$A=\frac{\sigma}{\varepsilon} \qquad \beta=\frac{B}{2}$$

$$b=\frac{2DA-B}{1-D} \qquad c=\frac{DA^2}{D-1}$$

$$P_1=\frac{1}{2}\left(b+\sqrt{b^2-4c}\right) \qquad P_2=\frac{1}{2}\left(b-\sqrt{b^2-4c}\right)$$

$$E=B-A\left(1-\sqrt{D}\right) \qquad F=A^2\sqrt{D}$$

$$K_1=\frac{EP_1+F}{P_1-P_2} \qquad K_2=\frac{EP_2+F}{P_2-P_1}$$

$$K_3=\frac{P_1+A}{P_1-P_2} \qquad K_4=\frac{P_2+A}{P_2-P_1}.$$

It is noted that (2.3-6) is valid under the condition that $P_2 < P_1 < 0$. This requires $D > 1$, and thus

$$\theta_0 < \sin^{-1}\left(\frac{\varepsilon_r}{\varepsilon_r + 1}\right) = \theta_B$$

where θ_B is the Brewster angle when $\sigma = 0$. Like TE polarization, the first term in (2.3-6) is the specular reflection coefficient identical to the lossless case, while the remainder, designated $R(t)$, results from the dispersive nature of the conducting medium. Equation (2.3-6) is in a form similar to (2.3-1) for TE polarization but is considerably more complicated.

Using (2.3-2) and (2.3-3), (2.3-6) can be finally written as

$$R(t) = -\frac{2\beta\sqrt{D}\,K_3 u(t)}{D-1}\int_0^\infty e^{-u}\left[Q\left(\beta t + \frac{\beta}{P_1}u\right) - Q(\beta t)\right]du$$

$$-\frac{2\beta\sqrt{D}\,K_4 u(t)}{D-1}\int_0^\infty e^{-u}\left[Q\left(\beta t + \frac{\beta}{P_2}u\right) - Q(\beta t)\right]du \qquad (2.3\text{-}7)$$

where $Q(x) = e^{-x}I(x)$.

2.4 COSSMANN, ROTHWELL AND KEMPEL'S METHOD

In the above presentations of the three techniques handling the transient reflection from a lossy half space, it is assumed that the the material parameters are independent of frequency. In practice, the permittivity, permeability and conductivity show a weak frequency dependence only within some frequency ranges, e.g., microwave bands, and so can be approximately treated as frequency independence quantities within these frequency ranges. When approaching the visible spectrum, permittivity and conductivity began to show a strong frequency dependence and cannot be considered frequency independent anymore. Cossmann, Rothwell and Kempel analytically determined the time domain reflection coefficients for a TE [35] and TM [36] polarized plane wave obliquely incident on a Lorentz medium half space whose permittivity obeys some specific relation with frequency. They utilized the inversion of the frequency domain reflection coefficients, and the

resulting expressions contain exponential and modified Bessel functions and require convolution operation to evaluate.

Consider a sinusoidal stead-state plane wave of frequency ω incident on an interface separating free space (region 1) from a homogeneous Lorentz medium (region 2). The angle of incidence measured from the normal to the interface is θ, and the electric field is polarized perpendicular to the plane of incidence (TE polarization). Region 1 is described by the permittivity ε_0 and permeability μ_0, while region 2 is described by the permittivity $\varepsilon(\omega)=\varepsilon_0\,\varepsilon_r(\omega)$ and permeability μ_0. The reflection coefficient, defined as the ratio of the tangential incident field to reflected electric field, is given by

$$\Gamma(\omega)=\frac{Z(\omega)-Z_0}{Z(\omega)+Z_0}, \tag{2.4-1}$$

where the wave impedance of the incident wave is $Z_0=\eta_0/\cos\theta$ and the wave impedance of the transmitted wave is

$$Z(\omega)=\frac{\eta(\omega)\,k(\omega)}{k_z(\omega)}. \tag{2.4-2}$$

Here $\eta_0=(\mu_0/\varepsilon_0)^{1/2}$, $\eta=(\mu_0/\varepsilon)^{1/2}$, $k_z=\left(k^2-k_0^2\sin^2\theta\right)^{1/2}$, $k_0=\omega(\mu_0\,\varepsilon_0)^{1/2}$ and $k=\omega(\mu_0\,\varepsilon)^{1/2}$.

The relative permittivity of a single resonance Lorentz medium has the form

$$\varepsilon_r(\omega)=1+\frac{b^2}{\omega_0^2-\omega^2+2j\omega\delta}. \tag{2.4-3}$$

Here ω_0 is the resonance frequency, δ is the damping coefficient, and b is the plasma frequency of the medium. Letting the Laplace transform variable be $s=j\omega$ and substituting Equation (2.4-3), then the Laplace domain reflection coefficient may be written in the form

$$\Gamma(s)=\frac{\left(s^2+2\delta s+\omega_0^2\right)^{1/2}-\left(s^2+2\delta s+\omega_0^2+B^2\right)^{1/2}}{\left(s^2+2\delta s+\omega_0^2\right)^{1/2}+\left(s^2+2\delta s+\omega_0^2+B^2\right)^{1/2}}, \tag{2.4-4}$$

where $B = b/\cos\theta$. Factoring the quadratic forms under the radicals gives the alternative form

$$\Gamma(s) = \frac{\left((s-s_1)(s-s_2)\right)^{1/2} - \left((s-s_3)(s-s_4)\right)^{1/2}}{\left((s-s_1)(s-s_2)\right)^{1/2} + \left((s-s_3)(s-s_4)\right)^{1/2}}, \tag{2.4-5}$$

where

$$s_{1,2} = -\delta \pm \lambda_1 \qquad \lambda_1 = \left(\delta^2 - \omega_0^2\right)^{1/2}, \tag{2.4-6}$$

$$s_{3,4} = -\delta \pm \lambda_3 \qquad \lambda_3 = \left(\delta^2 - \omega_0^2 - B^2\right)^{1/2}. \tag{2.4-7}$$

λ_1 and λ_3 may be either real or imaginary, depending on the values of ω_0, δ and B.

The reflection coefficient, Equation (2.4-5), may be put into a form amenable to inversion via a look-up table by rationalizing the denominator, leading to

$$\Gamma(s) = -\frac{\left(F(s)\right)^2}{B^2}, \tag{2.4-8}$$

where

$$F(s) = \left((s-s_1)(s-s_2)\right)^{1/2} - \left((s-s_3)(s-s_4)\right)^{1/2}. \tag{2.4-9}$$

Through mathematical manipulation, $F(s)$ can be written as

$$F(s) = s\left\{\left[\left(\frac{s-s_2}{s-s_1}\right)^{\frac{1}{2}} - 1\right] - \left[\left(\frac{s-s_4}{s-s_3}\right)^{\frac{1}{2}} - 1\right]\right\} - s_1\left[\left(\frac{s-s_2}{s-s_1}\right)^{\frac{1}{2}} - 1\right] + s_3\left[\left(\frac{s-s_4}{s-s_3}\right)^{\frac{1}{2}} - 1\right] - (s_1 - s_3). \tag{2.4-10}$$

Defining the transform pairs

$$\left(\frac{s-s_2}{s-s_1}\right)^{\frac{1}{2}} - 1 \leftrightarrow f_1(t), \tag{2.4-11}$$

$$\left(\frac{s-s_4}{s-s_3}\right)^{\frac{1}{2}} - 1 \leftrightarrow f_2(t), \tag{2.4-12}$$

with the differentiation theorem of Laplace transforms, the inversion of $F(s)$ can be written as

$$f(t) = L^{-1}\left(F(s)\right) = \frac{d}{dt}\left(f_1(t) - f_2(t)\right) - s_1 f_1(t) + s_3 f_2(t) - (s_1 - s_3)\,\delta(t). \tag{2.4-13}$$

Using the transform pair

$$\left(\frac{s-\alpha}{s-\beta}\right)^{\frac{1}{2}} - 1 \leftrightarrow \frac{1}{2}(-\alpha+\beta)\,e^{-\frac{1}{2}(-\alpha-\beta)t}\left[I_1\left(\frac{1}{2}(-\alpha+\beta)t\right) + I_0\left(\frac{1}{2}(-\alpha+\beta)t\right)\right]u(t), \tag{2.4-14}$$

and substituting from Equations, (2.4-6) and (2.4-5) give

$$f_1(t) = \lambda_1\, e^{-\delta t}\left[I_1(\lambda_1 t) + I_0(\lambda_1 t)\right]u(t), \tag{2.4-15}$$

$$f_2(t) = \lambda_3\, e^{-\delta t}\left[I_1(\lambda_3 t) + I_0(\lambda_3 t)\right]u(t). \tag{2.4-16}$$

Here $u(t)$ is the unit step function, and $I_0(x)$ and $I_1(x)$ are the modified Bessel functions of orders 0 and 1, respectively.

The derivatives required to specify $f(t)$ can be found through direct differentiation.

$$\frac{d f_1(t)}{dt} = \lambda_1 e^{-\delta t}\left[\lambda_1 I_1'(\lambda_1 t) + (\lambda_1 - \delta) I_1(\lambda_1 t) - \delta I_0(\lambda_1 t)\right]u(t) + \lambda_1\,\delta(t), \tag{2.4-17}$$

$$\frac{d f_2(t)}{dt} = \lambda_3 e^{-\delta t}\left[\lambda_3 I_1'(\lambda_3 t) + (\lambda_3 - \delta) I_1(\lambda_3 t) - \delta I_0(\lambda_3 t)\right]u(t) + \lambda_3\,\delta(t). \tag{2.4-18}$$

Substituting (2.4-17) and (2.4-18) into (2.4-13) gives

$$f(t) = \lambda_1^2\, e^{-\delta t}\left[I_1'(\lambda_1 t) - I_0(\lambda_1 t)\right]u(t) - \lambda_3^2\, e^{-\delta t}\left[I_1'(\lambda_3 t) - I_0(\lambda_3 t)\right]u(t). \tag{2.4-19}$$

Using the derivative identity

$$\frac{1}{x} I_1(x) = -I_1'(x) + I_0(x) \tag{2.4-20}$$

allows Equation (2.4-19) to be simplified to

$$f(t) = \left[-\lambda_1^2 \frac{I_1(\lambda_1 t)}{\lambda_1 t} + \lambda_3^2 \frac{I_1(\lambda_3 t)}{\lambda_3 t}\right] e^{-\delta t}\, u(t). \tag{2.4-21}$$

The time-domain reflection coefficient, $\Gamma(t)$, can be found by computing the inverse transform of Equation (2.4-8) and using convolution formula. Substitutig from Equation (2.4-21) for $f(t)$ leads to

$$-B^2\,\Gamma(t) = f(t) * f(t)$$

$$= e^{-\delta t}\left[\left(-\lambda_1{}^2\frac{I_1(\lambda_1 t)}{\lambda_1 t} + \lambda_3{}^2\frac{I_1(\lambda_3 t)}{\lambda_3 t}\right)u(t)\right] * \left[\left(-\lambda_1{}^2\frac{I_1(\lambda_1 t)}{\lambda_1 t} + \lambda_3{}^2\frac{I_1(\lambda_3 t)}{\lambda_3 t}\right)u(t)\right]$$

$$= e^{-\delta t}\left(\lambda_1{}^4 f_A(t) - 2\lambda_1{}^2\lambda_3{}^2 f_B(t) + \lambda_3{}^4 f_C(t)\right). \qquad (2.4\text{-}22)$$

The covolutions comprising $f_A(t)$ and $f_C(t)$ can be written explicitly. Writing $f_A(t)$ in integral form gives

$$f_A(t) = u(t)\int_0^t \frac{I_1(\lambda_1 t')}{\lambda_1 t'}\,\frac{I_1\left(\lambda_1(t-t')\right)}{\lambda_1(t-t')}\,dt'. \qquad (2.4\text{-}23)$$

Using the substitution $u = \lambda_1(t-t')$ gives

$$f_A(t) = u(t)\int_{\lambda_1 t}^0 \frac{I_1(\lambda_1 t - u)}{\lambda_1 t - u}\,\frac{I_1(u)}{u}\left(-\frac{1}{\lambda_1}\right)du. \qquad (2.4\text{-}24)$$

Defining $\tau = \lambda_1 t$ allows the integral to be evaluated as follows:

$$f_A(t) = -\frac{u(t)}{\lambda_1}\int_0^\tau \frac{I_1(\tau-u)}{\tau-u}\,\frac{I_1(u)}{u}\,du = \frac{u(t)}{\lambda_1}\left(\frac{2}{\tau}I_2(\tau)\right). \qquad (2.4\text{-}25)$$

Hence $f_A(t)$ and $f_C(t)$ can be written as

$$f_A(t) = \frac{2}{\lambda_1}\tilde{I}_2(\lambda_1 t) \qquad f_C(t) = \frac{2}{\lambda_3}\tilde{I}_2(\lambda_3 t), \qquad (2.4\text{-}26)$$

where

$$\tilde{I}_n(x) = \frac{I_n(x)}{x}u(x). \qquad (2.4\text{-}27)$$

With these, the time domain reflection coefficient becomes

$$\Gamma(t) = -\frac{2}{B^2} e^{-\delta t} \left(\lambda_1^3 \tilde{I}_2(\lambda_1 t) + \lambda_3^3 \tilde{I}_2(\lambda_3 t) - \lambda_1^2 \lambda_3^2 \tilde{I}_1(\lambda_1 t) * \tilde{I}_1(\lambda_3 t) \right). \tag{2.4-28}$$

Equation (2.4-28) is general valid. However, when λ_1 or λ_3 is imaginary, the modified Bessel functions may be replaced by ordinary Bessel functions according to three possible cases. Case 1 occurs when $\omega_0^2 > \delta^2$, making both λ_1 and λ_3 be purely imaginary. Defining

$$\bar{\lambda}_1 = \left(\omega_0^2 - \delta^2\right)^{1/2} \qquad \bar{\lambda}_3 = \left(\omega_0^2 + B^2 - \delta^2\right)^{1/2} \tag{2.4-29}$$

and using

$$I_n(jx) = j^n J_n(x) \tag{2.4-30}$$

lead to

$$\Gamma(t) = -\frac{2}{B^2} e^{-\delta t} \left(\bar{\lambda}_1^3 \tilde{J}_2(\bar{\lambda}_1 t) + \bar{\lambda}_3^3 \tilde{J}_2(\bar{\lambda}_3 t) - \bar{\lambda}_1^2 \bar{\lambda}_3^2 \tilde{J}_1(\bar{\lambda}_1 t) * \tilde{J}_1(\bar{\lambda}_3 t) \right), \tag{2.4-31}$$

where

$$\tilde{J}_n(x) = \frac{J_n(x)}{x} u(x). \tag{2.4-32}$$

Here $J_n(x)$ is the ordinary Bessel function of order n.

Case 2 occurs when $\omega_0^2 + B^2 < \delta^2$, making both λ_1 and λ_3 be purely real, then Equation (2.4-28) can be directly used. Case 3 occurs when $\omega_0^2 + B^2 > \delta^2$ and $\omega_0^2 < \delta^2$. In this case, λ_1 is purely real but λ_3 purely imaginary, leading to

$$\Gamma(t) = -\frac{2}{B^2} e^{-\delta t} \left(\lambda_1^3 \tilde{I}_2(\bar{\lambda}_1 t) + \bar{\lambda}_3^3 \tilde{J}_2(\bar{\lambda}_3 t) - \lambda_1^2 \bar{\lambda}_3^2 \tilde{I}_1(\lambda_1 t) * \tilde{J}_1(\bar{\lambda}_3 t) \right). \tag{2.4-33}$$

There are some interesting differences between the results obtained in the TE and TM cases. Because of the greater complexity of the TM frequency domain reflection coefficient, a more involved process is needed, including the introduction of a term that does not appear in the TE case. Interestingly, under some conditions this term is noncausal, although the final expression for the impulse response is causal. This is an artifact of the technique used to manipulate the frequency

domain expression and does not cause any difficulty in calculation. Also, it is found that when the incident angle is equal to 45^0, a special form of the reflection coefficient is obtained that does not involve the additional term.

For the case of TM polarization (magnetic field perpendicular to the plane of incidence), the originally defined reflection coefficient is still given by (2.4-1), the impedance of a plane wave in the free space (ratio of tangential electric field to tangential magnetic field at the interface) is $Z_0 = \eta_0 \cos\theta$, the impedance of a wave in the Lorentz medium is

$$Z(\omega) = \frac{\eta(\omega) k_z(\omega)}{k(\omega)}. \tag{2.4-34}$$

The incident angle θ is measured in the same way as in TE case, η_0, η, k_z, k_0, and k are the same as those for TE polarization, respectively. Letting the Laplace transform variable be $s = j\omega$ and substituting (2.4-3) and (2.4-34) into (2.4-1), the Laplace domain reflection coefficient may be written in the form

$$\Gamma(s) = \frac{\left((s-s_1)(s-s_2)(s-s_5)(s-s_6)\right)^{1/2} - \left((s-s_3)(s-s_4)\right)^{1/2}}{\left((s-s_1)(s-s_2)(s-s_5)(s-s_6)\right)^{1/2} + \left((s-s_3)(s-s_4)\right)^{1/2}} = \frac{N(s)}{D(s)}, \tag{2.4-35}$$

where

$$s_{1,2} = -\delta \pm \lambda_1 \qquad \lambda_1 = \left(\delta^2 - \omega_0^2\right)^{1/2}, \tag{2.4-36}$$

$$s_{3,4} = -\delta \pm \lambda_3 \qquad \lambda_3 = \left(\delta^2 - \omega_0^2 - b^2\right)^{1/2}, \tag{2.4-37}$$

$$s_{5,6} = -\delta \pm \lambda_5 \qquad \lambda_5 = \left(\delta^2 - \omega_0^2 - B^2\right)^{1/2}. \tag{2.4-38}$$

Here ω_0, δ, b and B are the same as those for TE polarization, and λ_1, λ_3 and λ_5 may be either real or imaginary, depending on the values of ω_0, δ, b and B.

The denominator in (2.4-35) is rationalized by the operation

$$\Gamma(s) = \frac{N(s)}{D(s)} \frac{N(s)}{N(s)}. \tag{2.4-39}$$

For $\theta \neq 45^0$, the denominator of (2.4-39) can be written as

$$D(s)N(s) = b^2\left(\tan^2\theta - 1\right)(s - s_A)(s - s_B), \tag{2.4-40}$$

where

$$s_{A,B} = -\delta \pm \lambda_A \qquad \lambda_A = \left(\delta^2 - \omega_0^2 - b^2/\left(\tan^2\theta - 1\right)\right)^{1/2}. \tag{2.4-41}$$

The numerator of (2.4-39) can be written as

$$\left(N(s)\right)^2 = (s - s_1)(s - s_2)G(s), \tag{2.4-42}$$

where

$$G(s) = g_1(s) + g_2(s) - 2b^2 g_3(s) + b^4 g_4(s) + 2b^2, \tag{2.4-43}$$

$$g_1(s) = (s - s_1)(s - s_2) - \left((s - s_1)(s - s_2)(s - s_5)(s - s_6)\right)^{1/2}, \tag{2.4-44}$$

$$g_2(s) = (s - s_5)(s - s_6) - \left((s - s_1)(s - s_2)(s - s_5)(s - s_6)\right)^{1/2}, \tag{2.4-45}$$

$$g_3(s) = \frac{(s - s_5)(s - s_6)}{\left((s - s_1)(s - s_2)(s - s_5)(s - s_6)\right)^{1/2}}, \tag{2.4-46}$$

$$g_4(s) = \frac{1}{(s - s_1)(s - s_2)}. \tag{2.4-47}$$

Using the convolution theorem of Laplace transforms, the time domain reflection coefficient can be written as

$$b^2\left(\tan^2\theta - 1\right)\Gamma(t) = c(t) * g(t), \tag{2.4-48}$$

where $g(t)$ is the inverse transform of $G(s)$ and is given by

$$g(t) = g_1(t) + g_2(t) - 2b^2 g_3(t) + b^4 g_4(t) + 2b^2\,\delta(t), \tag{2.4-49}$$

and $c(t)$ is the inverse transform of

$$C(s) = \frac{(s - s_1)(s - s_2)}{(s - s_A)(s - s_B)}. \tag{2.4-50}$$

The quantity $g(t)$ may be found by taking the inverse transform of each of the terms in (2.4-43). The terms $g_1(s)+g_2(s)$ are identical to the numerator of the reflection coefficient for the TE polarization, termed $(F(s))^2$ there. Using the inverse transform developed there gives

$$g_1(t)+g_2(t)=2e^{-\delta t}\left[\lambda_1^3\tilde{I}_2(\lambda_1 t)u(t)+\lambda_5^3\tilde{I}_2(\lambda_5 t)u(t)-\lambda_1^2\lambda_5^2\left(\tilde{I}_1(\lambda_1 t)u(t)\right)*\left(\tilde{I}_1(\lambda_5 t)u(t)\right)\right], \quad (2.4\text{-}51)$$

where $u(t)$ is the unit step function and

$$\tilde{I}_n(x)=\frac{I_n(x)}{x}, \quad (2.4\text{-}52)$$

with $I_n(x)$ as the modified Bessel function of the first kind of order n. This definition does not include the unit step function and thus differs from the definition in the TE case.

Using the transform pair

$$\frac{1}{(s+\rho)^{1/2}(s+\sigma)^{1/2}}\leftrightarrow e^{-(\rho+\sigma)\frac{t}{2}}I_0\left(-(\rho-\sigma)\frac{t}{2}\right)u(t) \quad (2.4\text{-}53)$$

and employing the differentiation theorem of Laplace transforms, the term $g_3(t)$ can be written as

$$g_3(t)=\left(\frac{d^2}{dt^2}+2\delta\frac{d}{dt}+\omega_0^2+\frac{b^2}{\cos^2\theta}\right)\bar{g}_3(t), \quad (2.4\text{-}54)$$

where

$$\bar{g}_3(t)=e^{-\delta t}\left[I_0(\lambda_1 t)u(t)\right]*\left[I_0(\lambda_5 t)u(t)\right]. \quad (2.4\text{-}55)$$

Using the definition of λ_5, (2.4-54) can be simplified as

$$g_3(t)=\left(\frac{d^2}{dt^2}-\lambda_5^2\right)\bar{g}_3(t). \quad (2.4\text{-}56)$$

Recalling that $\frac{du(t)}{dt}=\delta(t)$ and using the differentiation rule,

$$\frac{d}{dt}\left[f(t)*g(t)\right]=\frac{df(t)}{dt}*g(t)=f(t)*\frac{dg(t)}{dt}, \quad (2.4\text{-}57)$$

gives, after some simplification,

$$g_3(t) = e^{-\delta t}\left[-\lambda_5^2\left(I_0(\lambda_1 t)u(t)\right) * \left(\tilde{I}_1(\lambda_5 t)u(t)\right) + \lambda_1 I_1(\lambda_1 t)u(t)\right] + \delta(t). \tag{2.4-58}$$

The fourth term in (2.4-49) may be inverted by using the partial fraction expansion

$$g_4(s) = \frac{1}{(s-s_1)(s-s_2)} = \frac{1}{2\lambda_1}\left(\frac{1}{s-s_1} - \frac{1}{s-s_2}\right), \tag{2.4-59}$$

giving

$$g_4(t) = \frac{e^{-\delta t}}{\lambda_1}\sinh(\lambda_1 t)u(t). \tag{2.4-60}$$

Substituting (2.4-51), (2.4-58) and (2.4-60) into (2.4-49) then gives

$$g(t) = 2e^{-\delta t}\Big[\lambda_1^3\tilde{I}_2(\lambda_1 t)u(t) + \lambda_5^3\tilde{I}_2(\lambda_5 t)u(t) - \lambda_1^2\lambda_5^2\left(\tilde{I}_1(\lambda_1 t)u(t)\right) * \left(\tilde{I}_1(\lambda_5 t)u(t)\right)$$

$$+b^2\lambda_5^2\left(I_0(\lambda_1 t)u(t)\right) * \left(\tilde{I}_1(\lambda_5 t)u(t)\right) - b^2\lambda_1 I_1(\lambda_1 t)u(t) + \frac{b^4}{2\lambda_1}\sinh(\lambda_1 t)u(t)\Big]. \tag{2.4-61}$$

There are three possible variants of $g(t)$. Case 1 occurs when $\omega_0^2 > \delta^2$, making both λ_1 and λ_5 be imaginary. Using (2.4-30) and $\sinh(jx) = j\sin(x)$ and letting

$$\bar{\lambda}_1 = \left(\omega_0^2 - \delta^2\right)^{1/2} \qquad \bar{\lambda}_5 = \left(\omega_0^2 + B^2 - \delta^2\right)^{1/2} \tag{2.4-62}$$

give

$$g(t) = 2e^{-\delta t}\Big[\bar{\lambda}_1^3\tilde{J}_2(\bar{\lambda}_1 t)u(t) + \bar{\lambda}_5^3\tilde{J}_2(\bar{\lambda}_5 t)u(t) - \bar{\lambda}_1^2\bar{\lambda}_5^2\left(\tilde{J}_1(\bar{\lambda}_1 t)u(t)\right) * \left(\tilde{J}_1(\bar{\lambda}_5 t)u(t)\right)$$

$$-b^2\bar{\lambda}_5^2\left(J_0(\bar{\lambda}_1 t)u(t)\right) * \left(\tilde{J}_1(\bar{\lambda}_5 t)u(t)\right) + b^2\bar{\lambda}_1 J_1(\bar{\lambda}_1 t)u(t) + \frac{b^4}{2\bar{\lambda}_1}\sin(\bar{\lambda}_1 t)u(t)\Big]. \tag{2.4-63}$$

In case 2, $\omega_0^2 < \delta^2 - B^2$, then both λ_1 and λ_5 are real and Equation (2.4-61) can be directly used. Finally, case 3 occurs when $\delta^2 - B^2 < \omega_0^2 < \delta^2$, then λ_1 is real but λ_5 imaginary, and Equation (2.4-61) becomes

$$g(t) = 2e^{-\delta t}\Big[\lambda_1^3\tilde{I}_2(\lambda_1 t)u(t) + \bar{\lambda}_5^3\tilde{J}_2(\bar{\lambda}_5 t)u(t) - \lambda_1^2\bar{\lambda}_5^2\left(\tilde{I}_1(\lambda_1 t)u(t)\right) * \left(\tilde{J}_1(\bar{\lambda}_5 t)u(t)\right)$$

$$+b^2\bar{\lambda}_5^{\,2}\left(I_0\left(\bar{\lambda}_1 t\right)u(t)\right)*\left(\tilde{J}_1\left(\bar{\lambda}_5 t\right)u(t)\right)-b^2\lambda_1 I_1\left(\lambda_1 t\right)u(t)+\frac{b^4}{2\lambda_1}\sinh\left(\lambda_1 t\right)u(t)\Bigg]. \qquad (2.4\text{-}64)$$

The last step in determining the reflection coefficient is to invert $C(s)$. Expanding (2.4-50) in partial fractions gives

$$C(s)=1+\frac{b^2}{2\lambda_A\left(\tan^2\theta-1\right)}\left(\frac{1}{s-s_A}-\frac{1}{s-s_B}\right). \qquad (2.4\text{-}65)$$

The form of the inverse transform of this function depends on the values of s_A and s_B, with three possible cases. Case 1 occurs if $\delta^2+b^2/\left(\tan^2\theta-1\right)>\omega_0^2>b^2/\left(\tan^2\theta-1\right)$. Then the transform identity $1/(s+\beta)\leftrightarrow e^{-\beta t}u(t)$ can be used to give

$$c(t)=\delta(t)-\frac{b^2e^{-\delta t}}{\lambda_A\left(\tan^2\theta-1\right)}\sinh\left(\lambda_A t\right)u(t). \qquad (2.4\text{-}66)$$

Case 2 occurs if $\omega_0^2>\delta^2+b^2/\left(\tan^2\theta-1\right)$, for which λ_A is imaginary. Defining

$$\bar{\lambda}_A=\left(\omega_0^2-\delta^2+\frac{b^2}{\tan^2\theta-1}\right)^{1/2}, \qquad (2.4\text{-}67)$$

gives for this case

$$c(t)=\delta(t)+\frac{b^2e^{-\delta t}}{\bar{\lambda}_A\left(\tan^2\theta-1\right)}\sin\left(\bar{\lambda}_A t\right)u(t). \qquad (2.4\text{-}68)$$

Finally, case 3 occurs if $\omega_0^2<b^2/\left(\tan^2\theta-1\right)$. Then λ_A is real and greater than δ, resulting in $\mathrm{Re}(s_A)>0$. This requires use of the identity $1/(s-\beta)\leftrightarrow e^{\beta t}u(-t)$, giving

$$c(t)=\delta(t)+\frac{b^2e^{-\delta t}}{\lambda_A\left(\tan^2\theta-1\right)}\left(-e^{\lambda_A t}u(-t)-e^{-\lambda_A t}u(t)\right)=\delta(t)-\frac{b^2e^{-\delta t}}{\lambda_A\left(\tan^2\theta-1\right)}e^{-\lambda_A|t|}. \qquad (2.4\text{-}69)$$

With $c(t)$ determined, the reflection coefficient is found through the convolution described by (2.4-48). When $\omega_0^2<b^2/\left(\tan^2\theta-1\right)$, then $c(t)$, as given by (2.4-69), is noncausal. However, the numerical inversion of (2.4-35) shows that $\Gamma(t)$ is causal under all circumstances. This apparent

contradiction is the result of the rationalization process inherent in (2.4-39). Since this process is a multiplication by unity, there is no effect on the spectrum, and in the TE case the process leads to no difficulties. However, for the TM case, under certain circumstances, the inverse transform of the term $1/N(s)$ is noncausal, and so the convolution introduced by multiplication in frequency domain must somehow eliminate any noncausal effect.

When $\theta = 45^0$, the expressions achieved above cannot be used directly due to singularities. Since the denominator of (2.4-39) reduces to $N(s)D(s) = -b^4$ when $\theta = 45^0$, from (2.4-42) the reflection coefficient is given by

$$-b^4 \Gamma(s) = (s - s_1)(s - s_2) G(s) = (s^2 + 2\delta s + \omega_0^2) G(s). \tag{2.4-70}$$

Inverting (2.4-70) with the differentiation theorem gives

$$-b^4 \Gamma(t) = \left(\frac{d^2}{dt^2} + 2\delta \frac{d}{dt} + \omega_0^2 \right) g(t), \tag{2.4-71}$$

where $g(t)$ is given in (2.4-61). Using the definition of λ_1, (2.4-71) reduces to

$$-b^4 \Gamma(t) = 2e^{-\delta t} \left(\frac{d^2}{dt^2} - \lambda_1^2 \right) g_A(t), \tag{2.4-72}$$

where $g_A(t) = e^{\delta t} g(t)$. Computing the derivatives of $g_A(t)$ gives

$$\begin{aligned} g_A''(t) = &-\lambda_1^3 \lambda_5^3 \left[\tilde{I}_1'(\lambda_1 t) u(t) \right] * \left[\tilde{I}_1'(\lambda_5 t) u(t) \right] - \frac{1}{2} \lambda_1^3 \lambda_5^2 \tilde{I}_1'(\lambda_1 t) u(t) - \frac{1}{2} \lambda_5^5 \tilde{I}_1'(\lambda_5 t) u(t) \\ &+ \lambda_1^5 \tilde{I}_2''(\lambda_1 t) u(t) + \lambda_5^5 \tilde{I}_2''(\lambda_5 t) u(t) + b^2 \lambda_1^2 \lambda_5^2 \left[I_1'(\lambda_1 t) u(t) \right] * \left[\tilde{I}_1'(\lambda_5 t) u(t) \right] \\ &- b^2 \lambda_1^3 I_1''(\lambda_1 t) u(t) + \frac{1}{2} b^4 \lambda_1 \sinh(\lambda_1 t) u(t) \end{aligned} \tag{2.4-73}$$

where a prime (') indicates differentiation with respect to argument. Substituting this expression into (2.4-72) and using

$$\tilde{I}_n'(x) = \frac{n-1}{2n} \tilde{I}_{n-1}(x) + \frac{n+1}{2n} \tilde{I}_{n+1}(x), \tag{2.4-74}$$

produces, after some simplification, the reflection coefficient for $\theta = 45^0$,

$$\Gamma(t) = -\frac{2e^{-\delta t}}{b^4}\left\{-\lambda_1^3\lambda_5^3\left[\tilde{I}_2(\lambda_1 t)u(t)\right]*\left[\tilde{I}_2(\lambda_5 t)u(t)\right]+\frac{1}{2}\lambda_1^2\lambda_5^2\left(\lambda_1^2+\lambda_5^2\right)\left[\tilde{I}_1(\lambda_1 t)u(t)\right]*\left[\tilde{I}_1(\lambda_5 t)u(t)\right]\right.$$

$$\left.-\lambda_1^3\lambda_5^2\tilde{I}_2(\lambda_1 t)\,u(t)-\lambda_1^2\lambda_5^3\tilde{I}_2(\lambda_5 t)\,u(t)+\frac{1}{2}\lambda_1^5\tilde{I}_4(\lambda_1 t)\,u(t)+\frac{1}{2}\lambda_5^5\tilde{I}_4(\lambda_5 t)\,u(t)\right\} \qquad (2.4\text{-}75)$$

When λ_5 is imaginary or when both λ_1 and λ_5 are imaginary, then (2.4-75) can be modified as was done before. For example, when both λ_1 and λ_5 are imaginary, (2.4-75) becomes

$$\Gamma(t) = -\frac{2e^{-\delta t}}{b^4}\left\{-\bar{\lambda}_1^3\bar{\lambda}_5^3\left[\tilde{J}_2(\bar{\lambda}_1 t)u(t)\right]*\left[\tilde{J}_2(\bar{\lambda}_5 t)u(t)\right]+\frac{1}{2}\bar{\lambda}_1^2\bar{\lambda}_5^2\left(\bar{\lambda}_1^2+\bar{\lambda}_5^2\right)\left[\tilde{I}_1(\bar{\lambda}_1 t)u(t)\right]*\left[\tilde{I}_1(\bar{\lambda}_5 t)u(t)\right]\right.$$

$$\left.-\bar{\lambda}_1^3\bar{\lambda}_5^2\tilde{I}_2(\bar{\lambda}_1 t)\,u(t)-\bar{\lambda}_1^2\bar{\lambda}_5^3\tilde{I}_2(\bar{\lambda}_5 t)\,u(t)+\frac{1}{2}\bar{\lambda}_1^5\tilde{I}_4(\bar{\lambda}_1 t)\,u(t)+\frac{1}{2}\bar{\lambda}_5^5\tilde{I}_4(\bar{\lambda}_5 t)\,u(t)\right\} \qquad (2.4\text{-}76)$$

2.5 CONCLUDING REMARKS

This chapter reviews some major analytical methods to model transient reflection of horizontally and vertically polarized wave reflected from lossy and dispersive medium half spaces, and has shown that they are not good enough. The merits and limitations of each method are summarized as follows.

In section 2.1, the approximate form of a frequency-domain reflection coefficient permits one analytical expression for the impulse response of a lossy half space, but makes the solutions inaccurate or even invalid for large incident angles relative to the normal to the interface and/or for relative dielectric constants below the order of 10.

In section 2.2, the transient TE and TM plane waves obliquely incident on a conductive half space are first represented as inverse Laplace transforms, and then shown to consist of two canonical integrals that can be solved analytically. However, these inverse Laplace transform representations are derived only for the incidence of a double exponential signal. The solutions for the reflected and transmitted waves involve incomplete Lipschitz-Hankel integrals for which some specific software is needed for rapid calculation.

Section 2.3 introduces a rapidly converging series of the time-domain reflection coefficient into the analysis of transient reflection from a lossy half space, which is valid for all incident angles with the horizontal polarization, but only for incident angles less than the Brewster angle with the vertical polarization. Few terms provide good accuracy for late time, while many more terms may be required to approach acceptable accuracy for early time, making calculation complicated and time-consuming.

Section 2.4 presents the closed form solutions for both TE and TM transient reflection coefficients, which provide useful intuition about the response of a Lorentz medium half space. However, the mathematical derivations are lengthy and the solutions involve exponential and modified Bessel functions and require convolution operation to evaluate. Particularly, because of the greater complexity of the TM frequency domain reflection coefficient, a more involved process is needed, including the introduction of a term that does not appear in the TE case. Under some conditions this term is noncausal, although the final expression for the impulse response is causal. Moreover, when the incident angle is equal to 45^0, the general expressions cannot be used directly due to singularities, and a special form of TM time domain reflection coefficient is separately achieved.

In order to overcome the disadvantages of the above methods, we introduced one method based on the numerical inversion of Laplace transform into the transient analysis of electromagnetic waves in lossy and dispersive media. In next chapter, the theory on the numerical inversion of Laplace transform is discussed and the method is put on a firmer mathematical basis.

CHAPTER 3: THEORY ON NUMERICAL INVERSION OF LAPLACE TRANSFORM

All the analytical methods discussed in Chapter 2 for transient reflection and transmission rely on the evaluation or computation of inverse Fourier transforms or inverse Laplace transforms. As indicated in [61], the most straightforward numerical approach is to use the fast Fourier transform algorithm in a direct numerical synthesis of the Fourier integral representation of the dispersive pulse propagation problem. Unfortunately, the computational efficiency of this numerical procedure decreases rapidly when an attempt is made to calculate the fine high frequency field structure that is characteristic of the onset of the Sommerfeld precursor field. It has been found that FFT techniques require a large number of sample points for correct modeling of the early time behavior in dispersive regions [11] [12] [27] [28]. In fact, this is one of the reasons that some analytical methods like those in Chapter 2 are needed to be developed. However, as shown in the last chapter, a process for evaluating or calculating inverse transforms is lengthy, some skills in mathematical manipulation are often needed, and particularly, the procedure is relative complicated but not generic. For instance, the usage of the closed form representation in terms of incomplete Lipschitz-Hankel integrals (ILHI's) are more complex than the usage of FFT for the dispersion problems relevant to lossy materials in [11] [12] [26] [27], but cannot be directly applied to dispersion problems related to Lorentz material because of the complexity of the Lorentz model.

The inversion of Laplace transforms is a topic of fundamental importance in many fields of applied and computational sciences. For a transform with a suitable structure, the inverse function can be recovered by using tables of function-transform pairs [59] or by using the Bromwich integral and Cauchy integral theorem [67]. For more complicated transforms that are not given in these tables and for which the Bromwich integral and Cauchy integral theorem cannot be used, the numerical transform inversion would be a viable option. Many methods have been developed for performing numerical transform inversion. Davies [62] gives a good summary of the more popular methods.

Although no method is universally superior, one that boasts a good combination of accuracy, robustness and similicity and is well suited to technological applications is the Fourier series method, which is so-called because it involves approximating the inversion integral with an infinite Fourier series. The partial sums of a Fourier series thus formed are often slow to converge, so an effective convergence acceleration technique needs to be applied. Euler summation [63] is a classical scheme for accelerating the convergence of certain sequences. Simon et al [64] were the first to use Euler summation for Laplace transform inversion with the Fourier series approach. Hosono [65] [66] employed a more flexible Euler summation, made refinements to the basic Fourier series approach, and pioneered new areas of application. Since then, however, Hosono's algorithm has only found quite limited applications in electromagnetics and seems to have received less attention in the related fields over the last thirty years. The aims of this thesis are to further develop Hosono's algorithm and to extend and apply the inversion approach to transient analysis of electromagnetic pulses. In this chapter, Hosono's algorithm for numerical inversion of Laplace transform is discussed and treated under a strict theoretical framework.

3.1 Approximation of Exponential Function

The Laplace transform (image function in the complex frequency domain) $F(s)$ and the inverse Laplace transform (original function in the time domain) $f(t)$ are related by the forward transformation

$$L(f(t)) = F(s) = \int_0^\infty f(t)e^{-st}dt \tag{3.1-1}$$

and the inverse transformation

$$L^{-1}(F(s)) = f(t) = \frac{1}{2\pi j}\int_{\gamma-j\infty}^{\gamma+j\infty} F(s)e^{st}ds\,. \tag{3.1-2}$$

The most distinctive feature of this method lies in approximating e^{st} with some function, such as

$$E_{ec}(st,\rho)=\frac{e^{\rho}}{2cosh(\rho-st)}=\frac{e^{st}}{1+e^{-2(\rho-st)}}=e^{st}-e^{-2\rho}e^{3st}+e^{-4\rho}e^{5st}-\cdots \tag{3.1-3}$$

Hence,

$$e^{st}=\lim_{\rho\to\infty}E_{ec}(st,\rho). \tag{3.1-4}$$

e^{st} differs from $E_{ec}(st,\rho)$ in nature, because e^{st} is an entire function that has an essential singularity at infinity but has no finite-plane singularities, while $E_{ec}(st,\rho)$ is a meromorphic function that has any number of poles in the finite plane.

In order to conduct the complex integral, a partial-fraction expansion of $E_{ec}(st,\rho)$ which takes the form of an infinite series needs to be found. $E_{ec}(st,\rho)$ has first-order poles at

$$s=\frac{\rho+j(n-0.5)\pi}{t} \tag{3.1-5}$$

where n is an integer. According to the Mittag-Leffler theorem [67], $E_{ec}(st,\rho)$ can be expressed by

$$E_{ec}(st,\rho)=\sum_{n=-\infty}^{\infty}p_n(st,\rho) \tag{3.1-6}$$

where $p_n(st,\rho)$ is a single principal part arising from an expansion about each pole, if $E_{ec}(st,\rho)$ or $\left[cosh(\rho-st)\right]^{-1}$ is uniformly bounded on a set of curves. The square contours shown in Figure 3.1-1 can be chosen as the set of curves, on which it is checked whether $\left[cosh(\rho-st)\right]^{-1}$ is uniformly bounded or not.

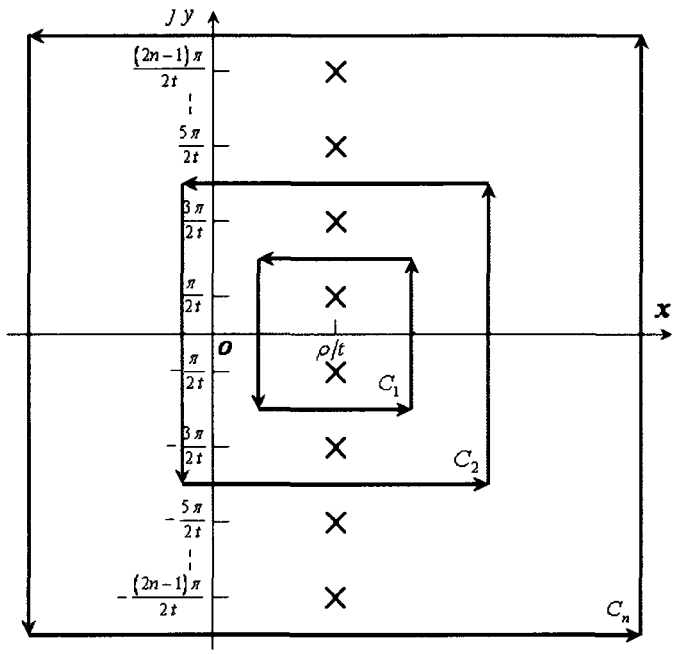

Figure 3.1-1: Contours used in obtaining the partial-fraction expansion of $E_{ec}(s\,t,\rho)$.

With $s = x + j\,y$,

$$\left|cosh(\rho - s\,t)\right|^2 = \left|cosh(\rho - x\,t - j\,y\,t)\right|^2 = sinh^2(\rho - x\,t) + cos^2(y\,t). \tag{3.1-7}$$

On a vertical side $x = \dfrac{\rho + n\,\pi}{t}$ $(n = \pm 1, \pm 2, \cdots)$,

$$\left|cosh(\rho - s\,t)\right|^2 = sinh^2(n\,\pi) + cos^2(y\,t) \geq sinh^2(n\,\pi) > 1. \tag{3.1-8}$$

On a horizontal side $y = \dfrac{n\,\pi}{t}$ $(n = \pm 1, \pm 2, \cdots)$,

$$\left|cosh(\rho - s\,t)\right|^2 = sinh^2(\rho - x\,t) + cos^2(n\,\pi) = sinh^2(\rho - x\,t) + 1 = cosh^2(\rho - x\,t) \geq 1. \tag{3.1-9}$$

Hence, on each contour shown in Figure 3.1-1,

$$\left|\frac{1}{cosh(\rho - s\,t)}\right| \leq 1 \tag{3.1-10}$$

which verifies that the conditions of the Mittag-Leffler theorem are satisfied. At each pole, the residue of $\left[cosh(\rho - s\,t)\right]^{-1}$ is

$$\lim_{s\to(\rho+j(n-0.5)\pi)/t}\frac{st-(\rho+j(n-0.5)\pi)}{\cosh(\rho-st)}=\left[\frac{1}{\sinh(st-\rho)}\right]_{s\to(\rho+j(n-0.5)\pi)/t}$$

$$=\frac{1}{\sinh(j(n-0.5)\pi)}=\frac{1}{j\sin\left(n\pi-\frac{\pi}{2}\right)}=\frac{j}{\cos(n\pi)}=j(-1)^n \tag{3.1-11}$$

so that

$$E_{ec}(st,\rho)=\frac{e^{\rho}}{2}\sum_{n=-\infty}^{\infty}\frac{(-1)^n j}{st-[\rho+j(n-0.5)\pi]}. \tag{3.1-12}$$

In [65] and [66], (3.1-12) was simply given without the derivation and verification that the conditions of the Mittag-Leffler theorem are met.

3.2 APPROXIMATION OF INVERSION OF LAPLACE TRANSFORM

The inversion of Laplace transform is approximated by a function $f_{ec}(t,\rho)$ that is defined as

$$f_{ec}(t,\rho)=\frac{1}{2\pi j}\int_{\gamma-j\infty}^{\gamma+j\infty}F(s)E_{ec}(st,\rho)\,ds. \tag{3.2-1}$$

Substituting (3.1-3) into (3.2-1) leads to

$$f_{ec}(t,\rho)=f(t)-e^{-2\rho}f(3t)+e^{-4\rho}f(5t)-\cdots \tag{3.2-2}$$

Thus,

$$f(t)=\lim_{\rho\to\infty}f_{ec}(t,\rho). \tag{3.2-3}$$

The evaluation of the Bromwich integral for $f_{ec}(t,\rho)$ in (3.2-1) was not strictly treated in [65] and [66]. This thesis attempts to present a more strict treatment as follows. The purpose is to transfer the Bromwich integral for $f_{ec}(t,\rho)$, under some conditions $F(s)$ satisfies, to an integral that encloses all the poles of $E_{ec}(st,\rho)$ but does not contains any singularity or branch point of $F(s)$, so that $f_{ec}(t,\rho)$ is evaluated as a summation of the residues of $F(s)E_{ec}(st,\rho)$ at all poles of $E_{ec}(st,\rho)$. If $E_{ec}(st,\rho)$ had a finite number of poles, the transfer could be done straightforwardly.

With $E_{ec}(s\,t,\rho)$ containing an infinite number of poles now, as indicated in the partial-fraction expansion given by (3.1-12), the transfer cannot be done straightforwardly, since the contour of integration will pass through singularities of $E_{ec}(s\,t,\rho)$ when $n\to\infty$.

Based on the properties of $F(s)$, such a number γ_0 can always be found that in the region of convergence, $0<\gamma_0<\mathrm{Re}(s)$, 1) $F(s)$ converges absolutely, 2) $\lim_{s\to\infty}F(s)=0$, 3) $F(s)$ does not have any singularity and branch point, and 4) $F(s^*)=F^*(s)$ where * denotes complex conjugate. Meanwhile, a number ρ in (3.1-3) can also be determined such that $\gamma_0<\frac{\rho}{t}$. With the partial-fraction expansion of the approximating function $E_{ec}(s\,t,\rho)$ given by (3.1-12), the Bromwich integral for $f_{ec}(t,\rho)$ in (3.2-1) can be transferred to the integral around the poles of $E_{ec}(s\,t,\rho)$ when $F(s)$ satisfies the above four conditions. The procedure is justified below.

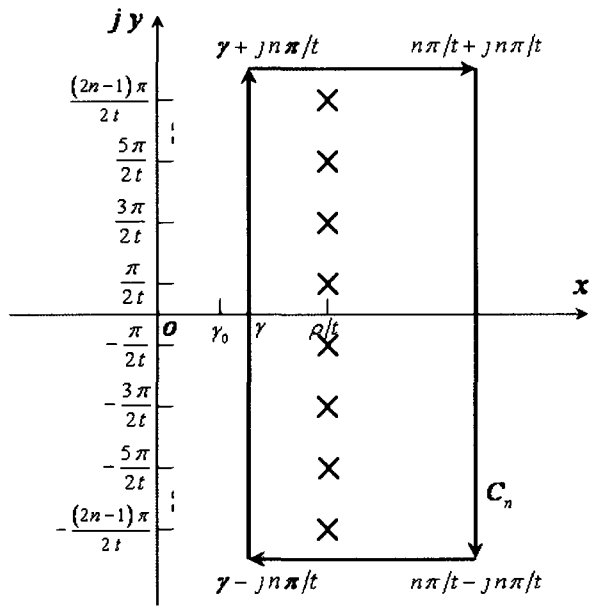

Figure 3.2-1: Bromwich integral path for $f_{ec}(t,\rho)$.

As shown in Figure 3.2-1, $\gamma_0 < \gamma < \frac{\rho}{t}$, a sequence of expanding closed rectangular contours are chosen in such a way that no contour passes through any pole of $E_{ec}(s\,t,\rho)$. When n increases to infinity through the positive integers ($n \to \infty$), the height $\frac{2\,n\,\pi}{t}$ and width $2\left(\frac{n\,\pi}{t} - \gamma\right)$ of the rectangular contour go to infinity through discrete values and the closed contour will enclose all the poles of $E_{ec}(s\,t,\rho)$. The Bromwich integral for $f_{ec}(t,\rho)$ is evaluated as follows.

$$\frac{1}{2\pi j}\int_{\gamma-j\frac{n\,\pi}{t}}^{\gamma+j\frac{n\,\pi}{t}} F(s)E_{ec}(s\,t,\rho)\,ds = \frac{1}{2\pi j}\oint_{C_n} F(s)E_{ec}(s\,t,\rho)\,ds - I_1 - I_2 - I_3 \tag{3.2-4}$$

where

$$I_1 = \frac{1}{2\pi j}\int_{\gamma}^{\frac{n\,\pi}{t}} F\left(x + j\frac{n\,\pi}{t}\right)E_{ec}(x\,t + j\,n\,\pi,\rho)\,dx, \tag{3.2-5}$$

$$I_2 = \frac{1}{2\pi j}\int_{\frac{n\,\pi}{t}}^{\frac{n\,\pi}{t}} F\left(\frac{n\,\pi}{t} + j\,y\right)E_{ec}(n\,\pi + j\,y\,t,\rho)\,dy, \tag{3.2-6}$$

$$I_3 = \frac{1}{2\pi j}\int_{\frac{n\,\pi}{t}}^{\gamma} F\left(x - j\frac{n\,\pi}{t}\right)E_{ec}(x\,t - j\,n\,\pi,\rho)\,dx. \tag{3.2-7}$$

The goal is to argue that the integrals $I_k\,(k = 1, 2, 3)$ vanish as $n \to \infty$. With the above first condition on $F(s)$, such a number ε can be found that

$$\left|F\left(x + j\frac{n\,\pi}{t}\right)\right| \le \varepsilon, \quad \gamma \le x \le \frac{n\,\pi}{t}, \tag{3.2-8}$$

Hence,

$$|I_1| \le \frac{1}{2\pi}\int_{\gamma}^{\frac{n\,\pi}{t}} \left|F\left(x + j\frac{n\,\pi}{t}\right)\right| \left|E_{ec}(x\,t + j\,n\,\pi,\rho)\right| dx \le \frac{\varepsilon\,e^{\rho}}{4\pi}\int_{\gamma}^{\frac{n\,\pi}{t}} \left|\frac{1}{\cosh(\rho - x\,t - j\,n\,\pi)}\right| dx$$

$$= \frac{\varepsilon\,e^{\rho}}{4\pi}\int_{\gamma}^{\frac{n\,\pi}{t}} \frac{1}{\sqrt{\sinh^2(\rho - x\,t) + \cos^2(n\,\pi)}}\,dx = \frac{\varepsilon\,e^{\rho}}{4\pi}\int_{\gamma}^{\frac{n\,\pi}{t}} \frac{1}{\cosh(\rho - x\,t)}\,dx$$

$$= \frac{\varepsilon\, e^{\rho}}{4\pi t}\int_{\gamma t}^{n\pi}\frac{1}{\cosh(\rho-\bar{x})}\,d\bar{x} \quad (\bar{x}=x\,t) \quad = \frac{\varepsilon\, e^{\rho}}{4\pi t}\,2\left[-\arctan\left(e^{\rho-\bar{x}}\right)\right]_{\gamma t}^{n\pi}$$

$$= \frac{\varepsilon\, e^{\rho}}{2\pi t}\left(\arctan\left(e^{\rho-\gamma t}\right)-\arctan\left(e^{\rho-n\pi}\right)\right).$$

With the above second condition on $F(s)$, $n\to\infty$ is making ε arbitrarily small and

$$|I_1| \to \frac{\varepsilon\, e^{\rho}}{2\pi t}\arctan\left(e^{\rho-\gamma t}\right)\to 0. \tag{3.2-9}$$

Then consider I_2,

$$|I_2| \le \frac{1}{2\pi}\int_{-\frac{n\pi}{t}}^{\frac{n\pi}{t}}\left|F\left(\frac{n\pi}{t}+jy\right)\right|\left|E_{ec}\left(n\pi+jyt,\rho\right)\right|dy \le \frac{\varepsilon e^{\rho}}{4\pi}\int_{-\frac{n\pi}{t}}^{\frac{n\pi}{t}}\left|\frac{1}{\cosh\left(\rho-n\pi-jyt\right)}\right|dy$$

$$= \frac{\varepsilon e^{\rho}}{4\pi}\int_{-\frac{n\pi}{t}}^{\frac{n\pi}{t}}\frac{1}{\sqrt{\sinh^2(\rho-n\pi)+\cos^2(yt)}}\,dy \le \frac{\varepsilon e^{\rho}}{4\pi}\int_{-\frac{n\pi}{t}}^{\frac{n\pi}{t}}\frac{1}{\left|\sinh(\rho-n\pi)\right|}\,dy$$

$$= \frac{\varepsilon e^{\rho}}{2\pi t}\frac{n\pi}{\left|\sinh(\rho-n\pi)\right|}\to 0 \quad (n\to\infty). \tag{3.2-10}$$

Similar to I_1,

$$|I_3| \le \frac{1}{2\pi}\int_{\gamma}^{\frac{n\pi}{t}}\left|F\left(x-j\frac{n\pi}{t}\right)\right|\left|E_{ec}\left(xt-jn\pi,\rho\right)\right|dx \le \frac{\varepsilon e^{\rho}}{4\pi}\int_{\gamma}^{\frac{n\pi}{t}}\left|\frac{1}{\cosh\left(\rho-xt+jn\pi\right)}\right|dx$$

$$= \frac{\varepsilon\, e^{\rho}}{2\pi t}\left(\arctan\left(e^{\rho-\gamma t}\right)-\arctan\left(e^{\rho-n\pi}\right)\right)\to 0 \quad (n\to\infty). \tag{3.2-11}$$

From (3.2-9), (3.2-10) and (3.2-11),

$$\lim_{n\to\infty} I_k = 0 \quad (k=1,2,3). \tag{3.2-12}$$

Applying (3.2-12) to (3.2-4) leads to

$$\frac{1}{2\pi j}\int_{\gamma-j\infty}^{\gamma+j\infty}F(s)E_{ec}(st,\rho)\,ds = \frac{1}{2\pi j}\oint_{C_n}F(s)E_{ec}(st,\rho)\,ds. \tag{3.2-13}$$

So the Bromwich integral for $f_{ec}(t,\rho)$ is transferred to the integral around the poles of $E_{ec}(st,\rho)$ with the above three conditions on $F(s)$. From the residue theorem,

$$\frac{1}{2\pi j}\int_{\gamma-j\infty}^{\gamma+j\infty} F(s)E_{ec}(st,\rho)\,ds = -\sum_{residues} F(s)E_{ec}(st,\rho) \text{ at all poles of } E_{ec}(st,\rho) \tag{3.2-14}$$

Substituting (3.1-12) into (3.2-14) results in

$$f_{ec}(t,\rho) = \sum_{n=-\infty}^{\infty} \lim_{s\to(\rho+j(n-0.5)\pi)/t}\left[F(s)\,E_{ec}(st,\rho)\right]$$

$$= \frac{e^{\rho}}{2t}\sum_{n=-\infty}^{\infty}(-1)^{n+1}\,j\,F\left(\frac{\rho+j(n-0.5)\pi}{t}\right). \tag{3.2-15}$$

Using the above fourth condition on $F(s)$, it can be obtained from (3.2-15) that

$$f_{ec}(t,\rho) = \frac{e^{\rho}}{t}\sum_{n=1}^{\infty} F_n \tag{3.2-16}$$

where

$$F_n = (-1)^n \,\mathrm{Im}\,F\left(\frac{\rho+j(n-0.5)\pi}{t}\right). \tag{3.2-17}$$

Theoretically, $f_{ec}(t,\rho)$ can be evaluated from (3.2-16), which gives a good approximation to $f(t)$ when $\rho >> 1$, based on (3.2-2).

3.3 Practical Computation of Inversion of Laplace Transform

In practice, the infinite series in (3.2-16) has to be truncated after a proper number of terms. Since the infinite series is a slowly convergent alternating series, truncating it to a small number of terms leads to a significant error and thus is not practical. An effective approach using the Euler transformation has been developed, which works under the following conditions [63]:

a) There exists an integer $k \geq 1$ such that the signs of F_n given by (3.2-17) alternate for $n \geq k$.

b) For $n \geq k$, $\frac{1}{2} < |F_{n+1}/F_n| \leq 1$.

With the conditions a) and b), (3.2-16) can be truncated with $f_{ec}^{lm}(t,\rho)$, which has $N = l+m$ terms and is given by

$$f_{ec}^{lm}(t,\rho)=\left(e^{\rho}/t\right)\left(\sum_{n=1}^{l-1}F_n+2^{-m-1}\sum_{n=0}^{m}A_{mn}F_{l+n}\right), \tag{3.3-1}$$

where A_{mn} are defined recursively by

$$A_{mm}=1, \qquad A_{mn-1}=A_{mn}+\binom{m+1}{n}. \tag{3.3-2}$$

3.4 ERROR ESTIMATION

In this method, there are three kinds of errors: truncation errors, approximation errors and round-off errors. The truncation errors increase with t and decrease with $N=l+m$. For a typical value of t, the calculation is repeated by increasing N to determine a proper number of terms in (3.2-16), which makes the truncation errors small enough. The upper bound of the truncation errors is given by

$$R^{lm}=\left|f_{ec}^{l+1,m}(t,\rho)-f_{ec}^{l,m}(t,\rho)\right|. \tag{3.4-1}$$

For the approximation errors, according to (14), the upper bound is given by

$$\left|f_{ec}(t,\rho)-f(t)\right|\approx M\,e^{-2\rho}, \tag{3.4-2}$$

if

$$\left|f(t)\right|\le M \qquad \text{for all} \quad t>0.$$

The round-off errors depend on the significant digits used, the complexity of the image function $F(s)$, the number of terms in the summation, the order of operations, and so on. Usually, the round-off errors are so small that they can be neglected if a computer with significant digits of no less than nine is used.

3.5 CONCLUDING REMARKS

In this chapter, the theory on numerical inversion of Laplace transform is discussed, and the scheme is put on a firmer mathematical basis. The conditions under which the scheme is developed

and can be applied in practice are clarified. In next chapter, this scheme is extended and applied to modeling pulses reflected from a conductive half space, and is combined with Prony's method to characterize pulses propagating through a lossy dielectric slab.

CHAPTER 4: PULSE REFLECTION FROM A CONDUCTIVE HALF SPACE AND PROPAGATION THROUGH A LOSSY DIELECTRIC SLAB

The waveform analysis for pulses propagating through and interacting with different media is a topic of importance in many technological fields. In this chapter, an efficient time domain technique is developed on the basis of the numerical inversion of the Laplace transform discussed in last chapter and Prony's method for the analyses of electromagnetic pulses reflected from a conductive interface and propagating through a lossy dielectric slab. First, using the numerical inversion of the Laplace transform but without using Prony's method, the reflection excited by exponentially decaying incident pulses impinging on a conducting half space is analyzed for both horizontal and vertical polarizations. Then the technique is directly applied to the case of the vertical polarization with an incident angle not smaller than the Brewster angle. For arbitrary incident signals, it is clarified that the technique based on the algorithm discussed in Chapter 3 is still usable but needs to be combined with Prony's method. Following this clarification, the details on Prony's method and some associated practical problems in the combination with Prony's method are discussed. After that, the approach combining the numerical inversion of the Laplace transform with Prony's method is applied to the analyses of arbitrary pulses reflected from a conductive interface. Our numerical results are illustrated and compared with those published in the literature. A good agreement between the two validates the correctness and effectiveness of this approach. Based on the studies of pulses reflected from a conducting half space, characterization of arbitrary pulses propagating through a lossy dielectric slab is pursued. Comparison between the results obtained with this technique and previously published results and those obtained using the FDTD technique indicates a good agreement. Moreover, the concern on whether the treatment of permittivity and conductivity in this chapter accords with the Kramers–Kronig relations is properly addressed. Finally, this approach is summarized and the significance of this work is discussed. In Appendix A, a mathematical proof is presented, showing that the numerical inversion of the Laplace transform is applicable to the

characterization of the reflected pulse due to an incident pulse that is a linear combination of exponentially decaying signals and is impinging upon a conductive interface at any incident angle for both polarizations.

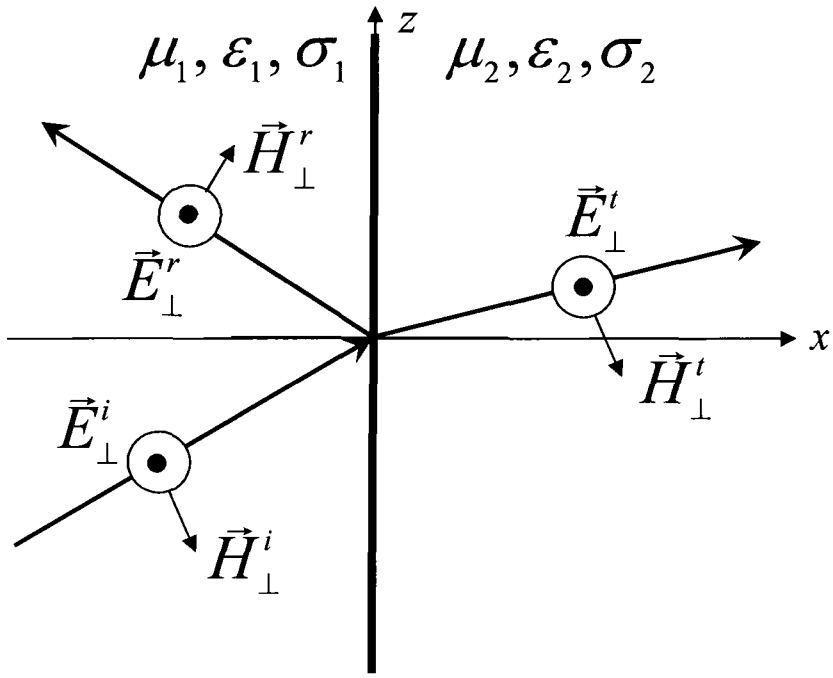

Figure 4.1-1: Horizontal, transverse electric (TE) or perpendicular polarization.

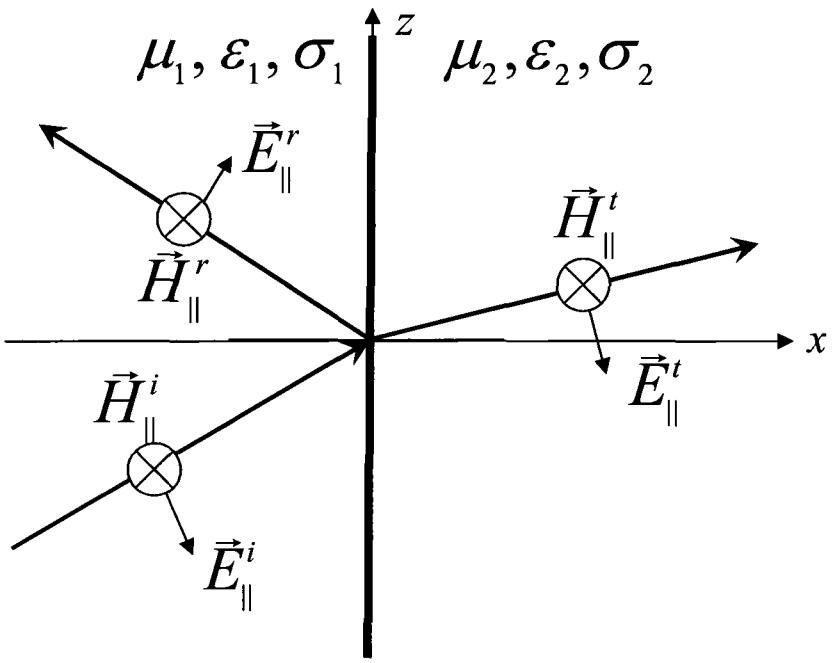

Figure 4.1-2: Vertical, transverse magnetic (TM) or parallel polarization.

4.1 REFLECTION OF EXPOENTIALLY DECAYING PULSES FROM A CONDUCTING HALF SPACE

For the convenient discussions in this chapter and in next chapter, the horizontal and vertical polarizations, the transverse electric (TE) and transverse magnetic (TM) polarizations, and the perpendicular and parallel polarizations are defined firstly. The horizontal polarization is called when the electric field is parallel to the interface between two media, which is identical to the transverse electric (TE) polarization since the electric field is transverse to the normal of the interface or to the wave propagation direction, and is also identical to the perpendicular polarization since the electric field is perpendicular to the plane of incidence (xz plane), as shown in Figure 4.1-1. The vertical polarization is called when a component of the electric field is perpendicular to the interface, which is identical to the transverse magnetic (TM) polarization since the magnetic field is transverse to the normal of the interface or to the wave propagation direction, and is also identical to the parallel polarization since the electric field is parallel to the plane of incidence, as shown in Figure 4.1-2.

The plane pulsive wave is incident from free space onto an interface between free space and a lossy material with the conductivity σ and the relative dielectric constant ε_r. The reflection coefficients in complex frequency domain for vertical and horizontal polarizations are given by (2.1-2) and (2.1-3), respectively. In order to compare our results with those in [10], the same parameters for the conducting half space, $\varepsilon_r = 10$, $\sigma = 10$ mS/m, and the same incident angle $\theta = 45^0$ are chosen, and the same Bell Laboratory waveform incident field is used as in [10]. Such an incident field is plotted by the dotted line in Figure 4.1-3, and is given by

$$E^{inc}(t) = A_0\left(e^{-\alpha t} - e^{-\beta t}\right) \tag{4.1-1}$$

with $A_0 = 52.5$ (kV/m), $\alpha = 4\times10^6$ (1/s), and $\beta = 4.76\times10^8$ (1/s). This double decaying exponential incident pulse has the spectral representation

$$E^{inc}(s) = A_0\left(\frac{1}{s+\alpha} - \frac{1}{s+\beta}\right). \tag{4.1-2}$$

The image functions $F_v(\theta,s)=R_v(\theta,s)E^{inc}(s)$ and $F_h(\theta,s)=R_h(\theta,s)E^{inc}(s)$ not only clearly satisfy the four conditions under which equation (3.2-16) holds, but also obey the two conditions in section 3.3 under which $f_{ec}^{lm}(t,\rho)$ can be used to approximate $f_{ec}(t,\rho)$, for which a proof is given in Appendix A. The following results are obtained with $\rho=6$ and $N=20$ ($l=14$, $m=6$).

For problems involving a lossy soil, typical values of σ range from 1 to 30 mS/m, although conductivities as high as 100 mS/m are sometimes encountered in the literature, while typical values of ε_r range from 10 to 30 [10].

The reflected field is calculated when $\theta=45^0$, σ = 10 mS/m and ε_r = 10, 20, 30, and is plotted in Figure 4.1-3 and Figure 4.1-4, for vertical and horizontal polarizations, respectively. Both figures show that, change of ε_r values only results in a little change of the waveforms of the reflected field pulse. The reflected field when $\theta=45^0$, ε_r = 10 and σ = 1, 10, 30 mS/m is also calculated, and is plotted in Figure 4.1-5 and Figure 4.1-6, for vertical and horizontal polarizations, respectively. From these two figures, it is seen that, as σ becomes larger, the amplitude of the reflected field significantly increases in early time, and slightly decreases in late time. This agrees with the fact that, with the increase of the conductivity of a medium, the reflected field from this medium increases more significantly at high frequencies than at low frequencies, while the early and late time responses are associated with the high and low frequency components of the reflected field, respectively.

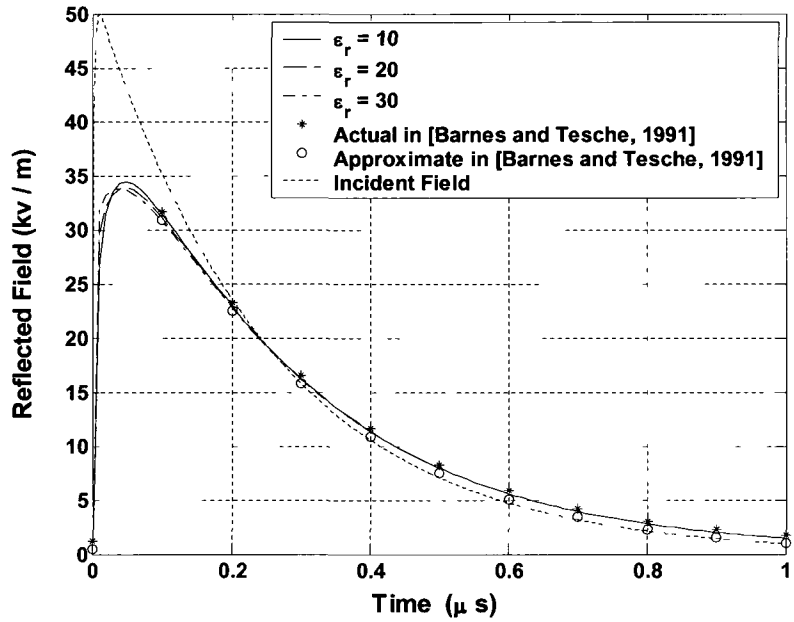

Figure 4.1-3: Reflected field for vertical polarization ($\theta = 45^0$, $\sigma = 10$ mS/m and $\varepsilon_r = 10, 20, 30$).

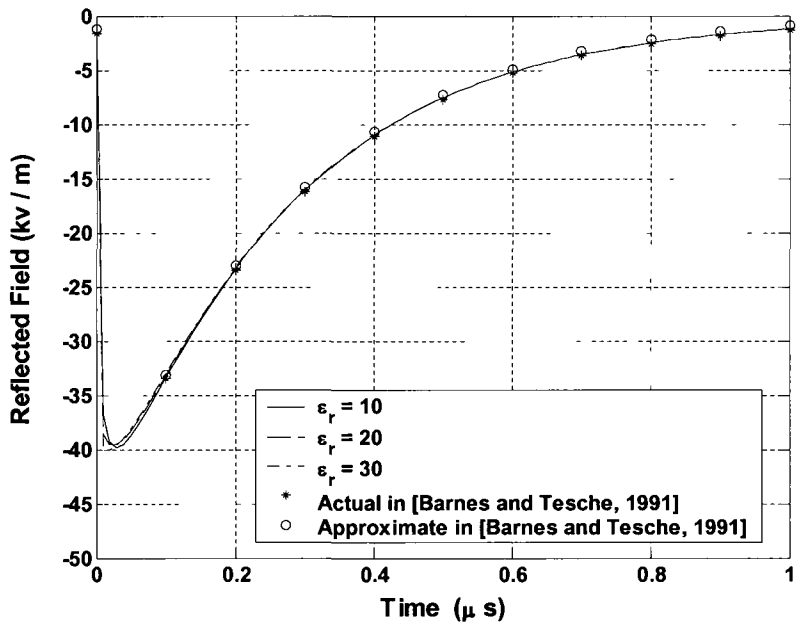

Figure 4.1-4: Reflected field for horizontal polarization ($\theta = 45^0$, $\sigma = 10$ mS/m and $\varepsilon_r = 10, 20, 30$).

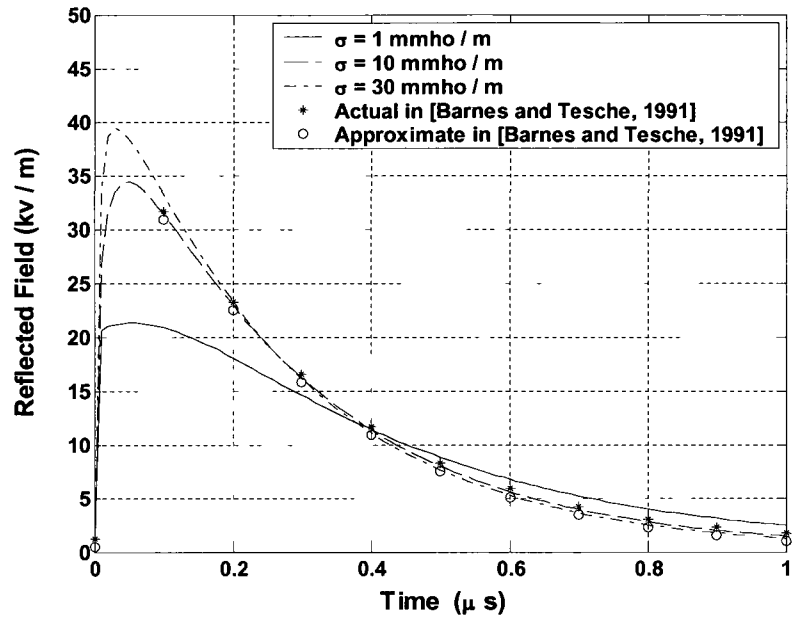

Figure 4.1-5: Reflected field for vertical polarization ($\theta = 45^0$, $\varepsilon_r = 10$ and $\sigma = 1$, 10, 30 mS/m).

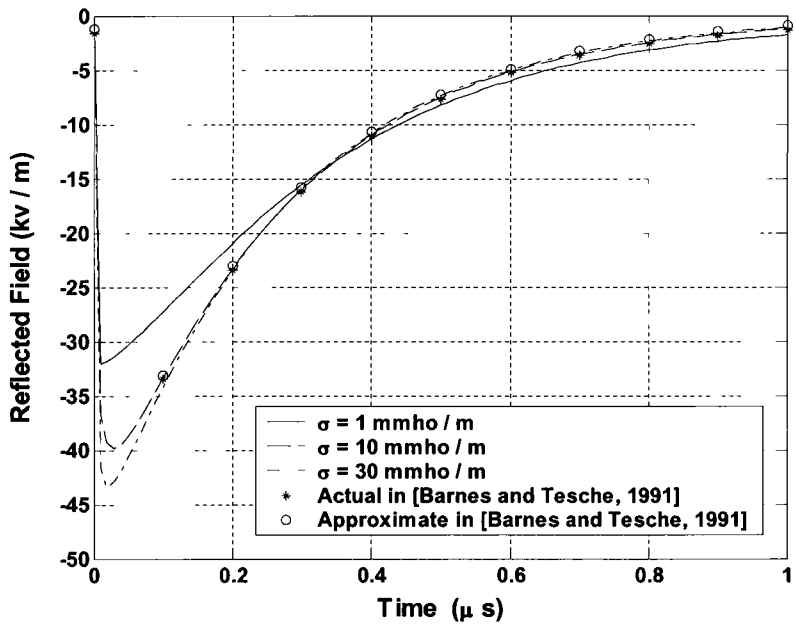

Figure 4.1-6: Reflected field for horizontal polarization ($\theta = 45^0$, $\varepsilon_r = 10$ and $\sigma = 1$, 10, 30 mS/m).

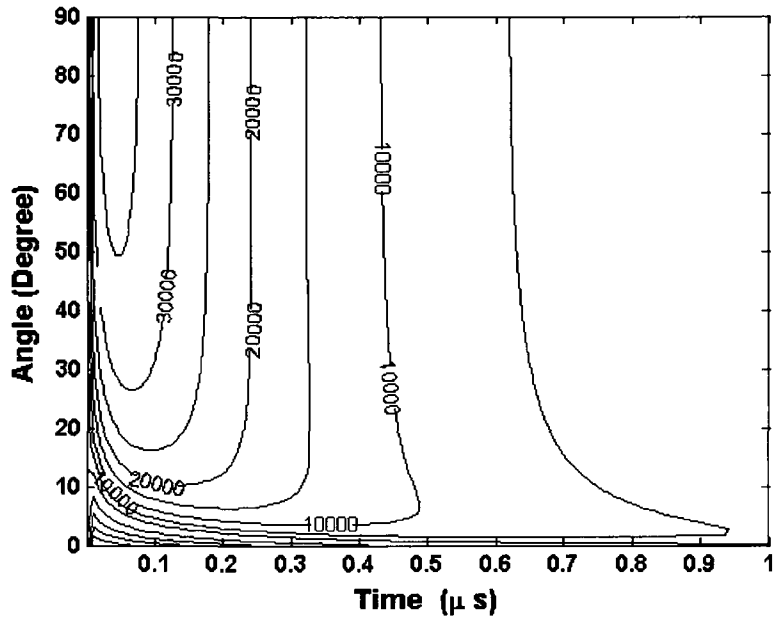

(a)

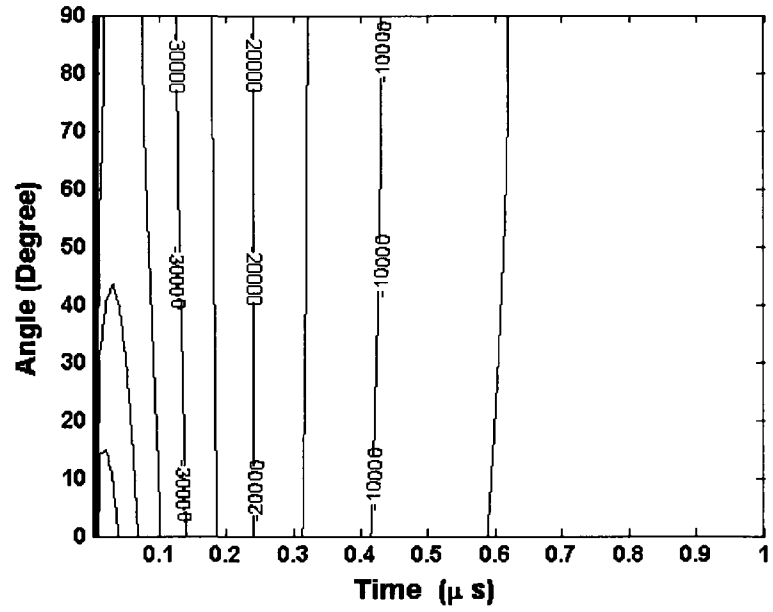

(b)

Figure 4.1-7: Contour plots of reflected fields for (a) vertical polarization and (b) horizontal polarization.

The reflected field values for $\theta = 45^0$, $\varepsilon_r = 10$ and $\sigma = 10$ mS/m in Figures 4.1-3, 4.1-4, 4.1-5 and 4.1-6 are closer to the actual values given in Figure 5 of [10] than the approximate values also given in Figure 5 of [10]. To show this clearly, the actual and approximate values in Figure 5 of [10] are indicated by stars and circles from Figure 4.1-3 to Figure 4.1-6, respectively. In order to check overall behavior of our approximation to reflected field, a series of calculations are carried out for a number of different incident angles and the results are given as contour plots in Figure 4.1-7 (a) and (b), for vertical and polarizations, respectively. Comparing Figure 4.1-7 (a) with Figure 6 (a) (b) in [10] and Figure 4.1-7 (b) with Figure 7 (a) (b) in [10] confirms that our results are closer to the actual values than the approximate values in [10], particularly for small incident angles and late time in the case of vertical polarization.

It is worthwhile to mention that the results obtained with $\rho = 3$ and $N = 15$ ($l = 9$, $m = 6$) and with $\rho = 6$ and $N = 25$ ($l = 14$, $m = 11$) are almost the same as the above results, indicating the truncation errors are very small [69].

For comparing our results with those in [68], the same parameters for the conducting half space, $\varepsilon_r = 10$, $\sigma = 10$ mS/m, and the same incident angles of $\theta = 72.45^0$ and $\theta = 85^0$ are chosen, and the above incident pulse is used as in [68]. Both incident and reflected fields are plotted in Figure 4.1-8, which shows a good agreement between our results and the published ones, and validates the correctness and effectiveness of this approach.

To obtain the general variation trend of the reflected pulse for both polarizations with the incident angle, the reflected pulses is calculated for any incident angle with $\sigma = 10$ mS/m, $\varepsilon_r = 10$, and is plotted for horizontal polarization in Figure 4.1-9 and for vertical polarization in Figure 4.1-10, respectively. The two figures indicate the following important points. (1) For horizontal polarization, the reflected pulse always has negative values for all incident angles, considering that the reflection coefficient R_h is negative for all incident angles. (2) For vertical polarization, the reflected pulse has positive values for the incident angles that are smaller than some angle denoted

by θ_B here. On the other hand, the reflected pulse may become negative in some early time for an incident angle larger than θ_B, and then become positive (it certainly tends to zero eventually).

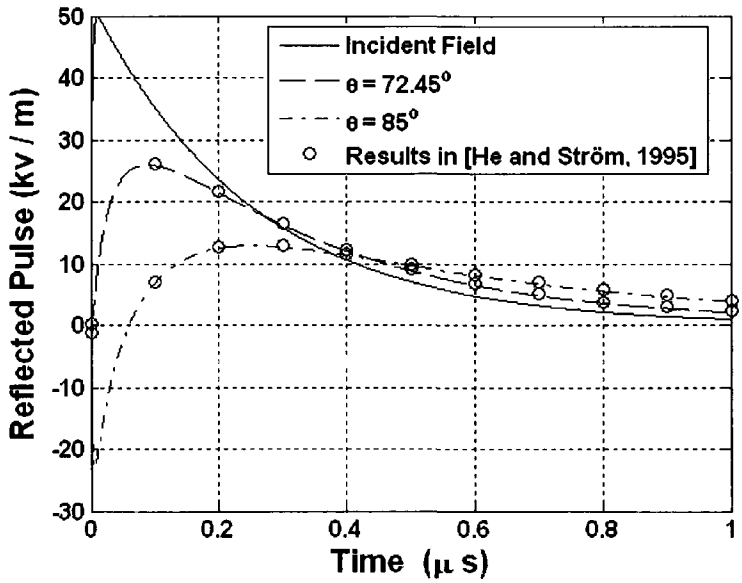

Figure 4.1-8: Reflected pulse for vertical polarization, σ = 10 mS/m, ε_r = 10, $\theta = 72.45^0$ and $\theta = 85^0$.

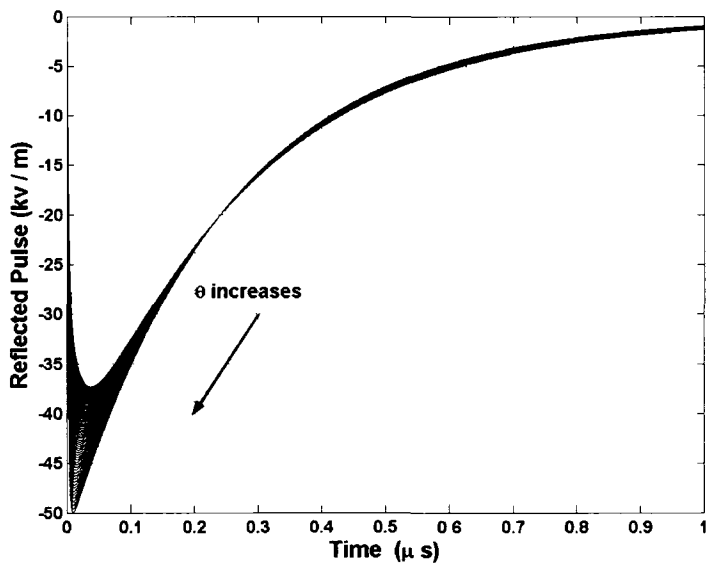

Figure 4.1-9: Variation trend of reflected pulse for horizontal polarization with incident angle θ, $\sigma = 10$ mS/m and $\varepsilon_r = 10$.

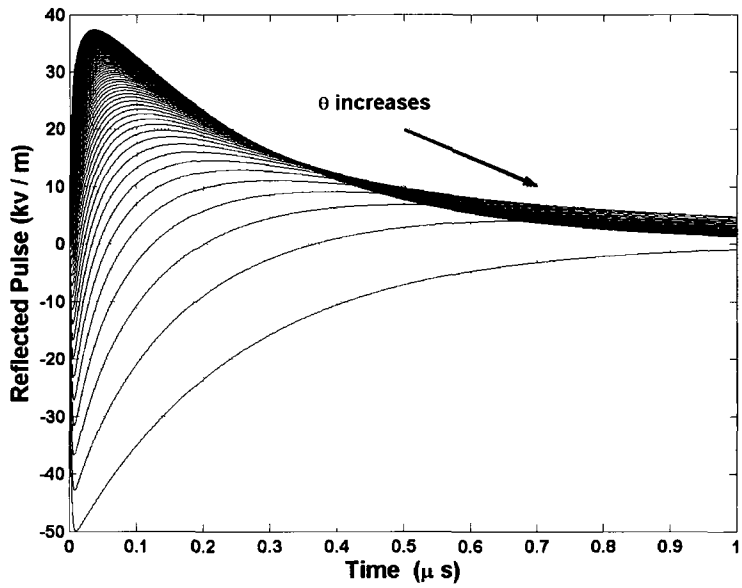

Figure 4.1-10: Variation trend of reflected pulse for vertical polarization with incident angle θ, $\sigma = 10$ mS/m and $\varepsilon_r = 10$.

This phenomenon can be attributed to a pseudo Brewster angle [12] [70]. From (2.1-3), the reflection coefficient in frequency domain for vertical polarization is given by

$$R_v(\omega) = \frac{\left(\varepsilon_r - j\frac{\sigma}{\omega\varepsilon_0}\right)\cos\theta - \sqrt{\varepsilon_r - j\frac{\sigma}{\omega\varepsilon_0} - \sin^2\theta}}{\left(\varepsilon_r - j\frac{\sigma}{\omega\varepsilon_0}\right)\cos\theta + \sqrt{\varepsilon_r - j\frac{\sigma}{\omega\varepsilon_0} - \sin^2\theta}}. \tag{4.1-3}$$

The Brewster angle is defined by $R_v = 0$, and then can be determined by

$$\cos\theta_B = \frac{1}{\sqrt{\varepsilon_r - j\frac{\sigma}{\omega\varepsilon_0} + 1}}. \tag{4.1-4}$$

Although (4.1-4) only has real solution in the limiting cases $\omega \to \infty$ or $\sigma \to 0$, the reflected pulse is small when $\theta > \theta_B$ if the conduction current is small in comparison with the displacement current,

$$\text{i.e., } \frac{\sigma}{\omega\varepsilon_0} << 1,$$

which shows that the pseudo Brewster angle effect is strongest at high frequencies. In the high frequency limit, the reflection coefficient (4.1-3) and the Brewster angle (4.1-4) reduce to the lossless case, respectively,

$$R_{\nu} = \frac{\varepsilon_r \cos\theta - \sqrt{\varepsilon_r - \sin^2\theta}}{\varepsilon_r \cos\theta + \sqrt{\varepsilon_r - \sin^2\theta}}, \tag{4.1-5}$$

and

$$\cos\theta_B = \frac{1}{\sqrt{\varepsilon_r + 1}}. \tag{4.1-6}$$

The reflection coefficient R_{ν} in (4.1-5) is positive and negative for an incident angle smaller and larger than the Brewster angle respectively, which is $\theta = 72.45^0$ for this material parameter and is determined through (4.1-6). Since the early time response is associated with high frequency components, the early time pulse changes sign when the incident angle passes the Brewster angle. In contrast, since the late time response is associated with low frequency components, which experience little of the pseudo Brewster angle effect, the late time pulse does not change sign when the incident angle passes the Brewster angle. The curve for $\theta = 85^0$ in Figure 4.1-8 clearly illustrates this effect.

4.2 PRONY'S METHOD AND ITS APPLICATION TO DECOMPOSITION OF ARBITRARY SIGNALS

Last section demonstrates the method based on a numerical inversion of the Laplace transform has been applied to the transient analysis of the reflected pulse due to a double exponential pulse incident on a lossy interface for the horizontal and vertical polarizations. This method eliminates the restrictions in [10] on the relative dielectric constant and the incidence angle, leads to good accuracy in both late and early times, and has a simple algorithm, short calculation time, and small required memory size. However, double exponential pulses are only one kind of electromagnetic signals. When the incident pulses are some other kind of signals, e.g., a Gaussian monocycle that has popularly been used as a UWB signal recently, numerical inversion of the Laplace transform may

not be applied directly to the transient analysis of the reflected pulses for the following three reasons. 1) Direct use of numerical inversion of the Laplace transform needs an analytical expression of the Laplace transform (image function) of the incident signal, which is not available for a number of commonly used signals. 2) Even if a signal has an analytical image function, it can be one function defined only in some real domain, while the argument of the image function takes a complex value in the numerical inversion of the Laplace transform. For instance, the analytical image function of a Gaussian monocycle contains the complementary error function $erfc(x)$, which is defined only in the real domain. 3) Even though a signal has an analytical image function defined in some complex domain, it does not mean that direct application of a numerical inversion of the Laplace transform can definitely be carried out. It is required that the final image function, viz., the product of the frequency domain reflection coefficient and the image function of an incident signal, obey some conditions for numerical inversion of the Laplace transform. Although these conditions are often satisfied by the final image function, numerical inversion of the Laplace transform also involves an infinite sum of a slowly convergent alternating series. Simply truncating it and retaining only some terms leads to a relatively large error and thus is not practical. An effective approach using the Euler transformation has to be used, which requires that the final image function meet two additional conditions. Hence, numerical inversion of the Laplace transform can be applied directly to the transient analysis of the reflected pulses, only if the final image function is defined in some complex domain, satisfies some conditions for numerical inversion of the Laplace transform, and two additional conditions for the Euler transformation.

Now an interesting and meaningful question arises: How to overcome the limitations mentioned above and be able to apply numerical inversion of the Laplace transform to the transient analysis of the reflected pulses with an arbitrary incident signal? It has been shown in Section 4.1 that numerical inversion of the Laplace transform can be utilized for the transient analysis of the reflected pulse when an incident signal is a linear combination of two real decaying exponential functions. Thus it

can be imagined that numerical inversion of the Laplace transform would also work when an incident signal is a linear combination of a finite number of complex attenuating exponential functions. An arbitrary realistic signal can be approximated by a series of finite attenuating exponential functions. Prony's method has been widely used for this purpose [9] [71] [72]. Although decomposing a signal into a series of finite attenuating exponential functions will incur numerical errors, some criterion can be set and some measures can be adopted to achieve required accuracy.

A signal can be represented as a superposition of exponential functions, i.e.,

$$E(t)=\sum_{p=1}^{q} C_p e^{-\alpha_p t}, \tag{4.2-1}$$

where the number of exponential functions, q, can be an infinite or a finite number. Only the case where q is finite or can be truncated to a finite number is considered in this work; when α_p is nonnegative, C_p is a real; when α_p is a complex number with a nonnegative real part, C_p is a complex number, and the corresponding conjugate term, $C_p^* e^{-\alpha_p^* t}$, must be included in (4.2-1) in this case. C_p and α_p can be determined directly from one set of sample values of $E(t)$. This technique is known as Prony's method [71]. Rewrite (4.2-1) as

$$E(t)=\sum_{p=1}^{q} C_p \gamma_p{}^t, \tag{4.2-2}$$

where $\gamma_p = e^{-\alpha_p}$. Assume that values of $E(t)$ are specified at equally spaced points over some time range. Then

$$E(t_0 + m_s \Delta)=\sum_{p=1}^{q} C_p \gamma_p{}^{(t_0+m_s\Delta)}, \tag{4.2-3}$$

where $m_s = 0, 1, 2, \cdots, M$, M is the number of sampling points, t_0 is the starting time, and Δ is the time increment.

The difficulty in solving (4.2-3) lies in that it is nonlinear in terms of γ_p. However, this difficulty can be minimized as follows. $E(t)$ satisfies the difference equation

$$E(t_0+q\Delta)-\beta_1 E(t_0+(q-1)\Delta)-\cdots-\beta_q E(t_0)=\sum_{p=1}^{q} C_p \gamma_p{}^{t_0}\left[\left(\gamma_p{}^{\Delta}\right)^q-\beta_1\left(\gamma_p{}^{\Delta}\right)^{q-1}-\cdots-\beta_q\right]. \quad (4.2\text{-}4)$$

Let $\gamma_1{}^{\Delta}$, $\gamma_2{}^{\Delta}$, ..., $\gamma_q{}^{\Delta}$ be the roots of the algebraic equation

$$\gamma^q-\beta_1\gamma^{q-1}-\beta_2\gamma^{q-2}-\cdots-\beta_{q-1}\gamma-\beta_q=0. \quad (4.2\text{-}5)$$

If the β_p $(p=1,2,\cdots,q)$ are known, then (4.2-5) can easily be solved for γ_p. On the other hand, since γ_p^{Δ} is a root of (4.2-5), (4.2-4) reduces to

$$\beta_1 E(t_0+(q-1)\Delta)+\cdots+\beta_q E(t_0)=E(t_0+q\Delta). \quad (4.2\text{-}6)$$

By changing q to $q+1$, $q+2$, ..., $q+m_s$, generalize (4.2-6) to form a set of linear equations of γ_p as

$$\sum_{p=1}^{q}\beta_p E(t_0+(q+m_s-p)\Delta)=E(t_0+(q+m_s)\Delta), \quad (4.2\text{-}7)$$

where $m_s=0,1,2,\cdots,M-q$.

From this set of $M-q+1$ linear equations, q β's can be determined when $M=2q-1$, or can be over-determined by applying a least square error algorithm to the entire equation set when $M\geq 2q$. After β_p is determined, γ_p can be found through (4.2-5). Then (4.2-3) becomes linear in terms of C_p and can be solved in the same manner as solving (4.2-7). Therefore, C_p and α_p are completely determined through Prony's method.

In this work, over-determination of β_p and C_p is adopted, since a large number of numerical trials have shown that over-determining β_p and C_p makes computational accuracy much higher

than determination of β_p and C_p. In [9], the number of exponential functions, $q = 20$, is simply chosen. In this work, q is selected through a series of numerical trials to meet some accuracy requirement, as shown in next section. The list of γ_p is sorted and any duplicates will be removed. Then the β's are determined from this reduced set of linear equations. For a complicated shape of an incident pulse, a large number of exponential functions may be needed to meet some accuracy requirement. Nevertheless, if the complicated waveform has a very short pulse length, which is the case for most UWB pulses, this waveform can still be efficiently expanded into a series of exponentials within some short time interval, i.e., reasonable accuracy can be maintained without significantly increasing the number of exponential functions. This will be also illustrated in next section.

4.3 Reflection of Arbitrary Pulses from a Conducting Half Space

A pulse which is a linear combination of a finite number of exponential functions is expressed by (4.2-1), and is incident from free space onto an interface between free space and a lossy material with conductivity σ and relative dielectric constant ε_r. The reflection coefficients in the frequency domain for the vertical and horizontal polarizations are given by (2.1-2) and (2.1-3), respectively. The image function of $E(t)$ in (4.2-1) is

$$E(s) = \sum_{p=1}^{q} \frac{C_p}{s + \alpha_p}. \tag{4.3-1}$$

The final image functions, $F_v(\theta, s) = R_v(\theta, s)E(s)$ and $F_h(\theta, s) = R_h(\theta, s)E(s)$, obviously satisfy conditions 2) – 4) listed in Section 3.2. A proof is given in Appendix A that, for $s = \left[\rho + j(n - 0.5)\pi\right]/t$, $F_v(\theta, s)$ and $F_h(\theta, s)$ also obey the above two conditions a) and b) described in Section 3.3, under which $f_{ec}^{lm}(t, \rho)$ can be used to approximate $f_{ec}(t, \rho)$.

4.3.1 Gaussian Monocycle as an Incident Signal

In order to compare our results with those in [9], the same Gaussian monocycle pulse as that in [9] is used as the incident pulse, which is called the differentiated Gaussian pulse in [9] and is expressed as

$$E(t)=\frac{t-t_s}{\tau_p}\exp\left(0.5-0.5\left(\frac{t-t_s}{\tau_p}\right)^2\right), \tag{4.3-2}$$

where the amplitude has been normalized to unity, τ_p is the parameter used to control the pulse width and is actually the time from the zero crossing to the peak of the pulse, and t_s is time shift with $t_s = 4\,\tau_p$ in the calculation.

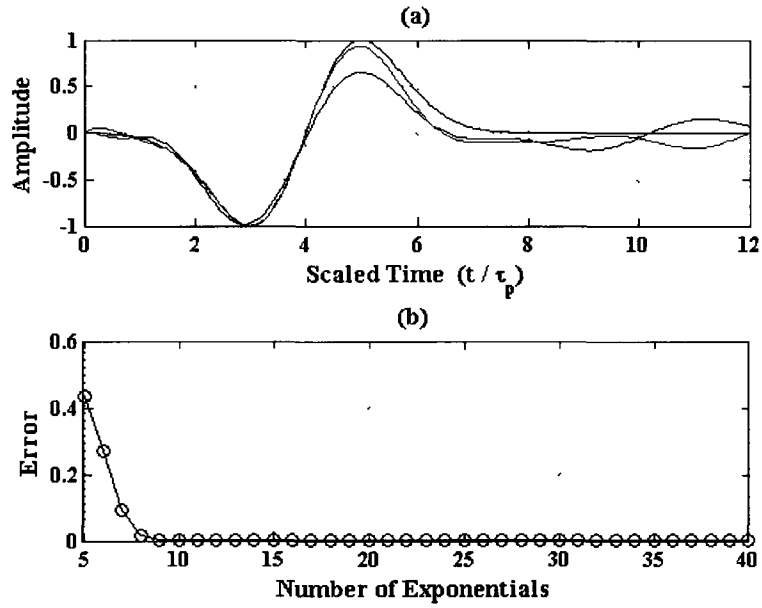

Figure 4.3-1: (a) Incident pulse (black line) and approximating pulses with 5 (blue line) and 6 (red line) exponentials. (b) Error versus number of exponential functions.

First, a series of numerical trials with Prony's method are carried out for selecting a proper number of exponential functions. Figure 4.3-1 (a) plots the incident pulse and two approximations with 5 and 6 exponential functions, respectively, versus the scaled time, t/τ_p. It is seen that different

approximation errors occur at different instants. A reasonable error measure should reflect the cumulative error over the entire time range considered, and can be defined as

$$error = \frac{\sum_{m=0}^{M} \left| E_a(t_0 + m\Delta) - E(t_0 + m\Delta) \right|}{\sum_{m=0}^{M} \left| E(t_0 + m\Delta) \right|} \tag{4.3-3}$$

where $E_a(t)$ is the approximating waveform. Figure 4.3-1 (b) plots the cumulative error versus the number of exponential functions, indicating that the error first rapidly decreases with the number of exponentials and then does not significantly decrease when the number of exponentials is above 10. Thus, at least 10 exponentials should be used for approximating this Gaussian monocycle pulse to obtain good computational accuracy.

Next, the transient analysis of the reflected pulse from a conductive interface is performed with the approximating incident pulse and the numerical inversion of the Laplace transform. For an easy comparison between our results and those in [9], following the expression of the frequency domain reflection coefficients for the horizontal polarization in [9], (2.1-3) is rewritten as

$$R_h(s) = \frac{\cos\theta - \sqrt{\varepsilon_r \left(1 + \frac{p_{2p}}{s\tau_p} \right) - \sin^2\theta}}{\cos\theta + \sqrt{\varepsilon_r \left(1 + \frac{p_{2p}}{s\tau_p} \right) - \sin^2\theta}}, \tag{4.3-4}$$

where p_{2p} is the loss tangent at the peak frequency ω_s of (4.3-2), $p_{2p} = \sigma/\omega_s\varepsilon$, and the peak frequency $\omega_s = 1/\tau_p$. This representation is used for the final generating function. The incident pulse is approximated by a linear combination of 31 exponentials. The reflected field is calculated when $\theta = 45^0$, $\varepsilon_r = 1.0$ and p_{2p} = 0.1, 1.0, 10.0, and is plotted versus the scaled time in Figure 4.3-2 and Figure 4.3-3, for the horizontal and vertical polarizations, respectively. From these two figures, it is seen that, as p_{2p} becomes larger, the peak amplitude of the reflected pulse significantly increases

and the reflected pulse goes through less distortion for both polarizations. Figure 4.3-2 compares our results with the exact ones in [9] and demonstrates good agreement between the two.

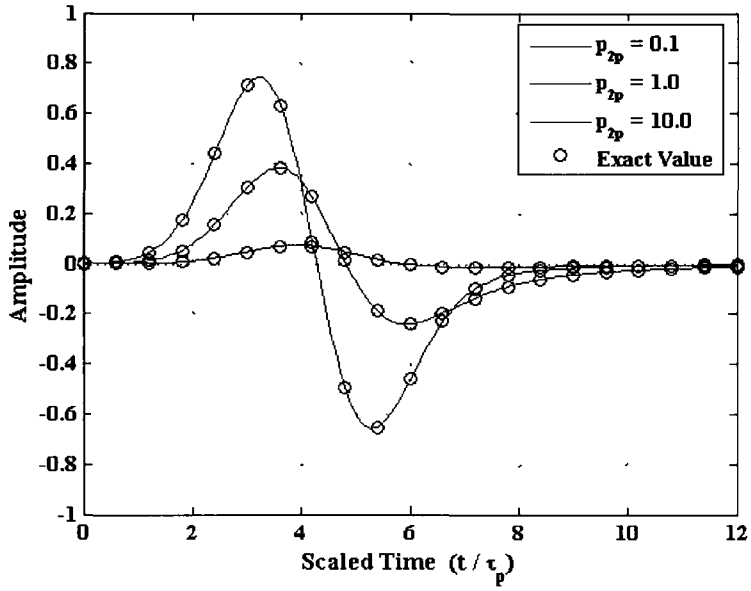

Figure 4.3-2: Reflected field for the horizontal polarization ($\theta = 45^0$, $\varepsilon_r = 1.0$ and p_{2p} = 0.1, 1.0, 10.0).

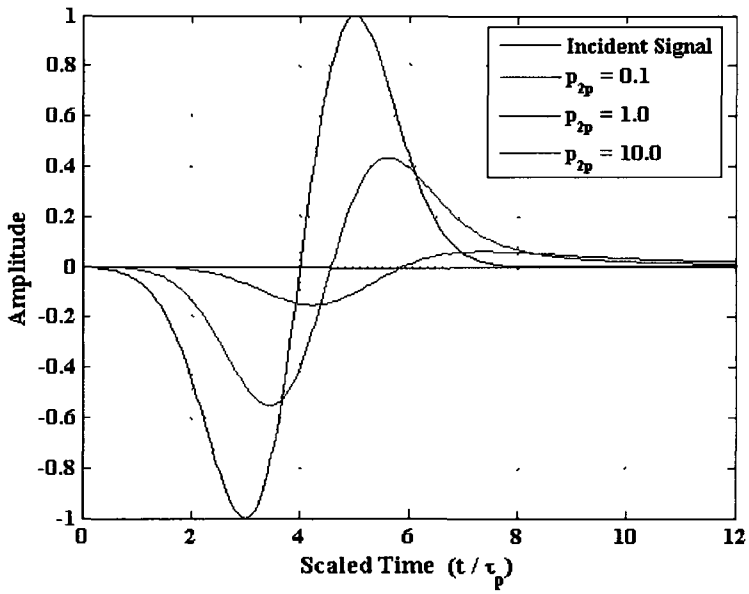

Figure 4.3-3: Reflected field for the vertical polarization ($\theta = 45^0$, $\varepsilon_r = 1.0$ and p_{2p} = 0.1, 1.0, 10.0).

4.3.2 Gaussian Doublet as an Incident Signal

For comparing our result with that in [73], the same Gaussian doublet pulse as that in [73] is used as the incident pulse, which is the second derivative of a Gaussian pulse and is given by

$$E(t)=\left[1-4\pi\left(\frac{t-t_s}{\tau_p}\right)^2\right]\exp\left(-2\pi\left(\frac{t-t_s}{\tau_p}\right)^2\right) \tag{4.3-5}$$

where the waveform parameter τ_p = 1.7262 ns and the time shift t_s = 0.75 ns in the calculation.

Since the waveform of a Gaussian doublet is more complicated than that of a Gaussian monocycle, more exponential functions would be needed to approximate it with good accuracy. However, the Gaussian doublet has a short pulse length and thus can be approximated with good accuracy within a short time range without using significantly more exponential functions. Several numerical trials are carried out for approximating the Gaussian doublet by a series of exponentials within the time interval of 0.3 – 1.2 ns.

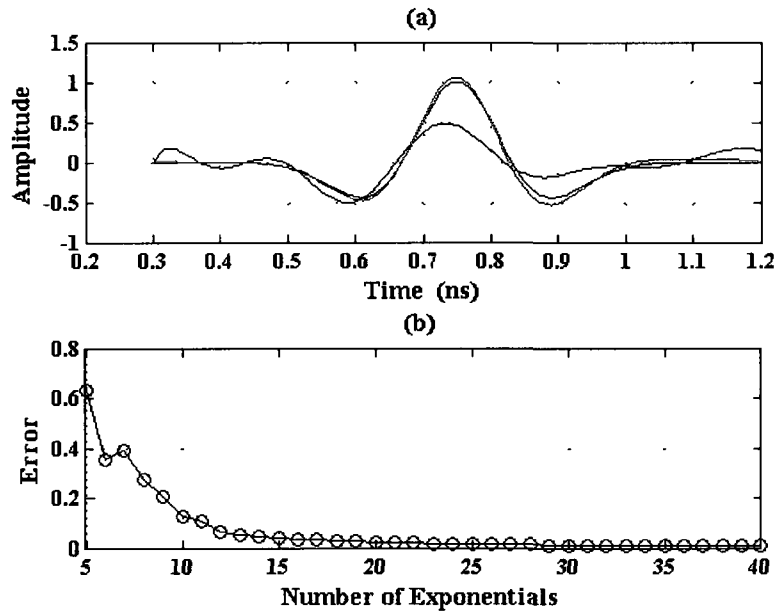

Figure 4.3-4: (a) Incident pulse (black line) and approximating pulses with 5 (blue line) and 10 (red line) exponentials. (b) Error with number of exponential functions.

Figure 4.3-4 (a) plots the incident pulse and two approximating pulses with 5 and 10 exponential functions, respectively, while Figure 4.3-4 (b) plots the cumulative error against the number of exponential functions, showing the error first decreases rapidly with the number of exponentials and then does not significantly decrease if the number of exponentials is above 20. Hence, more than 20 exponential functions should be used for approximating the Gaussian doublet pulse with good accuracy.

Equations (2.1-2) and (2.1-3) are used for the final generating functions. The incident pulse is approximated by a linear combination of 40 exponentials. The reflected field is calculated when $\theta = 45^0$, $\varepsilon_r = 10$, 25, 40 and $\sigma = 0.1$ mho/m, and is plotted in Figure 4.3-5 and Figure 4.3-6 for the horizontal and vertical polarizations, respectively. These two figures illustrate that the reflected pulse has less distortion for both polarizations in this case, and the peak amplitude of the reflected pulse increases with the increase of ε_r. Comparison between the two figures indicates that the reflected pulse has smaller peak amplitudes for the vertical polarization than for the horizontal polarization. Figure 4.3-6 compares our results with those in [73] and shows good agreement. It is worthwhile to point out that the result in [73] is accurate in this case where the incident angle is not large and the relative electric constant is on the order of 10.

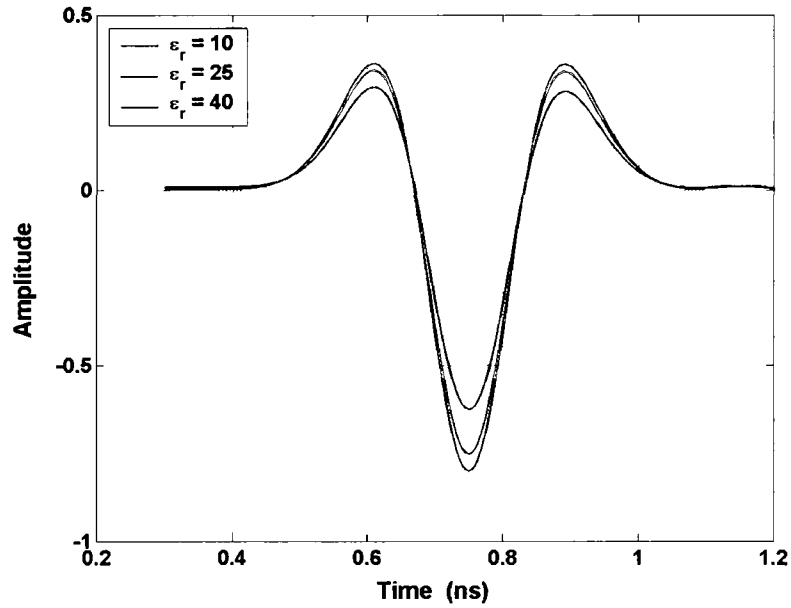

Figure 4.3-5: Reflected field for the horizontal polarization ($\theta = 45^0, \varepsilon_r$ = 10, 25, 40 and $\sigma = 0.1$ mho/m).

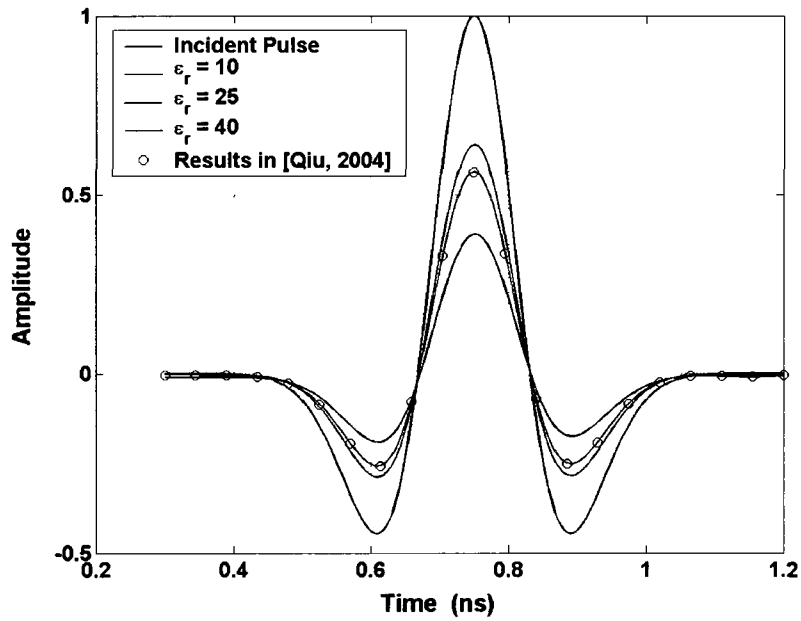

Figure 4.3-6: Reflected field for the vertical polarization ($\theta = 45^0, \varepsilon_r$ = 10, 25, 40 and $\sigma = 0.1$ mho/m).

4.4 PROPAGATION OF ARBITRARY PULSES THROUGH A LOSSY DIELECTRIC SLAB

The transient analysis of pulses propagating through a lossy dielectric slab is of great significance in a number of engineering fields, such as material characterization and diagnosis, wall penetration radar, and pulse radio. In fact, this kind of analysis can provide valuable insights into the appreciation of the capabilities and limitations of UWB communication for indoor and indoor-outdoor scenarios [74]. As discussed in Section 2.1, the approximation to a frequency-domain reflection coefficient permits one analytical expression of the impulse response of a lossy half space [10], but makes the solutions inaccurate or even invalid in some cases, e.g., for large incident angles. Based on the approximate form in [10], the time domain solutions for pulse transmission through a lossy dielectric slab were achieved and some related UWB issues were addressed [73] [75]. These solutions contain infinite sums of modified Bessel functions and time domain convolutions, and are implemented in three directions, perpendicular polarization, normal and tangential parallel polarizations [75] (wrongly written as "normal and tangential perpendicular polarizations" in [75]), leading to considerable calculations.

In this section, based on the discussion in the three sections above, the technique combining numerical inversion of Laplace transform with Prony's method is extended to the transient analysis of pulses propagating through a lossy dielectric slab. Comparison between our results obtained and those obtained using the FDTD technique indicates a good agreement. The waveforms and strengths of the transmitted signals are governed by four main parameters, thickness, relative permittivity and conductivity of the slab and incident angles. The analysis of transmitted signal waveforms is conducted for four different parameters and the results are shown to be comparable to those given by [75]. Based on this waveform analysis, the transmission loss is discussed for different parameters and the results are shown to be consistent with the previously published results [75]. Our approach also yields the results for a large incident angle, these being unavailable using alternative approaches [75]. In this investigation, the Gaussian doublet pulse with the same waveform parameter and time

shift as in Section 4.3 is used as the incident pulse. Figure 4.4-1 plots the incident pulse and the approximating pulse with 40 exponential functions, showing a good approximation.

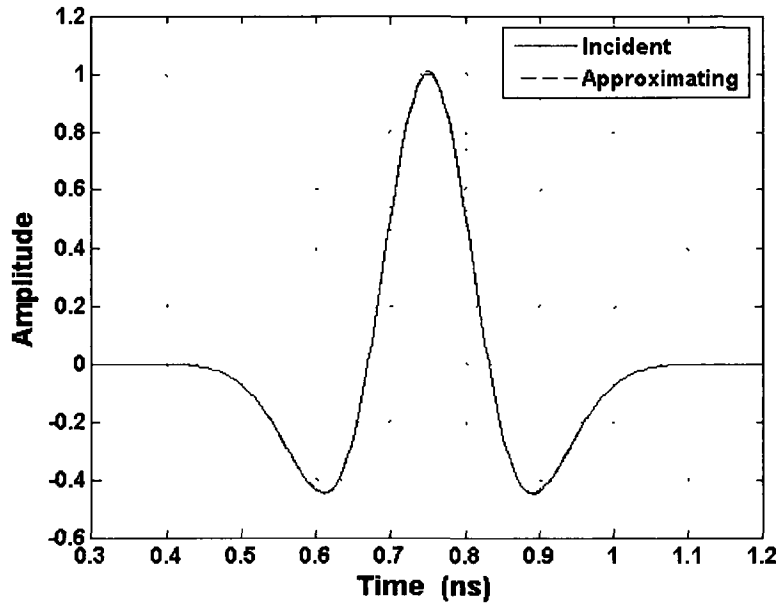

Figure 4.4-1: Incident pulse and approximating pulse with 40 exponentials.

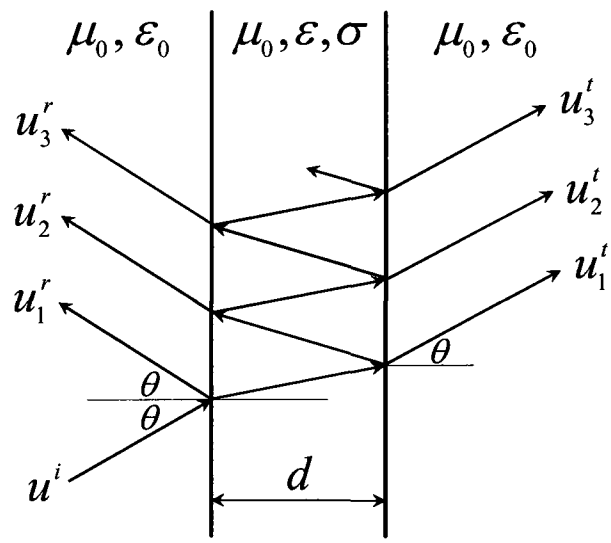

Figure 4.4-2: Pulse is impinging on lossy dielectric slab.

Figure 4.4-2 shows that the pulse is impinging on a homogeneous lossy slab at an incident angle of θ. The slab has an thickness of d, permeability of μ_0, conductivity σ and permittivity of $\varepsilon = \varepsilon_0 \varepsilon_r$ where ε_0 is the permittivity of vacuum and ε_r is the relative permittivity of the slab. The transmission through a dielectric layer is governed by the equation [76]

$$T = \frac{t_{0n}\, t_{n0}\, e^{-j\varphi}}{1 - r_{0n}\, r_{n0}\, e^{-j2\varphi}} \tag{4.4-1}$$

where r and t denote the reflection and transmission coefficients of the interface, respectively. The subscripts $0n$ and $n0$ mean that the pulse is incident from air onto the layer and from the layer onto air. The quantity φ is the complex frequency dependent electrical length of the layer as seen by the wave and is given by

$$\varphi(s) = \frac{s}{j}\frac{d}{c}\sqrt{\varepsilon_r - \sin^2\theta + \frac{\sigma}{s\varepsilon_0}} \tag{4.4-2}$$

where s is the complex frequency and c is the phase velocity of the wave in vacuum.

With $t_{0n}\, t_{n0} - r_{0n}\, r_{n0} = 1$ and $r_{0n} = -r_{n0}$ [76], (4.4-1) is written as

$$T(s) = \frac{\left(1 - r_{0n}^{\ 2}(s)\right)e^{-j\varphi(s)}}{1 - r_{0n}^{\ 2}(s)\, e^{-j2\varphi(s)}} \tag{4.4-3}$$

where $r_{0n}(s)$ is the reflection coefficient in complex frequency domain and is given by (2.1-2) for vertical polarization, or by (2.1-3) for horizontal polarization.

The image function of the approximating pulse is

$$E^{inc}(s) = \sum_{p=1}^{q} \frac{C_p}{s + \alpha_p}. \tag{4.4-4}$$

The final image functions is

$$F(s) = T(s) E^{inc}(s). \tag{4.4-5}$$

It satisfies the four conditions specified in Section 3.2 under which $f(t)$ can be approximated by $f_{ec}(t,\rho)$. For $s=[\rho+j(n-0.5)\pi]/t$, $F(s)$ does not obey the two conditions in Section 3.3 under which $f_{ec}^{lm}(t,\rho)$ can be used to approximate $f_{ec}(t,\rho)$.

The total transmitted field can be decomposed into a series of successive transmitted components,

$$T=u_1^t+u_2^t+u_3^t+\cdots=t_{0n}t_{n0}e^{-j\varphi}\left[1+r_{n0}{}^2e^{-j2\varphi}+\left(r_{n0}{}^2e^{-j2\varphi}\right)^2+\cdots\right]. \tag{4.4-6}$$

Consider the first term modeling two transmissions through two surfaces of the layer,

$$u_1^t=t_{0n}t_{n0}e^{-j\varphi}=\left(1-r_{0n}{}^2\right)e^{-j\varphi}. \tag{4.4-7}$$

$F_1(s)=u_1^t(s)E^{inc}(s)$ still does not satisfy the two conditions for Euler summation due to the phase factor $e^{-j\varphi}$ when $s=[\rho+j(n-0.5)\pi]/t$.

From (4.4-2), it is observed that, when $s\to\infty$,

$$\varphi(s)\to\varphi_m(s)=\frac{s}{j}\frac{d}{c}\sqrt{\varepsilon_r-\sin^2\theta}. \tag{4.4-8}$$

The replacement image function for $F_1(s)$ is defined as

$$F_{r1}(s)=u_1^t(s)E^{inc}(s)e^{j\phi_m(s)}=F_1(s)e^{s\tau} \tag{4.4-9}$$

and satisfies the four conditions listed in Section 3.2 and the two conditions specified in Section 3.3, where $e^{j\varphi_m(s)}$ is the modifying phase factor and the time shift is

$$\tau=\frac{d}{c}\sqrt{\varepsilon_r-\sin^2\theta}. \tag{4.4-10}$$

Hence, (3.3-1) is applicable to calculate $f_{r1,ec}^{lm}(t,\rho)$ which approximates $f_{r1,ec}(t,\rho)$, the original function of $F_{r1}(s)$. From (4.4-9), the relationship between $f_{r1,ec}^{lm}(t,\rho)$ and $f_{1,ec}^{lm}(t,\rho)$ which approximates $f_{1,ec}(t,\rho)$, the original function of $F_1(s)$, is given by

$$f_{1,ec}^{lm}(t,\rho) = f_{r1,ec}^{lm}(t-\tau,\rho). \tag{4.4-11}$$

Similarly, consider the second term in (4.4-6), which characterizes two transmissions through two surfaces and two reflections between two surfaces,

$$u_2^t = t_{0n}\, t_{n0}\, r_{n0}^2\, e^{-j3\varphi} = \left(1 - r_{0n}{}^2\right) r_{n0}^2\, e^{-j3\varphi}. \tag{4.4-12}$$

$F_2(s) = u_2^t(s)\, E^{inc}(s)$ does not satisfy the second of the two conditions above due to the phase factor $e^{-j3\varphi}$ when $s = [\rho + j(n-0.5)\pi]/t$. The replacement image function for $F_2(s)$ is

$$F_{r2}(s) = u_2^t(s)\, E^{inc}(s)\, e^{j3\phi_m(s)} = F_2(s)\, e^{3s\tau} \tag{4.4-13}$$

and meets the four conditions listed in Section 3.2 and the two conditions for Euler summation. $f_{r2,ec}^{lm}(t,\rho)$ can be calculated by using (3.3-1), and is a good approximation to $f_{r2,ec}(t,\rho)$, the original function of $F_{r2}(s)$. From (4.4-13), the relationship between $f_{r2,ec}^{lm}(t,\rho)$ and $f_{2,ec}^{lm}(t,\rho)$ which approximates $f_{2,ec}(t,\rho)$, the original function of $F_2(s)$, is given by

$$f_{2,ec}^{lm}(t,\rho) = f_{r2,ec}^{lm}(t-3\tau,\rho). \tag{4.4-14}$$

Following the above procedure, $f_{i,ec}^{lm}(t,\rho)$ can be achieved and is a good approximation to $f_{i,ec}(t,\rho)$, the original functions of $F_i(s) = u_i^t(s) E^{inc}(s)$, $i = 1, 2, 3, \cdots$.

From

$$F = F_1 + F_2 + F_3 + \cdots, \tag{4.4-15}$$

the final original function can be given approximately by

$$\begin{aligned} f(t) &\approx f_{ec}(t,\rho) = f_{1,ec}(t,\rho) + f_{2,ec}(t,\rho) + f_{3,ec}(t,\rho) + \cdots \\ &\approx f_{1,ec}^{lm}(t,\rho) + f_{2,ec}^{lm}(t,\rho) + f_{3,ec}^{lm}(t,\rho) + \cdots \end{aligned} \tag{4.4-16}$$

In general, the terms beyond the first term have much weaker impacts than the first one in (4.4-16), and then only taking the first term $f_{r1,ec}^{lm}(t,\rho)$ leads to a high accuracy. If a very high accuracy is required for some specific purposes, the first several terms in (4.4-16) will be added together. In

the following discussion, only the first term in (4.4-16) is taken into account. Figure 4.4-3 plots the waveform of the transmitted pulse at the layer's back surface, and shows that our results agree quite well with FDTD results. In our calculation, only the first term in (4.4-16) is taken as the transmission coefficient.

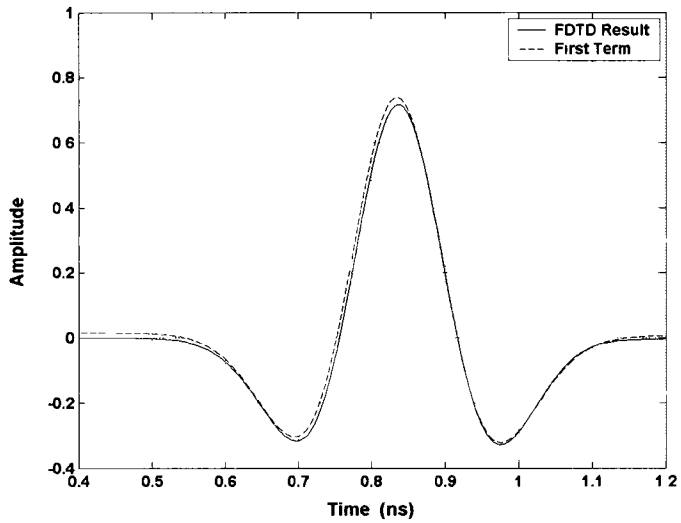

(a)

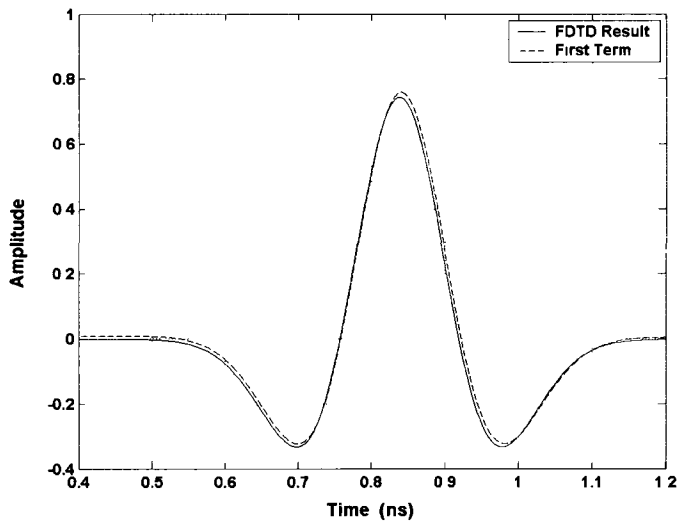

(b)

Figure 4.4-3: Waveforms of transmitted signal obtained using this method and using FDTD. (a) horizontal polarization; (b) vertical polarization. $d = 0.02$ m, $\varepsilon_r = 2$, $\sigma = 0.1$ S/m and $\theta = 30^0$.

Figures 4.4-4 to 4.4-7 illustrate the waveforms of the transmitted signal through a slab with different thickness, relative permittivity, conductivity and incident angles. With reference to the incident pulse shown in Figure 4.4-1, the attenuation, delay and distortion of the transmitted pulse can be seen and compared with each other in the different cases.

Figure 4.4-4 shows that the amplitude of the transmitted signal decreases, the delay increases and the distortion becomes larger with the increase of the thickness. In Figure 4.4-5, the amplitude becomes a little smaller, the distortion becomes a little larger and it takes longer for the pulse to go through the layer as the relative permittivity increases. Figure 4.4-6 illustrates that the amplitude decreases, the distortion increases but the delay almost remain the same when the conductivity increases.

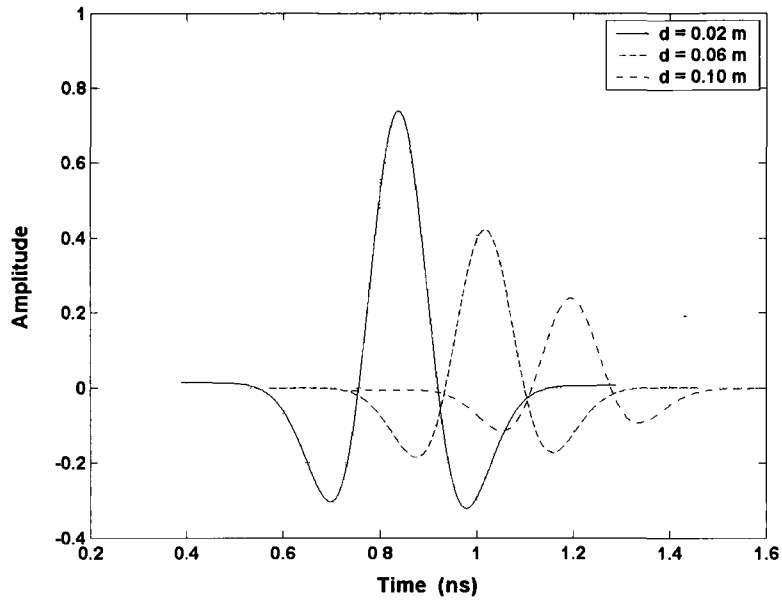

(a)

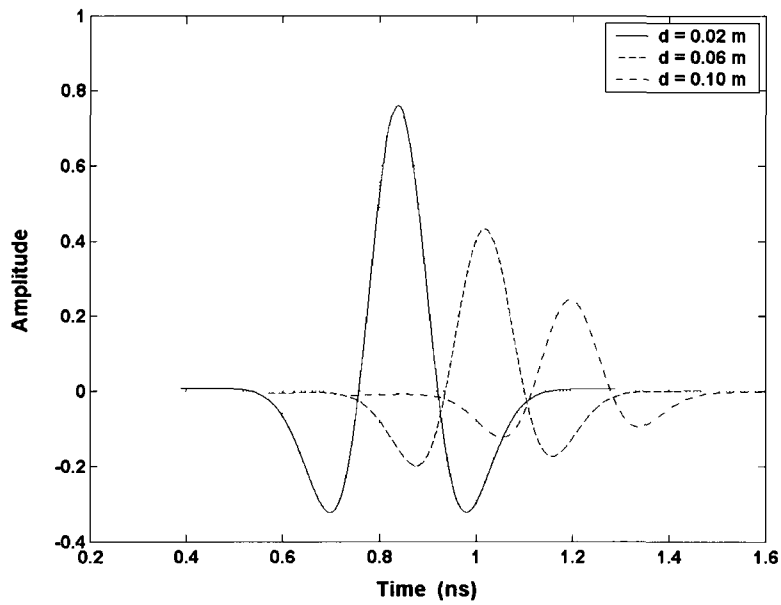

(b)

Figure 4.4-4: Waveforms of transmitted signal. (a) horizontal polarization; (b) vertical polarization. Varying d, $\varepsilon_r = 2$, $\sigma = 0.1$ S/m and $\theta = 30^0$.

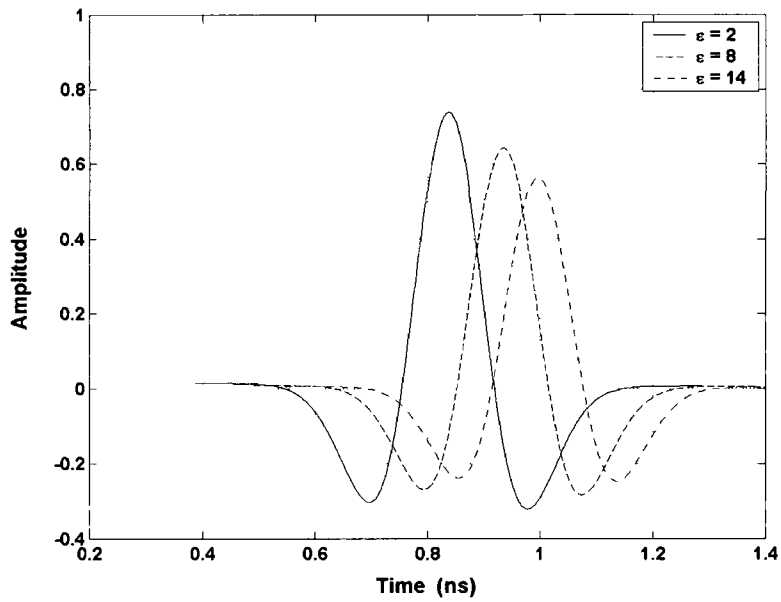

(a)

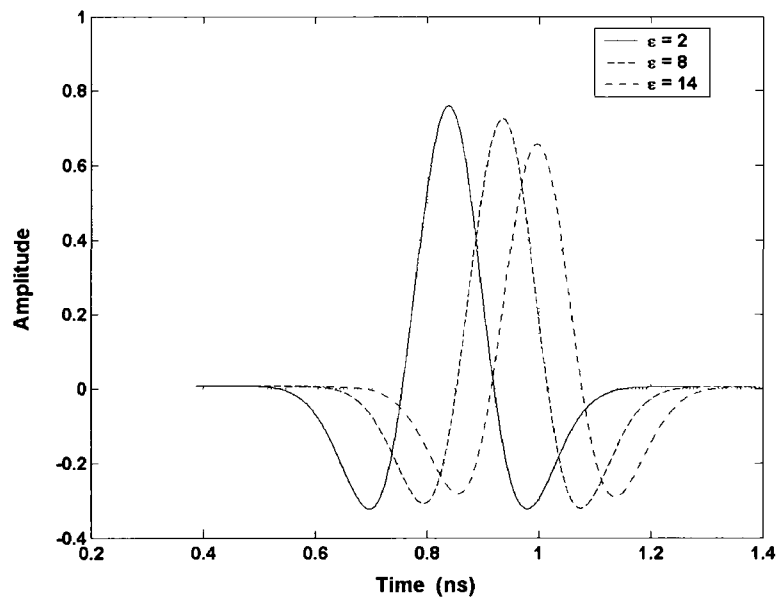

(b)

Figure 4.4-5: Waveforms of transmitted signal. (a) horizontal polarization; (b) vertical polarization. Varying ε_r, $d = 0.02$ m, $\sigma = 0.1$ S/m and $\theta = 30^0$.

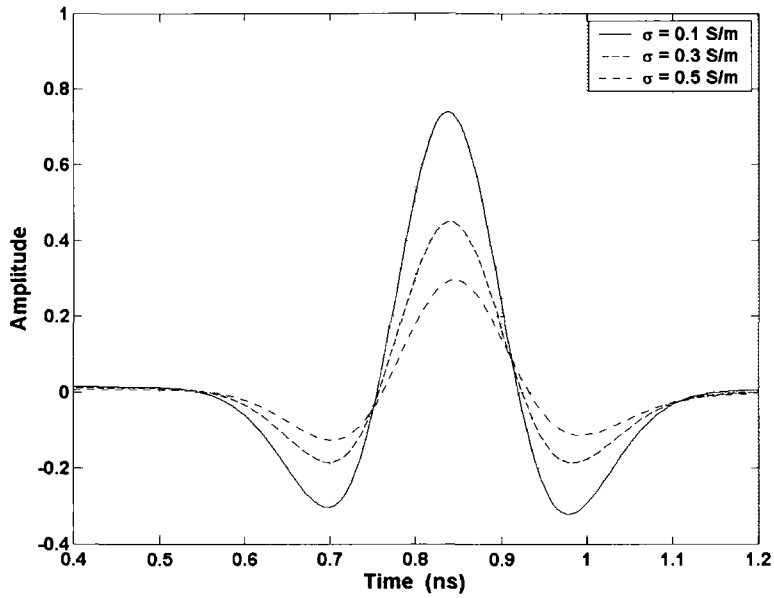

(a)

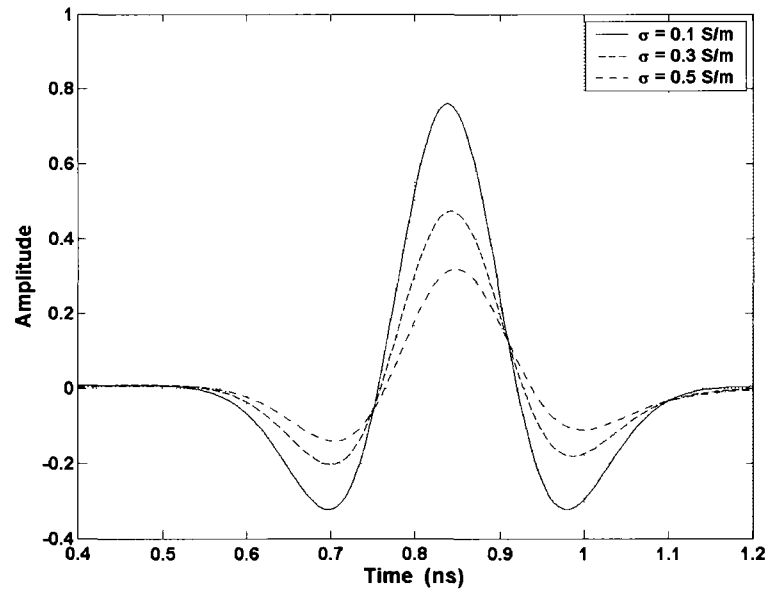

(b)

Figure 4.4-6: Waveforms of transmitted signal. (a) horizontal polarization; (b) vertical polarization. Varying σ, $d = 0.02$ m, $\varepsilon_r = 2$ and $\theta = 30^0$.

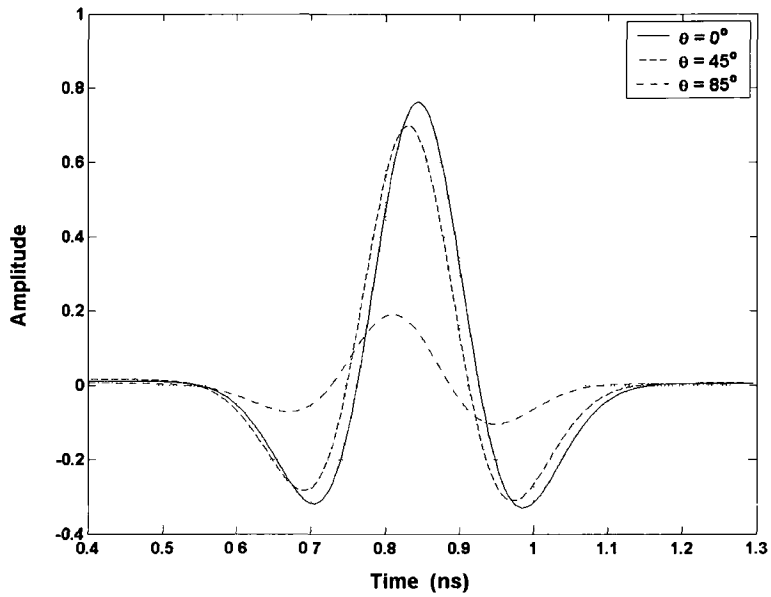

(a)

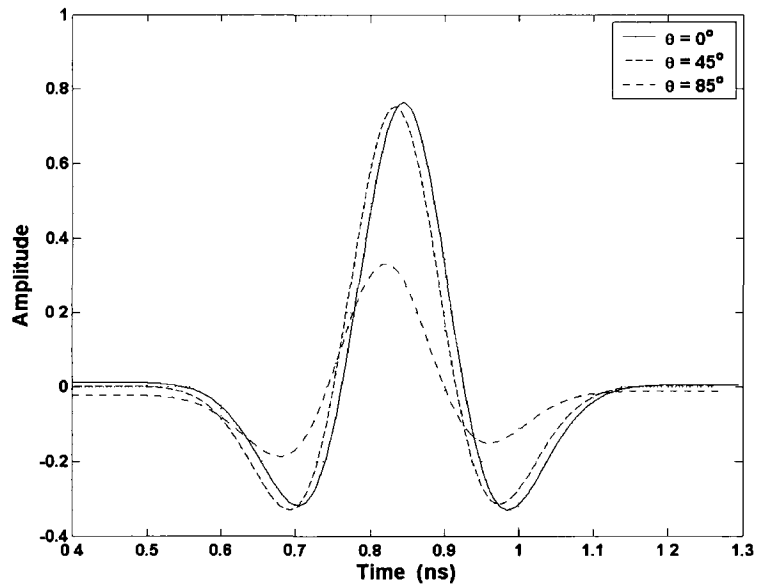

(b)

Figure 4.4-7: Waveforms of transmitted signal. (a) horizontal polarization; (b) vertical polarization. Varying θ, $d = 0.02$ m, $\varepsilon_r = 2$ and $\sigma = 0.1$ S/m.

In the above three cases, the incident angle is fixed and the other three parameters are varying, the transmitted pulse experiences roughly the same variation for both polarizations. On the other hand, when the incident angle is varying, the transmitted pulse undergoes different variations for two different polarizations. As shown in Figure 4.4-7, when the incident angle increases, the amplitude decreases, the delay decreases slightly and the distortion becomes larger. Meanwhile, the transmitted pulse undergoes larger variation for horizontal polarization than for vertical polarization. The above results accord with those in [75]. Nevertheless, Figure 4.4-7 demonstrates that the amplitude and distortion largely change when the incident angle is close to 90^0, This case was not discussed in [75].

On the basis of the above results, the transmission loss through a layer is discussed for different parameters. Figure 4.4-8 (a) illustrates that the transmission loss is basically proportional to the thickness and increases with the increase of the conductivity. As the conductivity becomes larger, the change rate of the transmission loss with the conductivity becomes larger. Figure 4.4-8 (b) shows that the transmission loss has the minimal value for a normal incidence, and slightly increases as the relative permittivity increases. The comparison between Figure 4.4-8 (a) and Figure 4.4-8 (b) indicates that the thickness and conductivity have much larger impacts on the transmission loss than the other two parameters, the relative permittivity and incident angle. These conclusions are consistent with those drawn in [75]. In Figure 4.4-8 (b), it is seen that the transmission loss for the incident angle close to 90^0 is much larger, and increases much faster with the increase of the relative permittivity than that for a small incident angle, which is not addressed in [75] and then is added here.

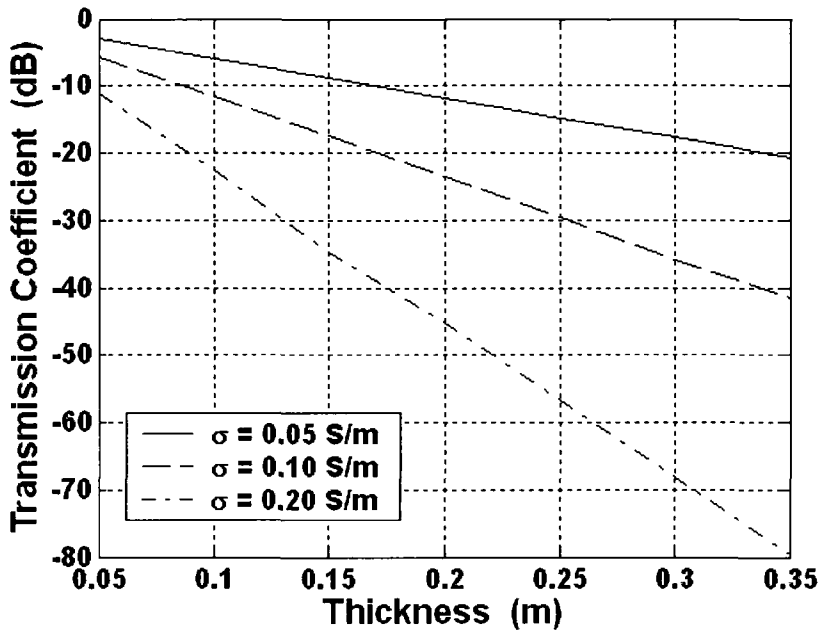

(a)

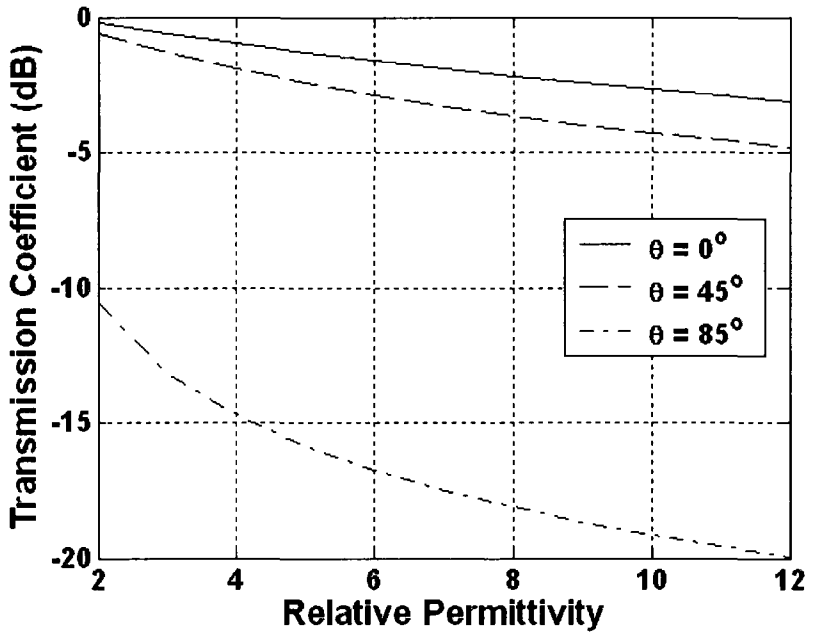

(b)

Figure 4.4-8: Transmission coefficient of slabs with different parameters. (a) thickness and conductivity; (b) relative permittivity and incident angle.

4.5 ADDITIONAL COMMENTS

As is well known, the principle of causality stating that the response cannot come before the stimulus leads to the Kramers–Kronig relations describing the interdependence of the real and imaginary parts of the susceptibility $\chi(\omega)$ [77] [78]. The Kramers–Kronig relations compose one of the most elegant and general theorems in physics, since they depend for their validity only on the principle of causality. As applied to wave propagation, the real part of susceptibility describes essentially the index of refraction and imaginary part the absorbstion coefficient of a medium. Thus, the Kramers–Kronig relations explain in the most fundamental and general terms, completely independent of the underlying physical mechanisms, the intimate connection between refraction and absorption. Actually, given one, the other follows immediately. The Kramers–Kronig relations are given by

$$\mathrm{Re}\left[\chi(\omega)\right] = \frac{1}{\pi} P \int_{-\infty}^{\infty} \frac{\mathrm{Im}\left[\chi(\Omega)\right]}{\omega - \Omega} d\Omega \tag{4.5-1}$$

$$\mathrm{Im}\left[\chi(\omega)\right] = -\frac{1}{\pi} P \int_{-\infty}^{\infty} \frac{\mathrm{Re}\left[\chi(\Omega)\right]}{\omega - \Omega} d\Omega \tag{4.5-2}$$

where P stands for principal part. The expressions show that causality requires the real and imaginary parts of the dielectric susceptibility (permittivity) or magnetic susceptibility (permeability) to depend on each other through the Hilbert transform pair.

Without losing generality, we focus on isotropic dieletecric materials. For narrowband modeling, the complex permittivity $\varepsilon_c(\omega) = \varepsilon(\omega) - j\frac{\sigma(\omega)}{\omega}$ can be determined for a fixed operating frequency. For wideband and ultra wideband modeling, the frequency dependence of the permittivity $\varepsilon(\omega)$ and the conductivity $\sigma(\omega)$ should be taken into account to appropriately characterize reflection and propagation mechanisms over some specified frequency range. In practice, the permittivity $\varepsilon(\omega)$ and the loss tangent $p(\omega)$ are measured for some materials over frequency bands, with the

relationship between $p(\omega)$, $\varepsilon(\omega)$ and $\sigma(\omega)$ being $p(\omega)=\frac{\sigma(\omega)}{\omega\,\varepsilon(\omega)}$, as specified in Section 4.3.1. Some measured values of $\varepsilon(\omega)$ and $p(\omega)$ for plywood have been used in modeling path loss of UWB signal propagation [79].

In Section 4.3.1, p_{2p} is the loss tangent at the peak frequency and varies when maintaining ε_r = 1.0, which seems not to obey the Kramers–Kronig relations but actually can be considered as the behaviors of permittivity and conductivity of a good conductor. The free electrons within a conductor can be considered as an electron gas that is free to move under the influence of an applied field. Since the electrons are not bound to the atoms of the conductor, there is no restoring force acting on them. However, there is a damping term associated with electron collisions. Hence a conductor can be modeled as a plasma, but with a very high collision frequency. The conductivity and permittivity of the plasma are given by [77]

$$\sigma(\omega)=\frac{\varepsilon_0\,\omega_p^2\,\nu}{\omega^2+\nu^2} \tag{4.5-3}$$

and

$$\varepsilon(\omega)=\varepsilon_0\left(1-\frac{\omega_p^2}{\omega^2+\nu^2}\right) \tag{4.5-4}$$

respectively, where ν is the electron collision frequency, ω_p is plasma frequency given by

$$\omega_p^2=\frac{Ne^2}{m\varepsilon_0} \tag{4.5-5}$$

where N represents the number of free electrons in a unit volume, m is the mass of an electron, and e denotes the charge. The complex permittivity

$$\varepsilon_c(\omega)=\varepsilon(\omega)-j\frac{\sigma(\omega)}{\omega}=\varepsilon_0\left(1-\frac{\omega_p^2}{\omega^2+\nu^2}\right)-j\frac{\varepsilon_0\,\omega_p^2\,\nu}{\omega\left(\omega^2+\nu^2\right)} \tag{4.5-6}$$

obeys the Kramers–Kronig relations.

For a good conductor ν is very large, then the conductivity and permittivity can be approximated by $\sigma(\omega)=\frac{\varepsilon_0\,\omega_p^2}{\nu}=\frac{N\,e^2}{m\,\nu}$ and $\varepsilon(\omega)=\varepsilon_0$, respectively. Therefore, it is reasonable for a good conductor that $p(\omega)$ or $\sigma(\omega)$ is independent of frequency and is varied when maintaining ε_r = 1.0.

In Section 4.1, Section 4.3.2 and Section 4.4, $\varepsilon(\omega)$ varies when $\sigma(\omega)$ is fixed, and $\sigma(\omega)$ varies when $\varepsilon(\omega)$ is fixed. This seems not to obey the Kramers–Kronig relations either but also can be considered as the approximations of permittivity and conductivity of a conductive dielectric at low frequencies. The complex permittivity of a dielectric is best described by the resonance model [77]

$$\varepsilon_c(\omega)=\varepsilon(\omega)+j\,\varepsilon''(\omega)=\varepsilon(\omega)-j\frac{\sigma(\omega)}{\omega}=\varepsilon_0+\sum_i\frac{\varepsilon_0\,\omega_{pi}^2}{\omega_i^2-\omega^2+j\,\omega\,2\,\Gamma_i^2}, \tag{4.5-7}$$

where $\omega_{pi}^2=\frac{N_i e^2}{m_i\,\varepsilon_0}$ is the plasma frequency of the i th resonance component, and ω_i and Γ_i are the oscillation frequency and damping coefficient, respectively, of this component. Splitting the permittvity into real and imaginary parts we have

$$\varepsilon(\omega)=\varepsilon_0\left(1+\sum_i\frac{\omega_{pi}^2\left(\omega_i^2-\omega^2\right)}{\left(\omega_i^2-\omega^2\right)^2+4\,\omega^2\,\Gamma_i^2}\right), \tag{4.5-8}$$

$$\varepsilon''(\omega)=-\varepsilon_0\sum_i\frac{2\,\omega\,\Gamma_i\,\omega_{pi}^2}{\left(\omega_i^2-\omega^2\right)^2+4\,\omega^2\,\Gamma_i^2}, \tag{4.5-9}$$

and then

$$\sigma(\omega)=-\omega\,\varepsilon''(\omega)=\varepsilon_0\sum_i\frac{2\,\omega^2\,\Gamma_i\,\omega_{pi}^2}{\left(\omega_i^2-\omega^2\right)^2+4\,\omega^2\,\Gamma_i^2}. \tag{4.5-10}$$

For low frequencies,

$$\varepsilon(\omega)\approx\varepsilon_0\left(1+\sum_i\frac{\omega_{pi}^2}{\omega_i^2}\right), \tag{4.5-11}$$

which is the static permittivity of material. A conductive dielectric has such small values of ω_i that the electrons become unbound. At low frequencies,

$$\sigma(\omega) \approx \varepsilon_0 \sum_i \frac{\omega_{pi}^2}{2\Gamma_i}, \tag{4.5-12}$$

which is the dc conductivity. Hence, it is not unreasonable for a conductive dielectric at low frequencies that $\varepsilon(\omega)$ and $\sigma(\omega)$ are approximately frequency independent and one of them varies when another is fixed. Even for modeling propagation of UWB signals in a typical band from 3 GHz to 10 GHz, the permittivity and conductivity of a construction material are still considered as constants independent in [80]. In [81], the permittivity (or conductivity) of a lossy dielectric varies when the conductivity (or permittivity) is fixed. In [82], one of the permittivity, permeability and conductivity of a conductive medium varies when fixing the rest.

4.6 CONCLUDING REMARKS

Section 4.1 shows that numerical inversion of Laplace transform is applied to the transient analysis of the reflected pulse for horizontal and vertical polarizations with a double exponential pulse incident on a lossy interface at an arbitrary angle [69] [70]. This method gets rid of the restrictions in [10] on the relative dielectric constant and the incident angle.

In Appendix A, it has been mathmaticall proved that numerical inversion of Laplace transform can be utilized for the transient analysis of the reflected pulses when an incident signal is a linear combination of finite complex attenuating exponential functions. Section 4.2 demonstrates that an arbitrary realistic signal can be approximated by a series of finite attenuating exponential functions with Prony's method. In Section 4.3, the approach combining numerical inversion of Laplace transform with Prony's method is applied to the analysis of transient reflection of non exponential pulses from a conductive interface [83]. This work has led to the following results: 1) the peak amplitude of the reflected pulse increases with the increase of the conductivity and/or the dielectric constant of the interface. 2) The distortion of the reflected pulse becomes less with the increases of

the conductivity and dielectric constant. 3) The reflected pulse has smaller peak amplitudes and is subject to more distortion for the vertical polarization than for the horizontal polarization.

Section 4.4 discusses propagation of non expontial pulses through a lossy dielectric slab [84]. The part transmitted through both interfaces without undergoing any reflection can be taken as the major part. Taking the phase difference between both interfaces into account as a factor makes the final image function not satisfy two additional conditions for Euler transformation. In order to override this obstacle, the original final image function is modified into the so-called replacement image function, which is the product of the original final image function and a modifying phase factor and satisfies two additional conditions for Euler transformation. In this way, the time domain technique on the basis of numerical inversion of Laplace transform and Prony's method is extended to the transient analysis of pulses transmitting through a lossy dielectric slab, with good accuracy and low computation costs.

In Sections 4.3 and 4.4, starting with Prony's method, the number of exponential functions is determined based on the compromise between the required accuracy and computational costs. Then, the incident pulse is approximated by a linear combination of exponentials. After that, numerical inversion of the Laplace transform is applied to the transient analyses of pulses reflected from a conductive interface and pulses propagating through a lossy dielectric slab, ending up with meaningful results and good agreement between the results achieved using this approach and those using the FDTD method and those published in the literature. The significance of this contribution is twofold: First, the corresponding results for an incident angle close to 90^0 can be provided with this technique, which can not be generated with the previous approaches. Second, this efficient time domain technique can be extended in a straightforward manner to the transient analysis of multiple reflections and transmissions in lossy media, and thus provide a powerful tool for electromagnetic analysis and design.

CHAPTER 5: PULSE PROPAGATION IN A DISPERSIVE MEDIUM AND REFLECTION FROM A DISPERSIVE MEDIUM HALF SPACE

All materials are to some extent dispersive. If a field applied to a material undergoes a sufficient rapid change, there is a time lag in the response of the polarization or magnetization of the atoms. It has been found that such materials have complex, frequency dependent constitutive parameters. On the one hand, the lossy material discussed in last chapter is dispersive since it has a complex, frequency dependent permittivity. On the other hand, the Kronig–Kramers relations imply that if the constitutive parameters of a material are frequency dependent, they must have both real and imaginary parts. Such a material, if isotropic, must be lossy. So dispersive materials are general lossy and must have both dissipative and energy storage characteristics. However, many materials have frequency range called transparency ranges over which the imaginary parts are smaller compared to real parts of constitutive parameters. If we restrict our interest to these ranges, we may approximate the material as lossless.

In this chapter, numerical inversion of Laplace transform is contiuously developed and extended to the modeling of pulse propagation in plasma and reflection from Lorentz, Debye and Cole–Cole media. All these four dispersive models satisfy the Kronig–Kramers relations required for a causal material [77]. Firstly, pulse propagation in plasma with a zero and nonzero electron collision frequency is discussed. Next, the time domain reflection coefficients, viz impulse responses, of Lorentz, Debye and Cole–Cole half spaces are achieved for both TE and TM cases. Then, the transient reflections of an arbitray pulse from these media are determined by convolving the incident pulse with the impulse responses of these media, instead of using Prony's method to decompose the incident pulse into a series of finite attenuating exponential signals as in last chapter. Based on the time domain analysis of reflected pulses from these dispersive half spaces, some waveform parameters are estimated and the material diagnosis is carried out. Lastly, the work on transient wave propagation in and reflection from dispersive media is summarized with some meaningful

conclusions. Our results show excellent agreement with those in the literature, validating the correctness and effectiveness of our technique.

5.1 PULSE PROPAGATION IN PLASMA

The advancement of radar technology has been driving the need to develop efficient time domain techniques for transient analysis of electromagnetic pulses propagating in plasma, which is used to represent a simplified model of the atmosphere. A plasma is an ioized gas in which the charged particles are free to move under the influence of an applied field and through particle-particle interaction. It differs from other materials in that there is no atomic lattice restricting the motion of the particles. However, even in a gas the interactions between the particles and the fields give rise to a polarization effect, causing the permittivity of the gas to differ from that of free space. In adition, exposing the gas to an external field will cause a secondary current to flow as a result of the Lorentz force on the particles. As the particles collide with each other, they relinquish their momentum, an effect describable in terms of a conductivity. In this section, the problem of plane wave propagation through the ionosphere is focused on. Without losing generality, a simple model of the ionosphere is employed where it is assumed that the plasma is homogeneous, that is, the number of free electrons does not depend on the altitude. If the earth's magnetic field is ignored, then a frequency domain, x-polarized plane wave propagating in the z-direction must satisfy the harmonic differential equation [27] [28],

$$\left(\frac{d^2}{dz^2}+k^2\right)E_x(z,\omega)=0 \tag{5.1-1}$$

where

$$k=\frac{1}{c}\sqrt{\omega^2-\frac{j\omega\omega_p^2}{\nu+j\omega}} \tag{5.1-2}$$

is the propagation constant, ν is the electron collision frequency, and c is the speed of light in a vacuum. The plasma cut-off frequency ω_p is given by

$$\omega_p^2 = \frac{Ne^2}{m\varepsilon_0}, \tag{5.1-3}$$

where N represents the number of free electrons in a unit volume, m is the mass of an electron, and e denotes the charge. The general solution for (5.1-1) is

$$E_x(z,\omega) = E_x(0,\omega)\left[\exp(-jkz) + \Gamma\exp(jkz)\right]. \tag{5.1-4}$$

Let $s = j\omega$, specify the incident field on the plane $z = 0$ (viz. $E_x(0,t)$) and assume that there are no reflected waves ($\Gamma = 0$), then

$$E_x(z,t) = \frac{1}{2\pi j}\int_{\gamma-\infty}^{\gamma+\infty} E_x(0,s)\,exp\left(st - \frac{sz}{c}\sqrt{1+\frac{\omega_p^{\,2}}{s(s+\nu)}}\right)ds \tag{5.1-5}$$

where

$$E_x(0,s) = \int_{-\infty}^{\infty} E_x(0,t)\,exp(-st)\,dt. \tag{5.1-6}$$

The image function

$$F(s) = E_x(0,s)\,exp\left(-\frac{sz}{c}\sqrt{1+\frac{\omega_p^{\,2}}{s(s+\nu)}}\right) \tag{5.1-7}$$

satisfies the four conditions specified in Section 3.2 under which $f(t)$ can be approximated by $f_{ec}(t,\rho)$. For $s = [\rho + j(n-0.5)\pi]/t$, $F(s)$ obey the first but does not obey the second of the two conditions in Section 3.3 under which $f_{ec}^{lm}(t,\rho)$ can be used to approximate $f_{ec}(t,\rho)$. $F(s)$ can be rewritten as

$$F(s) = E_x(0,s)\,exp\left(-s\tau_F(s)\right) \tag{5.1-8}$$

where

$$\tau_F(s) = \frac{z}{c}\sqrt{1+\frac{\omega_p^{\,2}}{s(s+\nu)}}. \tag{5.1-9}$$

As in Section 4.4, a replacement image function for $F(s)$ is defined as

$$F_r(s) = F(s)\,exp(s\tau(s)) \quad . \tag{5.1-10}$$

and meets the four conditions listed in Section 3.2 and the two conditions for Euler summation, where $exp(s\tau(s))$ is the modifying phase factor and the time shift is

$$\tau(s) = \lim_{s\to\infty} \tau_F(s) = \frac{z}{c} . \tag{5.1-11}$$

Hence $f_{r,ec}^{lm}(t,\rho)$ can be calculated by using (3.3-1), and is a good approximation to $f_{r,ec}(t,\rho)$, the original function of $F_r(s)$. From (5.1-10), the relationship between $f_{r,ec}^{lm}(t,\rho)$ and $f_{ec}^{lm}(t,\rho)$ which approximates $f_{ec}(t,\rho)$, the original function of $F(s)$, is given by

$$f_{ec}^{lm}(t,\rho) = f_{ec}^{lm}(t-\tau,\rho) . \tag{5.1-12}$$

In order to compare our results with those in [27], the same plasma parameters, $\omega_p = 1.0\times10^7$ sec^{-1}, $\nu = 0$ (collisionless plasma), are chosen, and the same incident signal is used as in [27]. The incident signal is a double exponential signal given by

$$E_x(0,t) = A\left(e^{-\alpha_1 t} - e^{-\alpha_2 t}\right)u(t) , \tag{5.1-13}$$

where $u(t)$ is the unit step function, $\alpha_1 = 1.0\times10^7$, $\alpha_2 = 1.0\times10^8$, and $A = 1.435$.

The same parameters for the collisionless plasma are chosen, and the same incident signal is used as in [20]. The incident signal is a step modulated carrier signal expressed by

$$E_x(0,t) = u(t)\sin\omega_0 t . \tag{5.1-14}$$

Figure 5.1-1 and Figure 5.1-2 plot the results for the two incident signals given by (5.1-13) and (5.1-14), respectively. Both figures demonstrate a good agreement between our results and those published in [27] and [20], verifying that our approach is correct and effective in modeling pulse propagation in collisionless plasma.

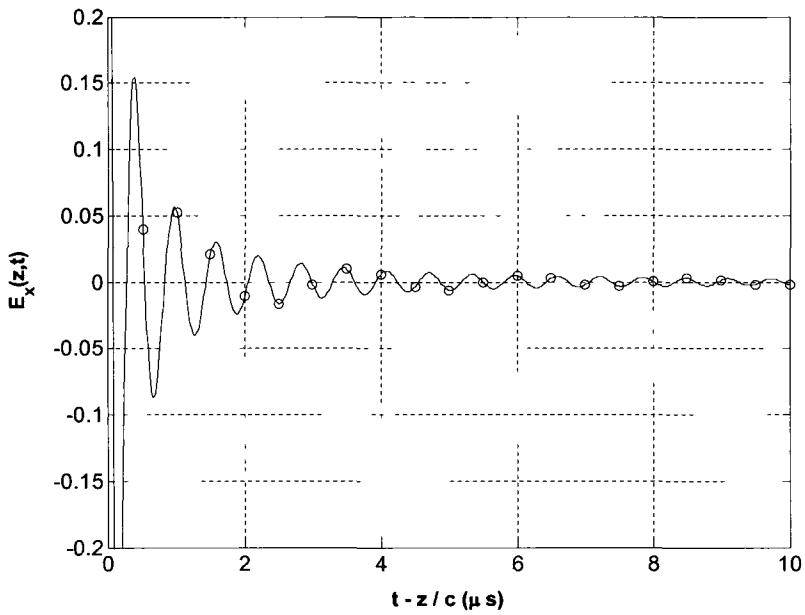

Figure 5.1-1 (a): Transient waveform at $z = 100$ m in the plasma ($\omega_p = 1.0 \times 10^7$ sec^{-1}, $\nu = 0$), due to incidence of a double exponential signal ($\alpha_1 = 1.0 \times 10^7$, $\alpha_2 = 1.0 \times 10^8$, $A = 1.435$).

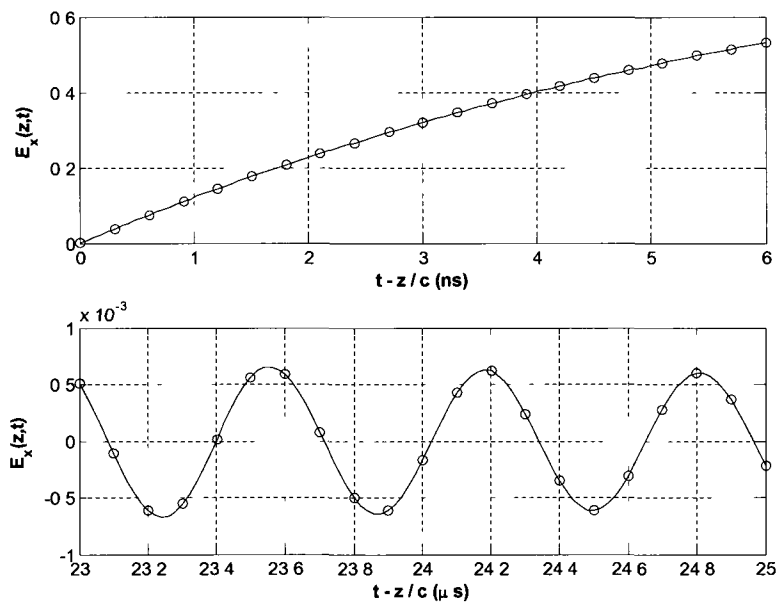

Figure 5.1-1 (b): Early time (above) and late time (below) transient waveform at $z = 100$ m in the plasma, due to incidence of the same double exponential signal as in Figure 5.1-1 (a).

Solid line: our results; Small circle: ILHI results in [27].

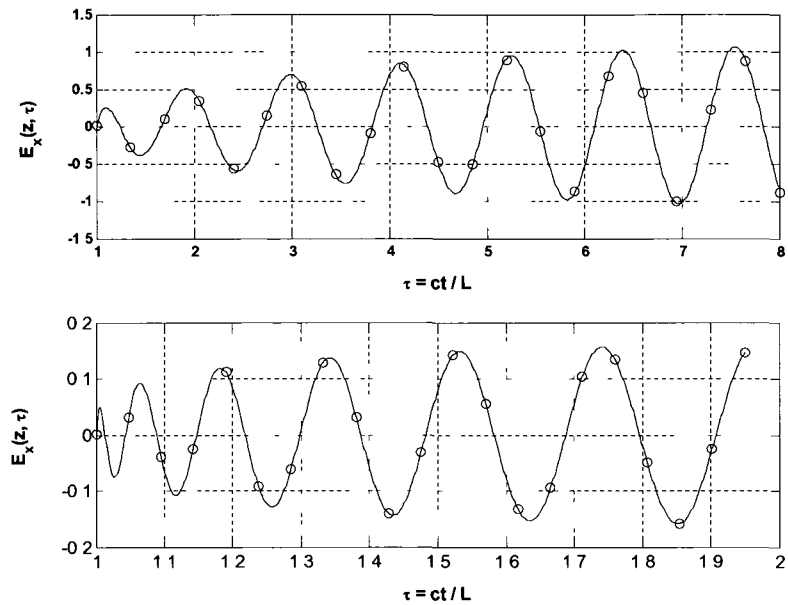

Figure 5.1-2: Transient waveform at $z = L$ in the plasma, due to incidence of a step modulated carrier signal (above: $\omega_0/\omega_p = 1.10$, $\dfrac{\omega_0 L}{2\pi c} = 0.875$; below: $\omega_0/\omega_p = 0.95$, $\dfrac{\omega_0 L}{2\pi c} = 3.58$).

Solid line: our results; Small circle: series results in [20].

For comparing our results with those in [28], the same double exponential signal given by (5.1-13) is used as the incident signal, and the same plasma parameters, $\omega_p = 1.0\times10^7$ sec^{-1} and $\nu = 1.0\times10^3$ Hz, are chosen as in [28]. Figure 5.1-3 illustrates that our results agree well with those in [28], which confirms our approach is also correct and effective for characterizing pulse propagation in plasma with a nonzero electron collision frequency.

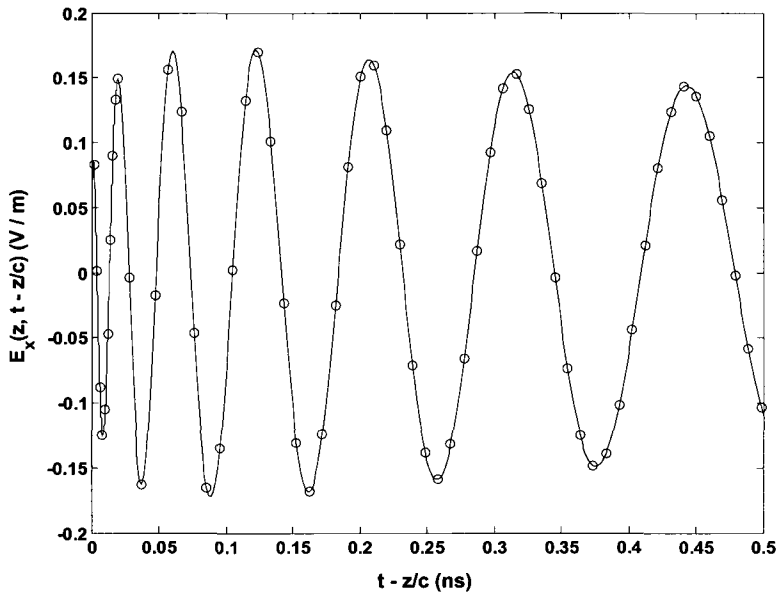

(a)

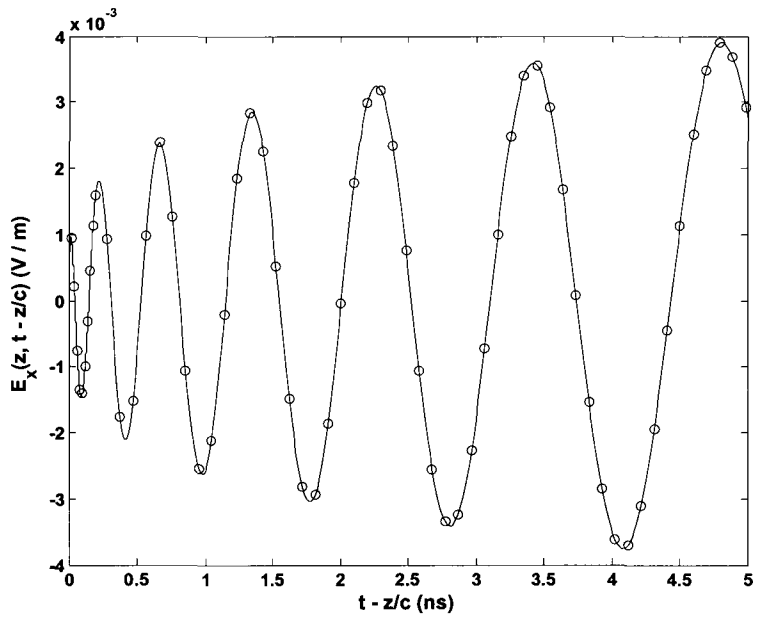

(b)

Figure 5.1-3: Transient waveforms in the plasma with $\omega_p = 1.0\times10^7$ sec^{-1} and $\nu = 1.0\times10^3$ Hz at z = 5 km (a) and z = 500 km (b). Solid line: our results; Small circle: series results in [28].

5.2 PULSE REFLECTION FROM A LORENTZ MEDIUM HALF SPACE

In Section 1.1 and Section 2.4, the significance and major analytical method for modeling pulses reflected from a Lorentz space have been addressed. In this section, following the formulations given in Section 2.4, we present our results achieved with numerical inversion of Laplace transform first for TE polarization and then for TM polarization.

The image function $\Gamma(s)$ given in (2.4-4) clearly satisfies the four conditions specified in Section 3.2 under which $f(t)$ can be approximated by $f_{ec}(t,\rho)$. Through a proof similar to that in Appendix A, it can be proved that $\Gamma(s)$ meets both two conditions in Section 3.3 under which $f_{ec}^{lm}(t,\rho)$ can be used to approximate $f_{ec}(t,\rho)$. So the transient reflection coefficient $\Gamma(t)$, the original function of $\Gamma(s)$, can be calculated using numerical inversion of Laplace transform. To compare our results with those in [35], the same incident angle and the same three sets of parameters are chosen as in [35], with each set of parameters corresponding to each of the three possible cases.

The first set of parameters is chosen as $\omega_0 = 4.0\times10^{16}s^{-1}$, $\delta = 0.28\times10^{16}s^{-1}$, $b^2 = 20.0\times10^{32}s^{-2}$, corresponding to case 1 for $\delta << \omega_0$. In this case, the analytical solution of $\Gamma(t)$ is given by (2.4-31), whose composition involves only the oscillatory ordinary Bessel functions, and so the waveform highly oscillates and only lightly damps. This is confirmed by our result plotted in Figure 5.2-1.

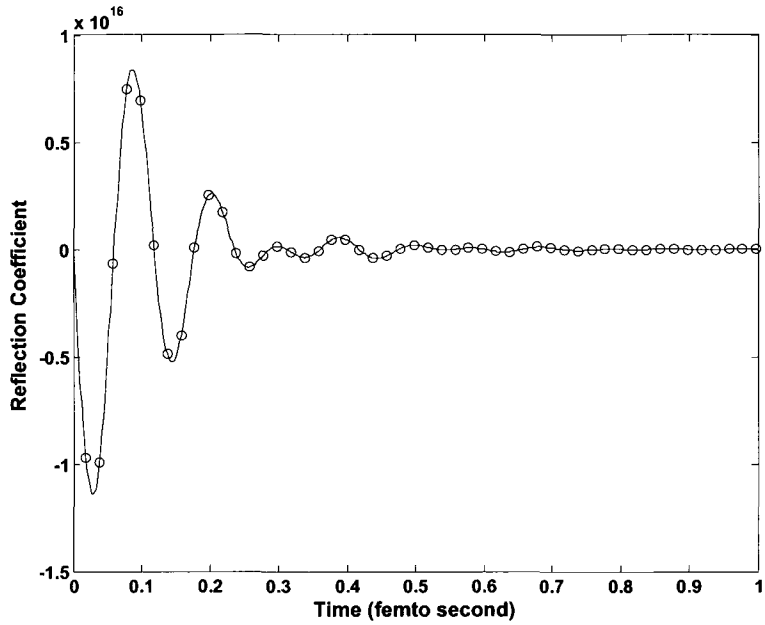

Figure 5.2-1: Transient reflection coefficient for TE polarization with incident angle $\theta = 30^0$ and material parameters, $\omega_0 = 4.0 \times 10^{16} s^{-1}$, $\delta = 0.28 \times 10^{16} s^{-1}$, $b^2 = 20.0 \times 10^{32} s^{-2}$, corresponding to case 1 for $\delta << \omega_0$. Solid line – our result; Small circle – result in [35].

The next set of parameters is $\omega_0 = 2.0 \times 10^{15} s^{-1}$, $\delta = 0.28 \times 10^{16} s^{-1}$, $b^2 = 20.0 \times 10^{29} s^{-2}$. This choice of parameter corresponds to case 2 for $\delta^2 > \omega_0^2 + B^2$ where equation (2.4-28) is used as the analytical solution of $\Gamma(t)$. Since the expression of $\Gamma(t)$ involves only modified Bessel functions that do not have oscillatory behavior of ordinary Bessel functions, the resulting waveform is overdamped and has only one single negative peak without any oscillation, which is verified by our result shown in Figure 5.2-2.

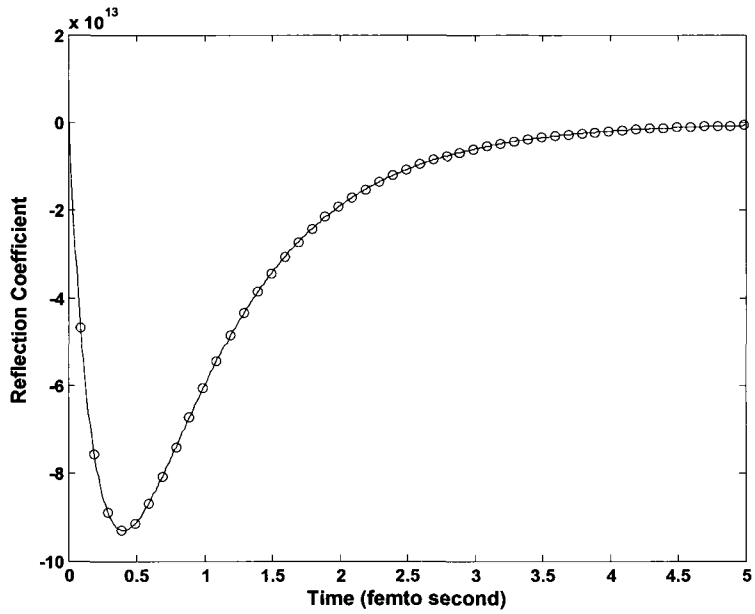

Figure 5.2-2: Transient reflection coefficient for TE polarization with incident angle $\theta = 30^0$ and material parameters, $\omega_0 = 2.0\times10^{15}s^{-1}$, $\delta = 0.28\times10^{16}s^{-1}$, $b^2 = 20.0\times10^{29}s^{-2}$, corresponding to case 2 for $\delta^2 > \omega_0^2 + B^2$. Solid line – our result; Small circle – result in [35].

The third choice of parameters is $\omega_0 = 2.0\times10^{15}s^{-1}$, $\delta = 0.28\times10^{16}s^{-1}$, $b^2 = 20.0\times10^{32}s^{-2}$, which corresponds to case 3 for $\delta > \omega_0$ but $\delta^2 < \omega_0^2 + B^2$. With this set parameters, the analytical expression of $\Gamma(t)$ given by (2.4-33) has a combination of ordinary and modified Bessel functions, so that the waveform has more damping and less oscillation than that in case 1, but has more oscillation than that in case 2. This is confirmed well by our result illustrated in Figure 5.2-3.

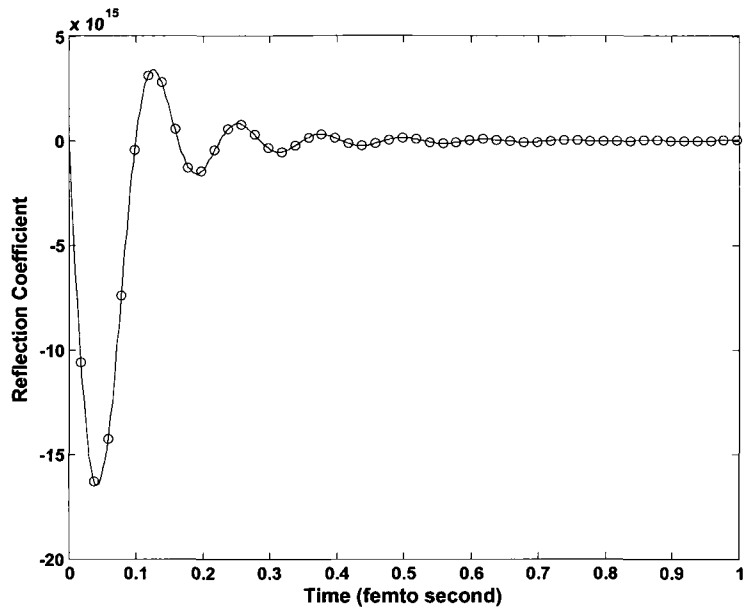

Figure 5.2-3: Transient reflection coefficient for TE polarization with incident angle $\theta = 30^0$ and material parameters, $\omega_0 = 2.0\times10^{15}s^{-1}$, $\delta = 0.28\times10^{16}s^{-1}$, $b^2 = 20.0\times10^{32}s^{-2}$, corresponding to case 3 for $\delta > \omega_0$ but $\delta^2 < \omega_0^2 + B^2$. Solid line – our result; Small circle – result in [35].

As indicated in Section 2.4, the solution of transient reflection coefficient in TM case is more complicated and involved than that in TE case. With the analytical method in Section 2.4, a term that does not appear in the TE case needs to be introduced and a special form of the time domain reflection coefficient needs to be separately solved when the incident angle is equal to 45^0 [36], which is however not needed with numerical Laplace transform. The image function $\Gamma(s)$ given in (2.4-35) clearly satisfies the four conditions in Section 3.2. Furthermore, through a process similar to Appendix A, it can be proved that $\Gamma(s)$ meets both two conditions in Section 3.3. So the time domain reflection coefficient $\Gamma(t)$, the original function of $\Gamma(s)$, can be calculated using numerical inversion of Laplace transform. To compare our results with those in [36], the same incident angles and the same sets of material parameters are chosen as in [36].

The first case uses $\theta = 30^0$ along with the material parameters, $\omega_0 = 4.0 \times 10^{16} s^{-1}$, $\delta = 0.28 \times 10^{16} s^{-1}$, and $b^2 = 20.0 \times 10^{32} s^{-2}$, corresponding to case 1 for $g(t)$ given by (2.4-63) and case 2 for $c(t)$ given by (2.4-68). Since $\delta << \omega_0$ and the composition of $g(t)$ involves only the oscillatory Bessel functions, the waveform of $\Gamma(t)$ is highly oscillatory and only lightly damped, which is confirmed by our result plotted in Figure 5.2-4.

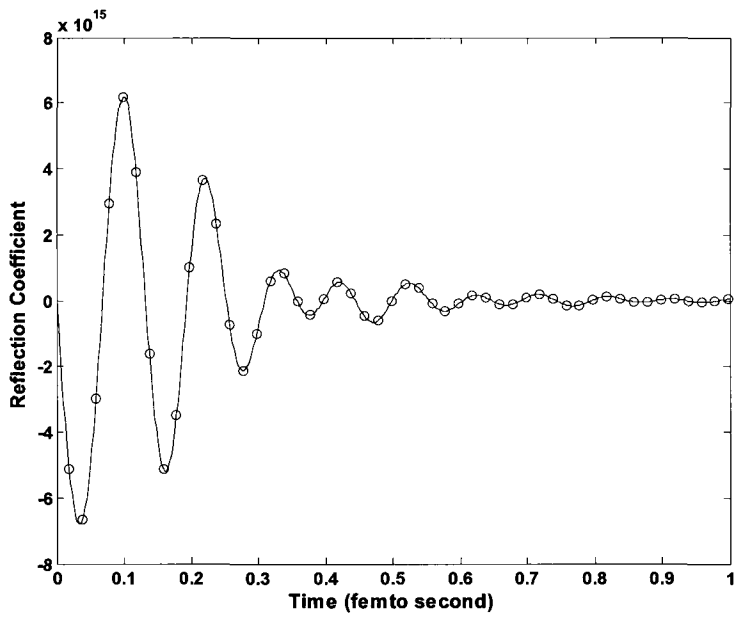

Figure 5.2-4: Transient reflection coefficient for TM polarization with incident angle $\theta = 30^0$ and material parameters, $\omega_0 = 4.0 \times 10^{16} s^{-1}$, $\delta = 0.28 \times 10^{16} s^{-1}$, $b^2 = 20.0 \times 10^{32} s^{-2}$, corresponding to case 1 for $g(t)$ and case 2 for $c(t)$, where $\delta << \omega_0$. Solid line – our result; Small circle – result in [36].

In the second case, the material parameters are chosen as $\omega_0 = 2.0 \times 10^{15} s^{-1}$, $\delta = 0.28 \times 10^{16} s^{-1}$, and $b^2 = 20.0 \times 10^{29} s^{-2}$, along with $\theta = 30^0$. This corresponds to case 2 for $g(t)$ given by (2.4-61) and case 1 for $c(t)$ given by (2.4-66). For this choice of parameters, $\delta^2 > \omega_0^2 + B^2$, and $g(t)$ is overdamped, while $c(t)$ is exponentially damped. Since $g(t)$ only involves modiefied Bessel

functions that do not oscillate like ordinary Bessel functions, the waveform of $\Gamma(t)$ shows no oscillatory behavior and only a single negative peak, which is verified by our result plotted in Figure 5.2-5.

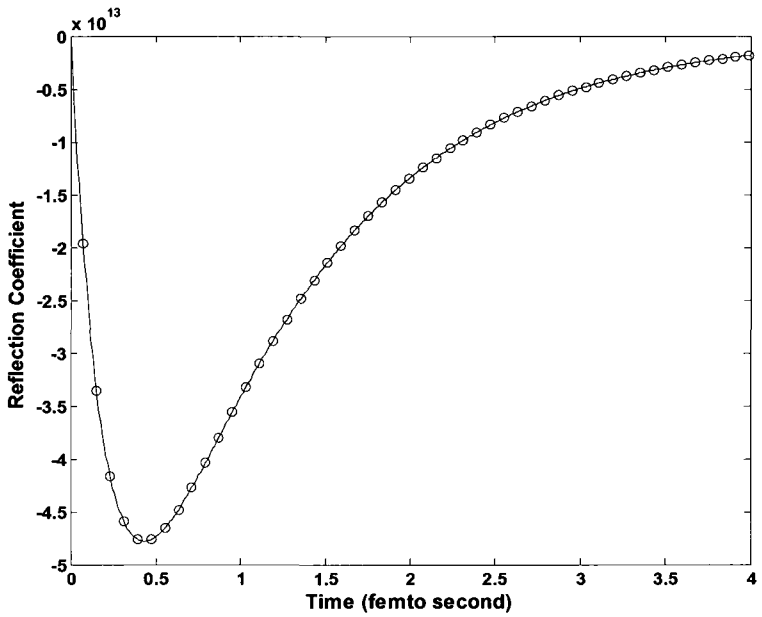

Figure 5.2-5: Transient reflection coefficient for TM polarization with incident angle $\theta = 30^0$ and material parameters, $\omega_0 = 2.0\times10^{15}s^{-1}$, $\delta = 0.28\times10^{16}s^{-1}$, $b^2 = 20.0\times10^{29}s^{-2}$, corresponding to case 2 for $g(t)$ and case 1 for $c(t)$, where $\delta^2 > \omega_0^2 + B^2$. Solid line – our result; Small circle – result in [36].

In the third case, the choice of parameters is $\omega_0 = 2.0\times10^{15}s^{-1}$, $\delta = 0.28\times10^{16}s^{-1}$, $b^2 = 20.0\times10^{32}s^{-2}$, again with $\theta = 30^0$, which corresponds to case 3 for $g(t)$ expressed by (2.4-64) and case 2 for $c(t)$ expressed by (2.4-68). Since $\delta > \omega_0$ but $\delta^2 < \omega_0^2 + B^2$, $g(t)$ has a combination of ordinary and modified Bessel functions, and so $\Gamma(t)$ is more damping and less oscillatory than with the first choice of parameters but more oscillatory than with the second choice of parameters. This is verified by our result shown in Figure 5.2-6.

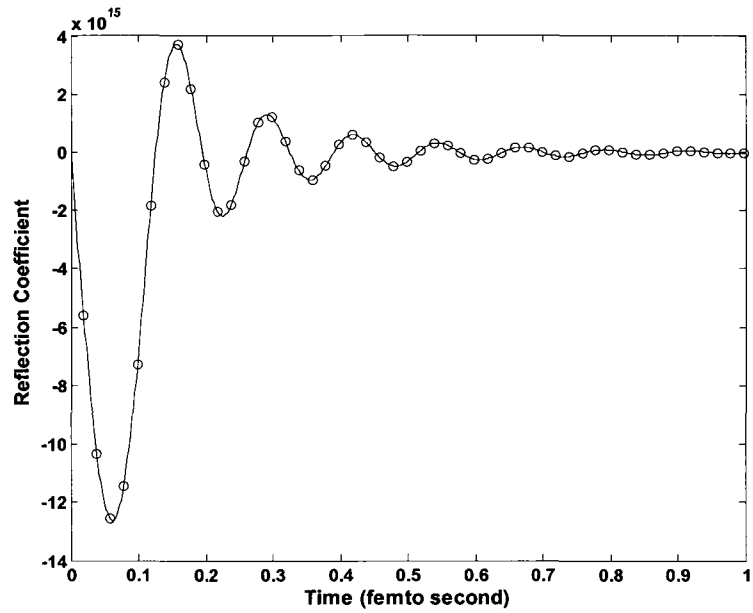

Figure 5.2-6: Transient reflection coefficient for TM polarization with incident angle $\theta = 30^0$ and material parameters, $\omega_0 = 2.0 \times 10^{15} s^{-1}$, $\delta = 0.28 \times 10^{16} s^{-1}$, $b^2 = 20.0 \times 10^{32} s^{-2}$, corresponding to case 3 for $g(t)$ and case 2 for $c(t)$, where $\delta > \omega_0$ but $\delta^2 < \omega_0^2 + B^2$. Solid line – our result; Small circle – result in [36].

In the fourth case, material parameters are the same as those in the first case, but $\theta = 50^0$ is used, corresponding to case 1 for $g(t)$ given by (2.4-63) and case 3 for a noncausal $c(t)$ given by (2.4-69). However, the convolution of $c(t)$ with $g(t)$ produces a causal result. This is confirmed by our result shown in Figure 5.2-7, which is achieved by directly using our approach that does not lead to any noncasual term.

The final case examines the special case of $\theta = 45^0$ with the same choice of material parameters as in the first case, which corresponds to the closed form expression of $\Gamma(t)$ given by (2.4-76). With our approach, this case does not need to be processed separately and can be treated as a general case

for any incident angle. This result is illustrated in Figure 5.2-8, and is very similar to that shown in Figure 5.2-7, since the incident angle in this case differs by only 5^0 from that in the fourth case.

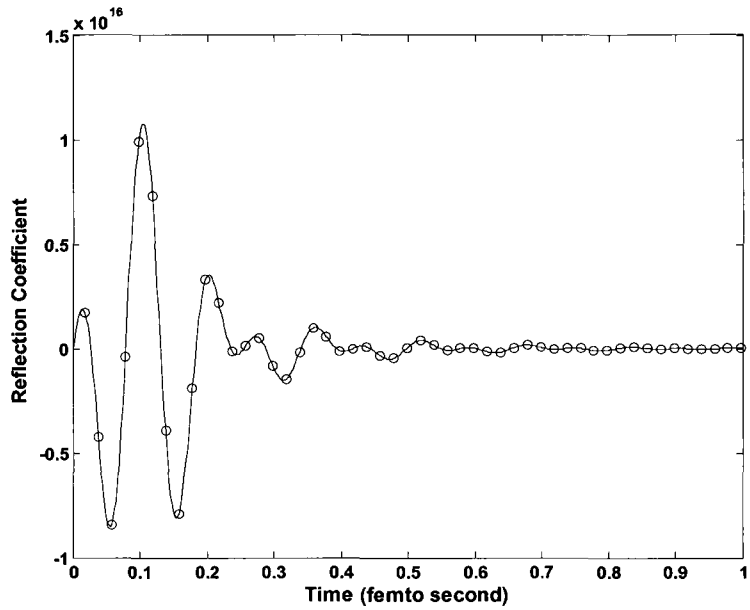

Figure 5.2-7: Transient reflection coefficient for TM polarization with incident angle $\theta = 50^0$ and material parameters, $\omega_0 = 4.0 \times 10^{16} s^{-1}$, $\delta = 0.28 \times 10^{16} s^{-1}$, $b^2 = 20.0 \times 10^{32} s^{-2}$, corresponding to case 1 for $g(t)$ and case 3 for $c(t)$, which results in a noncausal behavior of $c(t)$. Solid line – our result; Small circle -- result in [36].

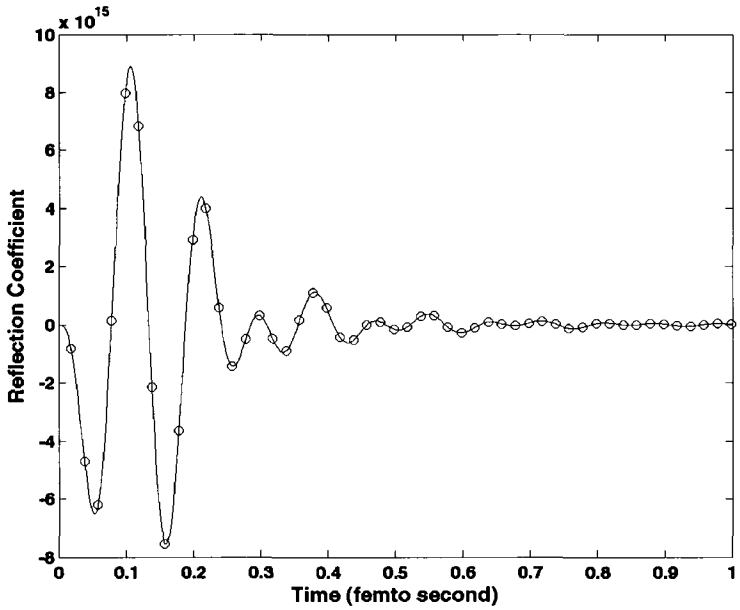

Figure 5.2-8: Transient reflection coefficient for TM polarization with incident angle $\theta = 45^0$ and material parameters, $\omega_0 = 4.0 \times 10^{16} s^{-1}$, $\delta = 0.28 \times 10^{16} s^{-1}$, $b^2 = 20.0 \times 10^{32} s^{-2}$, corresponding to the special case in [36]. Solid line – our result; Small circle – result in [36].

5.3 PULSE REFLECTION FROM A DEBYE AND COLE–COLE MEDIUM HALF SPACE

The knowledge of material properties is required in various technological fields, such as geophysics, material science and biomedical engineering. The characterization of bulk materials would be the most direct way to acquire this knowledge and greatly helpful to understand the underlying physics at the microscopic level, which is much more complicated in comparison with the existing formulations of the bulk effects. A typical approach to bulk material characterization is to examine reflected electromagnetic pulses from the interface between free space and the investigated material. Many kinds of materials show the relaxation-based dispersive properties that are commonly captured by the Debye [37] and Cole–Cole [47] models. Rothwell [46] worked out the time domain reflection coefficients of a Debye half space for both horizontal and vertical polarizations that involve exponential and modified Bessel functions and require convolution operations to evaluate.

To our knowledge, the time domain reflection coefficient of a Cole–Cole half space for any polarization has been not available so far. It is the purpose of this section to develop a new technique for transient analysis of pulse reflection from Debye and Cole–Cole media, and apply this technique to waveform parameter estimation and material characterization.

5.3.1 Time Domain Reflection Coefficients

Without losing generality and for the comparison with the results in [46], the one-order model with zero ionic conductivity is utilized in this work. Introduce the Laplace variable $s = j\omega$, and consider the interface between free space and a dielectric half space with unity permeability and a permittivity $\varepsilon(s) = \varepsilon_0 \varepsilon_r(s)$ described by the following unified equation

$$\varepsilon_r(s) = \varepsilon_\infty + \frac{\varepsilon_s - \varepsilon_\infty}{1 + (s\tau)^{1-\alpha}}, \tag{5.3-1}$$

where ε_s and ε_∞ are the static and optical dielectric constants ($\varepsilon_s > \varepsilon_\infty$), respectively, τ is the relaxation time, (11) becomes a one-pole Debye equation when $\alpha = 0$, and is a one-order Cole–Cole equation when $0 < \alpha \le 1$. A nonzero Cole–Cole parameter α is a measure for broadening dispersion, which tends to broaden the relaxation spectrum and results from a spread of relaxation times centered around τ [77]. A unified formulation for a Cole–Cole or Debye half space is given below.

A plane wave is obliquely incident onto a dispersive half space from free space, at an incidence angle θ relative to the normal to the interface. The reflection coefficients are given by

$$R_H(s) = \frac{\cos\theta - \sqrt{\varepsilon_r(s) - \sin^2\theta}}{\cos\theta + \sqrt{\varepsilon_r(s) - \sin^2\theta}} \tag{5.3-2}$$

and

$$R_V(s) = \frac{\sqrt{\varepsilon_r(s) - \sin^2\theta} - \varepsilon_r(s)\cos\theta}{\sqrt{\varepsilon_r(s) - \sin^2\theta} + \varepsilon_r(s)\cos\theta} \tag{5.3-3}$$

for horizontal and vertical polarizations, respectively. Substituting $\varepsilon_r(s)$ from (5.3-1) leads to

$$R_H(s)=\frac{\sqrt{s^{1-\alpha}+s_0}-K_H\sqrt{s^{1-\alpha}+s_1}}{\sqrt{s^{1-\alpha}+s_0}+K_H\sqrt{s^{1-\alpha}+s_1}} \tag{5.3-4}$$

and

$$R_V(s)=\frac{\sqrt{\varepsilon_r(s)-sin^2\theta}-\varepsilon_r(s)cos\theta}{\sqrt{\varepsilon_r(s)-sin^2\theta}+\varepsilon_r(s)cos\theta}, \tag{5.3-5}$$

where

$$s_0=\left(\frac{1}{\tau}\right)^{1-\alpha}, \qquad s_1=\left(\frac{1}{\tau}\right)^{1-\alpha}\frac{\varepsilon_s-sin^2\theta}{\varepsilon_\infty-sin^2\theta}>s_0, \qquad s_2=\left(\frac{1}{\tau}\right)^{1-\alpha}\frac{\varepsilon_s}{\varepsilon_\infty}, \tag{5.3-6}$$

$$K_H=\frac{\sqrt{\varepsilon_\infty-\sin^2\theta}}{\cos\theta}, \tag{5.3-7}$$

and

$$K_V=\frac{\varepsilon_\infty\cos\theta}{\sqrt{\varepsilon_\infty-\sin^2\theta}}. \tag{5.3-8}$$

Either $R_H(s)$ or $R_V(s)$ does not satisfy the third one of the four conditions listed in Section 3.2, that is, is not asymptotic to zero at high frequency, but instead

$$\lim_{s\to\infty}R_H(s)=R_H^\infty=\frac{1-K_H}{1+K_H}, \tag{5.3-9}$$

and

$$\lim_{s\to\infty}R_V(s)=R_V^\infty=\frac{1-K_V}{1+K_V}. \tag{5.3-10}$$

So $R_H(t)$ and $R_V(t)$ have the impulsive components, $R_H^\infty(t)$ and $R_V^\infty(t)$, with the amplitudes of R_H^∞ and R_V^∞, respectively. Subtracting the terms R_H^∞ and R_V^∞ from $R_H(s)$ and $R_V(s)$ respectively gives the "reduced" reflection coefficients,

$$\bar{R}_H(s)=R_H(s)-R_H^\infty=\frac{2K_H}{1+K_H}\frac{\sqrt{s^{1-\alpha}+s_0}-\sqrt{s^{1-\alpha}+s_1}}{\sqrt{s^{1-\alpha}+s_0}+K_H\sqrt{s^{1-\alpha}+s_1}}, \tag{5.3-11}$$

and

$$\bar{R}_V(s) = R_V(s) - R_V^{\infty} = \frac{2K_V}{1+K_V} \frac{\sqrt{s^{1-\alpha}+s_0}\sqrt{s^{1-\alpha}+s_1} - \left(s^{1-\alpha}+s_2\right)}{\sqrt{s^{1-\alpha}+s_0}\sqrt{s^{1-\alpha}+s_1} + K_V\left(s^{1-\alpha}+s_2\right)}. \tag{5.3-12}$$

Both $\bar{R}_H(s)$ and $\bar{R}_V(s)$ satisfy the four conditions in Section 3.2, under which $f(t)$ can be approximated by $f_{ec}(t,\rho)$. It can be proved that, for $s = \left[\rho + j(n-0.5)\pi\right]/t$, both $\bar{R}_H(s)$ and $\bar{R}_V(s)$ also obey the two conditions a) and b) in Section 3.3, under which $f_{ec}^{lm}(t,\rho)$ can be used to approximate $f_{ec}(t,\rho)$. The proof is similar to that given in Appendix A. Hence, both reduced time domain reflection coefficients $\bar{R}_H(t)$ and $\bar{R}_V(t)$ can be calculated using Equation (3.3-1). The required time domain reflection coefficients $R_H(t)$ and $R_V(t)$ are obtained by adding $R_H^{\infty}(t)$ and $R_V^{\infty}(t)$ to $\bar{R}_H(t)$ and $\bar{R}_V(t)$, respectively.

Before applying this technique to waveform parameter estimation and material characterization, its correctness and effectiveness are verified by comparing the reduced transient reflection coefficients with those in [46]. Several different cases are considered, each following the Debye model ($\alpha = 0$) with different values of the parameters ε_s, ε_∞ and τ. In the numerical trials, for each ρ value (ρ = 3, 6, 10 and 20), we set N = 15 (l = 9, m = 6), 20 (l = 14, m = 6), 39 (l = 20, m = 19), 59 (l = 29, m = 30), and 99 (l = 49, m = 50) and achieved almost the same results for $f_{ec}^{lm}(t,\rho)$, indicating that the truncation errors are small enough. In the following examples, ρ = 3 and N = 15 (l = 9, m = 6).

Figure 5.3-1 (a) illustrates the reduced reflection coefficients of water (at standard temperature and pressure) calculated using our technique, and compares them to the results in [46] with an excellent agreement. The reduced reflection coefficients do not include any impulsive component with the amplitude of R_H^{∞} or R_V^{∞}. The large scale on the vertical axis may be disconcerting at first look, but it should be noted that these reflection coefficients will be convolved with incident pulses with durations on the order of nanoseconds.

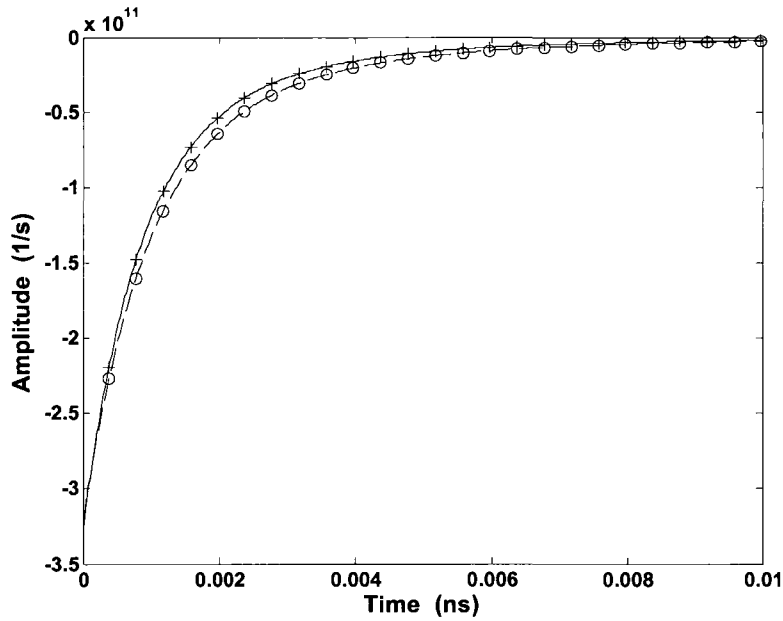
x 10^11
0
-0.5
-1
-1.5
-2
-2.5
-3
-3.5
Amplitude (1/s)
0
0.002
0.004
0.006
0.008
0.01
Time (ns)

(a)

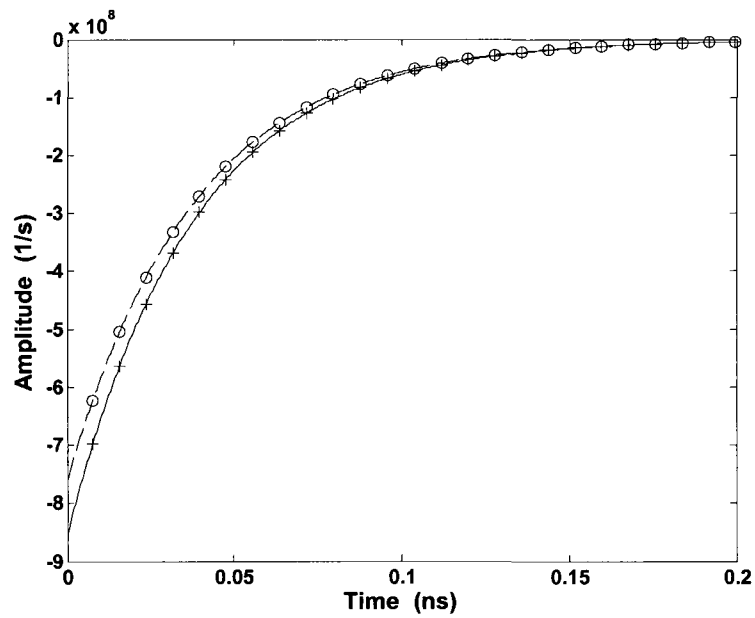
x 10^8
0
-1
-2
-3
-4
-5
-6
-7
-8
-9
Amplitude (1/s)
0
0.05
0.1
0.15
0.2
Time (ns)

(b)

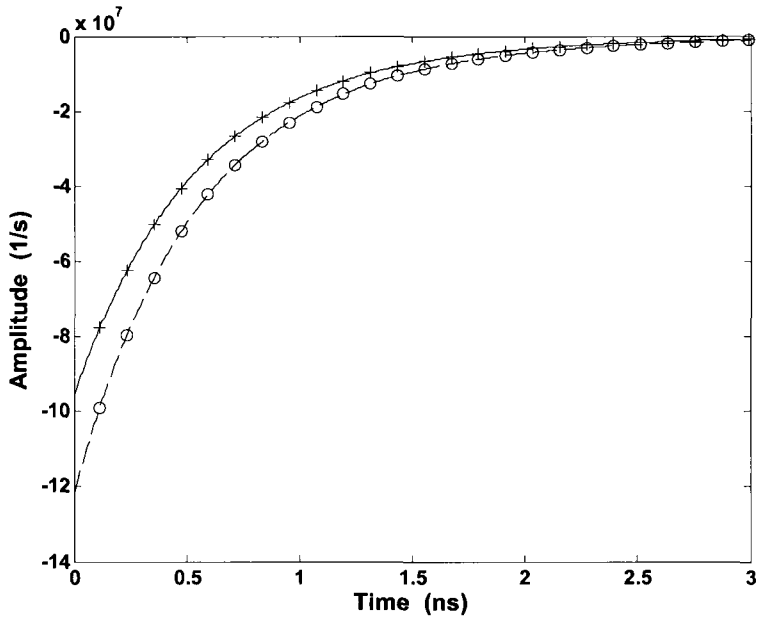

(c)

Figure 5.3-1: Time domain reduced reflection coefficients of Debye half space for $\theta = 30^0$.

(a) water, $\alpha = 0$, $\varepsilon_s = 78.3$, $\varepsilon_\infty = 5.0$, $\tau = 9.6 \times 10^{-12}$ s.

(b) Martian soil simulant. $\alpha = 0$, $\varepsilon_s = 3.57$, $\varepsilon_\infty = 3.12$, $\tau = 0.041 \times 10^{-9}$ s.

(c) ceramic. $\alpha = 0$, $\varepsilon_s = 494$, $\varepsilon_\infty = 155$, $\tau = 1.39 \times 10^{-9}$ s.

Solid line: Our results for horizontal polarization; Plus sign: Results for horizontal polarization in [46]; Dashed line: Our results for vertical polarization; Circle: Results for vertical polarization in [46].

Figure 5.3-1 (b) compares the reduced reflection coefficients of a Martian soil stimulant found using our technique to the results in [46]. Our results agree with those in [46] very well. Since the static and optical permittivities for the soil are comparable, the relaxation effect is less dramatic than that for water while the durations of transient reflection coefficients are longer than that for water due to the longer relaxation time.

Figure 5.3-1 (c) shows the reduced reflection coefficients of a Lanthanum modified $PbTiO_3$ ferroelectric ceramic. There is an excellent agreement between our results and those in [46]. The static and optical permittivities are much larger than those in the above two cases, but relaxation time is also quite large, making the durations of these reflection coefficients have the order of several nanoseconds.

Consider a Gaussian waveform incident upon a water half-space at $\theta = 30^0$. The incident field is horizontally polarized and has an amplitude of 1 V/m and a pulse width of 1 ps. The reflected waveform can be determined using the convolution,

$$E_H^r(t) = R_H(t) * E^i(t) = \bar{R}_H(t) * E^i(t) + R_H^\infty E^i(t), \tag{5.3-13}$$

where $\bar{R}_H(t)$ is shown in Figure 5.3-1 and R_H^∞ is given by (5.3-9). The reflected waveform is plotted in Figure 5.3-2, from which it is seen that the incident Gaussian waveform is maintained, but with a long tail contributed by the waveform of $\bar{R}_H(t)$ due to the relaxation effect.

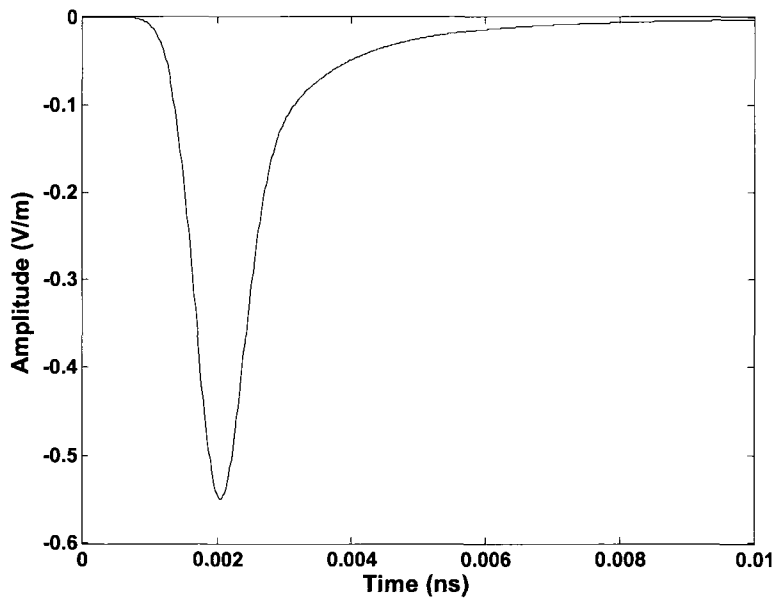

Figure 5.3-2: Reflected waveform for a horizontally polarized Gaussian pulse incident on a water half space at $\theta = 30^0$.

5.3.2 Waveform Parameter Estimation and Material Characterization

Based on the above transient analysis, this technique can be utilized for the estimation of waveform parameters of reflected pulses. As an example, consider a mixture of water and ethanol with a volume fraction v_F. Here, $v_F = 0$ corresponds to pure ethanol while $v_F = 1$ corresponds to pure water. Bao et al. have shown the permittivity of this mixture is described quite well by the Debye model and have measured the Debye parameters for various volume fractions. The parameters can be approximated by the following expressions [81]:

$$\varepsilon_\infty = -19.1\, v_F^{\,2} + 18.5\, v_F + 4.8, \tag{5.3-14}$$

$$\varepsilon_s - \varepsilon_\infty = 53\, v_F + 22, \tag{5.3-15}$$

$$\tau = 0.15 \times 10^{-1.27\, v_F} \text{ ns}. \tag{5.3-16}$$

For water the Cole–Cole parameter α is only 0.02, indicating that a Debye description is sufficient. However, not all polar materials have a permittivity that follows the Debye model as closely as water. Some oil has a Cole–Cole parameter α up to 0.23 [77]. In this work, assuming that the permittivity of the mixture above is described by the Debye and Cole–Cole equations, waveform parameters estimation and material diagnosis are explored, respectively, and the corresponding results in two cases are compared with each other.

One of the most important waveform parameters is the correlation between two waveforms. It indicates the degree to which two waveforms resemble and is defined by

$$C(t) = \left(\frac{\int_0^\infty s_1(t')\, s_2(t+t')\, dt'}{s_m} \right)^2 \tag{5.3-17}$$

$$s_m = \max\left(\int_0^\infty s_1^{\,2}(t')\, dt',\ \int_0^\infty s_2^{\,2}(t')\, dt' \right) \tag{5.3-18}$$

Let $s_1(t)$ and $s_2(t)$ be the incident and reflected waveforms, respectively, and consider the Guassian waveform in Section 3 incident upon a mixture half space. The maximum value $C_{\max}$ of

$C(t)$ is plotted versus the volume fraction v_F for three values of Cole–Cole parameter α and three incident angles in Figure 5.3-3 (left), and versus α for two v_F values and three incident angles in Figure 5.3-3 (right). It is seen that $C_{\max}$ increases with the increase of v_F, α and θ.

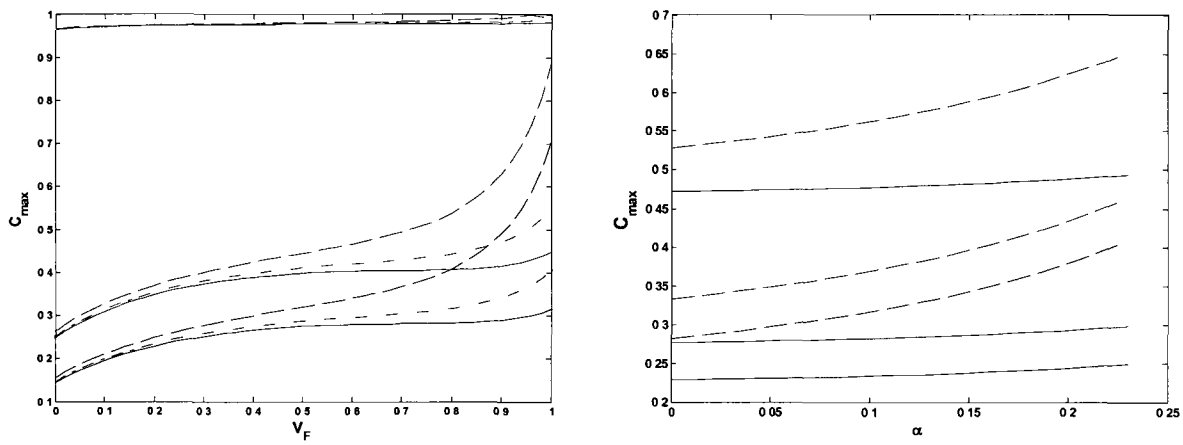

Figure 5.3-3: Maximum correlation between the incident and reflected waveforms for a mixture irradiated by a horizontally polarized Gaussian pulse.

Left: versus v_F for $\alpha = 0$ (solid lines), 0.1 (dash-dot lines) and 0.23 (dashed lines), and for $\theta = 0^0$ (blue lines), 45^0 (red lines) and 89^0 (green lines).

Right: versus α $(0 \le \alpha \le 0.23)$ for $v_F = 0.2$ (solid lines) and 0.8 (dashed lines), and for $\theta = 0^0$ (blue lines), 30^0 (red lines) and 60^0 (green lines).

Assume that a mixture with $\alpha = 0$ and $v_F = 0.7$ is desired. Whether this fraction has been achieved can be determined by examining the maximum correlation between two reduced reflected waveforms for the desired volume fraction and for the mixture to be determined. $C_{\max} = 1$ indicates that the mixture has the desired volume fraction, while $C_{\max} < 1$ means that the mixture has a different volume fraction from the desired one. Using a reduced reflected waveform obtained from $\bar{E}_H^r(t) = \bar{R}_H(t) * E^i(t)$ leads to a much higher detection accuracy than using a reflected waveform

calculated by $E_H^r(t) = R_H(t) * E^i(t)$. Figure 5.3-4 (right) shows that the desired mixture can be easily identified since $C_{\max}$ calculated using reduced reflected waveforms decreases sharply on two sides of the peak. Furthermore, increasing the incident angle even up to 89^0 (almost grazing incidence) will not deteriorate the detection accuracy. In contrast, Figure 5.3-4 (left) shows that it is not easy to detect the desired mixture because $C_{\max}$ calculated using reflected waveforms does not decrease quickly in the proximity of the peak. Moreover, increasing the incident angle will significantly deteriorate the detection accuracy. The peak nearly cannot be detected for larger incident angles.

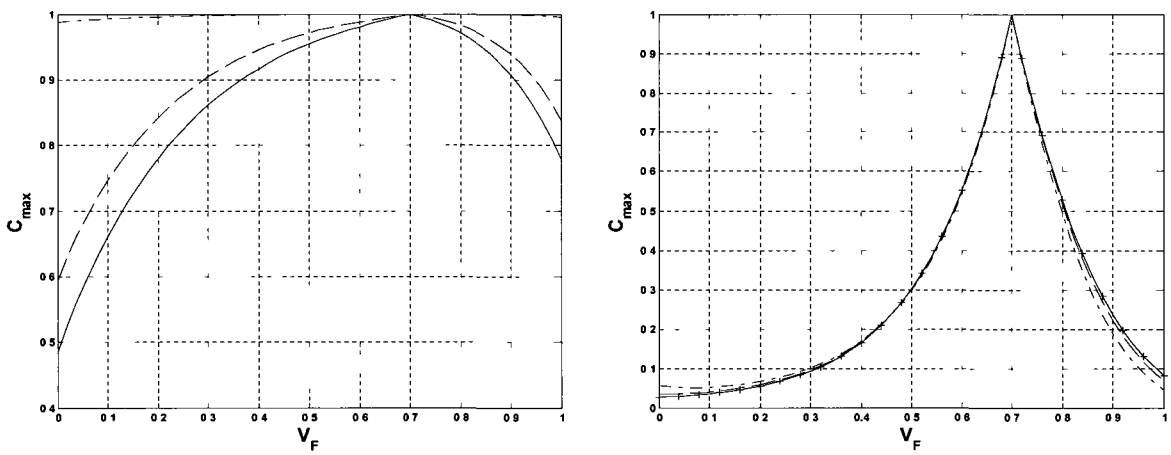

Figure 5.3-4: Maximum correlation between two reflected waveforms (left) and between two reduced reflected waveforms (right) for the desired volume fraction and for the mixture to be determined, with a horizontally polarized Gaussian pulse incident on the mixture at $\theta = 0^0$ (solid lines), 45^0 (dashed lines) and 89^0 (dash-dot lines), when $\alpha = 0$ and v_F varying. Plus sign: Corresponding results in [46].

Assume that a mixture with $\alpha = 0.1495$ and $v_F = 0.6$ is desired. Figure 5.3-5 (right) demonstrates that the desired mixture can be identified since $C_{\max}$ calculated using reduced reflected waveforms decreases on two sides of the peak. Meanwhile, increasing the incident angle even up to

89^0 will not deteriorate the detection accuracy basically. With the range of $C_{\max}$, Figure 5.3-5 (left) indicates that it is almost impossible to detect the desired mixture because $C_{\max}$ calculated using reflected waveforms does not significantly decrease on two sides of the peak. In addition, increasing the incident angle will further deteriorate the detection accuracy. Comparing Figure 5.3-5 (right) with Figure 5.3-4 (right), it is seen that detection of a mixture with a desired α value is much more difficult than detection of a mixture with a desired v_F value.

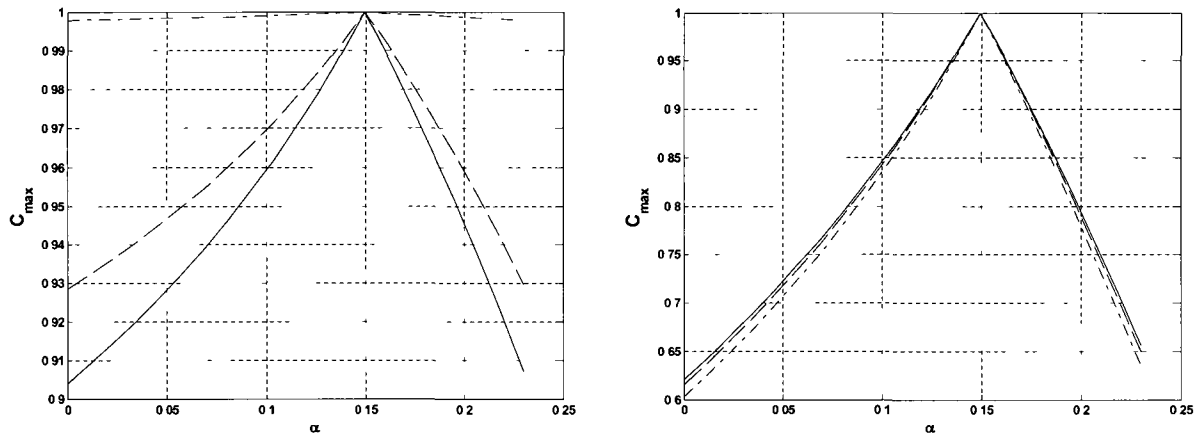

Figure 5.3-5: Maximum correlation between two reflected waveforms (left) or between two reduced reflected waveforms (right) for the desired volume fraction and for the mixture to be determined, with a horizontally polarized Gaussian pulse incident on the mixture at $\theta = 0^0$ (solid lines), 45^0 (dashed lines) and 89^0 (green lines), when $v_F = 6$ and α varying.

5.4 CONCLUDING REMARKS

Section 5.1 discusses pulse propagation in plasma with a zero and nonzero electron collision frequency. For an excitation like a double exponential signal that has the long tails in both time and frequency domains, a large number of sampling points are required to compute the tramsient response using fast Fourier transform (FFT). The closed form incomplete Lipschitz-Hankel integrals (ILHI) representation is more efficient than FFT but only can be used to model transient wave

propagation in plasma with a zero electron collision frequency [27]. For the plasma with a nonzero electron collision frequency, a hybrid method from ILHI representation and FFT can be employed in the following way. Because the plasma high-frequency behavior is approximately independent of electron collision frequency, an analytical frequency domain expression that is similar in form to the one encountered for the collisionless plasma encompasses this high-frequency behavior is substracted from the exact expression for the plasma with a nonzero electron collision frequency. The extracted term is evaluated analytically. The remaining expression, which can be transformed to the time domain with FFT, requires only a modest number of sampling points [28]. Using our method based on numerical inversion of Laplace transform (NILT), we do not need to extract the high-frequency behavior from the expression for the plasma with a nonzero electron collision frequency, since our method can be directly applied to plasma with a zero and nonzero electron collision frequency [86]. Furthermore, our approach is not only applicable to a double exponential signal but also to other signals. Although the application of our approach is not as wide as that of FDTD method, it is more cost effective for basic pulse propagation studies of import to the communications and radar communities. FDTD method can in principle be applied to the corresponding full three-dimensional vector problem. However, the standard FDTD approach cannot handle simulating the desired long propagation distances due to finite computing resources and the accumulation of phase errors associated with numerical dispersion. The results we present in this chapter can be used as validation cases for FDTD method and other numerical approaches in their regions of validity.

In this thesis research, two approaches are employed to analyze transient reflection and propagation. As shown in sections 4.2 and 4.3, one is to approximate an arbitrary incident signal with a finite number of attenuating exponential signals using Prony's method and to apply NILT to the final image function, which is the product of the frequency domain reflection or tramsimission coefficient and the image function of the approximating incident signal. The accuracy of this approach is limited by the numerical errors from both NILT and the decomposition of the original

incident signal into of a series of finite attenuating exponential signals. As shown in sections 5.2 and 5.3, another approach is to use NILT for determinating the transient reflection or transmission coefficient and to convolve the incident signal with the time domain reflection or transmission coefficient. The accuracy of this approach depends on both NILT and numerical convolution, which normally incurs smaller errors than decomposing an arbitrary signal into a series of finite attenuating exponential signals. Section 5.2 presents time domain reflection coefficients for both TE- and TM-polarized plane waves incident on a Lorentz medium half space using NILT. Three possible cases are discussed, each of which is determined by a different relationship between the damping coefficient, oscillation and plasma frequencies. The result is an exponentially damped waveform that oscillates based on the conditions of each case.

In section 5.3, the properties of a half space are described in frequency domain by the Debye and Cole–Cole models, respectively, which are commonly used to capture the relaxation-based dispersive properties. First, transient reflected pulses are analyzed and waveform parameters are estimated. Then, based on the estimation, the relationships between the waveform parameters of reflected pulses and the properties of dispersive material as well as incident angles are discussed. Meanwhile, the results obtained with the Debye model are compared to those obtained with the Cole–Cole model. The application of these results to material characterization and diagnosis is explored. It is shown that using the reduced time domain reflection coefficients often brings more physical insights and leads to an efficient algorithm and a robust scheme for dispersive material diagnosis. There is excellent agreement between our results and those in [46], which validates the correctness and effectiveness of this work [87] [88].

CHAPTER 6: CONCLUSIONS

6.1 SUMMARY OF THESIS WORK

This thesis addresses several issues regarding the transient analysis of short duration electromagnetic pulses propagating through a variety of media and some related subjects. Hosono introduced numerical inversion of Laplace transform (NILT) into electromagnetics and optics. Since then, however, his algorithm has only found quite limited applications in electromagnetics and seems to have received less attention in the related fields over the last thirty years. First of all, this thesis discusses and treats Hosono's algorithm for NILT under a strict theoretical framework.

The waveform analysis for pulses propagating through and interacting with different media is a topic of importance in many technological fields. An efficient time domain technique is developed on the basis of the numerical inversion of the Laplace transform and Prony's method for the analyses of electromagnetic pulses reflected from a conductive interface and propagating through a lossy dielectric slab. First, using numerical inversion of the Laplace transform but without using Prony's method, the reflection excited by exponential incident signals impinging on a conducting half space is analyzed for both horizontal and vertical polarizations. Then the technique is directly applied to the case of vertical polarizations with an incident angle not smaller than the Brewster angle. For non exponential incident signals, it is clarified that our technique is still usable but needs to be combined with Prony's method. Following this clarification, the details on Prony's method and some associated practical problems in the combination with Prony's method are discussed. After that, the approach combining a numerical inversion of the Laplace transform with Prony's method is applied to the analyses of non exponential pulses reflected from a conductive interface. Numerical results are illustrated and compared with those published in the literature. A good agreement between the two validates the correctness and effectiveness of this approach. Based on the studies of pulses reflected from a conducting half space, characterization of non exponential pulses propagating through a lossy dielectric slab is pursued. Comparison between the results obtained with this technique and

previously published results and those obtained using the FDTD technique indicates a good agreement. Moreover, the concern on whether the treatment of permittivity and conductivity in this chapter accords with the Kramers–Kronig relations is properly adressed. Finally, this approach is summarized and the significance of this work is discussed. A mathematical proof is presented, showing that the numerical inversion of the Laplace transform is applicable to the characterization of the reflected pulse due to an incident pulse that is a linear combination of exponential signals and is impinging upon a conductive interface at any incident angle for both polarizations.

Numerical inversion of Laplace transform is contiuously developed and extended to the modeling of pulse propagation in plasma and reflection from Lorentz, Debye and Cole–Cole media. All these four dispersive models satisfy the Kronig–Kramers relations required for a causal material. Firstly, pulse propagation in plasma with a zero and nonzero electron collision frequency is discussed. Next, the time domain reflection coefficients, viz impulse responses, of Lorentz, Debye and Cole–Cole half spaces are achieved for both TE and TM cases. Then, the transient reflections of an arbitray pulse from these media are determined by convolving the incident pulse with the impulse responses of these media, instead of using Prony's method to decompose the incident pulse into a series of finite attenuating exponential signals. Based on the time domain analysis of reflected pulses from these dispersive half spaces, some waveform parameters are estimated and the material diagnosis is carried out. Lastly, the work on transient wave propagation in and reflection from dispersive media is summarized with some meaningful conclusions. Our results show excellent agreement with those in the literature, validating the correctness and effectiveness of our technique.

6.2 FUTURE WORK

There are over 100 algorithms available for numerical inversion of Laplace transform (NILT). The technique developed in this thesis based on Hosono's algorithm is categorized into the method of Fourier series expansion. It is needed to choose some algorithms and compare them with each other and choose favorable ones for application to time domain electromagnetics.

We have extended and applied numerical inversion of Laplace transform to the analysis of transient waves in a stratified medium and achieved some preliminary results [89]. It is worthwhile to investigate the possibility to extend and apply numerical inversion of Laplace transform to transient analysis of plane waves reflected from and propagating in inhomogeneous media as well as non plane wave reflection and propagation.

A novel computational technique has been proposed very recently for transient electromagnetic scattering problems. This technique is based the combination of the method of moments (MoM) and numerical inversion of Laplace transform [90] and opens a door for further studies.

APPENDIX A

In this appendix, it will be proved that, for $s=\left[\rho+j(n-0.5)\pi\right]/t$, the final image functions, $F_v(s)$ and $F_h(s)$, satisfy the two conditions a) and b) mentioned in Section 2, under which $f_{ec}^{lm}(t,\rho)$ can be used to approximate $f_{ec}(t,\rho)$.

Here only the proof for $F_v(s)$ with α_p and C_p being real numbers is given, since the proofs for $F_v(s)$ with α_p and C_p being complex numbers and for $F_h(s)$ are similar. If we let

$$\left(\varepsilon_r+\frac{\sigma}{s\varepsilon_0}\right)\cos\theta=a+jb, \tag{A1}$$

$$\varepsilon_r+\frac{\sigma}{s\varepsilon_0}-\sin^2\theta=c_1+jd_1, \tag{A2}$$

$$\sqrt{\varepsilon_r+\frac{\sigma}{s\varepsilon_0}-\sin^2\theta}=c+jd, \tag{A3}$$

$$a=\left(\varepsilon_r+\frac{\rho\sigma t}{B}\right)\cos\theta, \quad b=-\frac{(n-0.5)\pi\sigma t}{B}\cos\theta, \quad B=\left[\rho^2+(n-0.5)^2\pi^2\right]\varepsilon_0, \tag{A4}$$

$$c_1=\varepsilon_r-\sin^2\theta+\frac{\rho\sigma t}{B}, \qquad d_1=-\frac{(n-0.5)\pi\sigma t}{B}, \tag{A5}$$

$$c=\pm\sqrt{\frac{c_1+\sqrt{c_1^2+d_1^2}}{2}}, \qquad d=\pm\frac{d_1}{|d_1|}\sqrt{\frac{\sqrt{c_1^2+d_1^2}-c_1}{2}}. \tag{A6}$$

If we denote

$$\sum_{p=1}^{q}\frac{C_p}{s+\alpha_p}=\sum_{p=1}^{q}(u_p+jv_p), \tag{A7}$$

then

$$u_p=\frac{(\rho+\alpha_p t)C_p t}{A}, \qquad v_p=-\frac{(n-0.5)\pi C_p t}{A}, \qquad A=(\rho+\alpha_p t)^2+(n-0.5)^2\pi^2. \tag{A8}$$

From $F_v(s)=R_v(s)E(s)$,

$$F_v(s)=\sum_{p=1}^{q}\frac{(a+jb)-(c+jd)}{(a+jb)+(c+jd)}\left(u_p+jv_p\right), \tag{A9}$$

then

$$F_n=(-1)^n\,Im\left(F_v(s)\right)=(-1)^n\,\frac{F_v(s)-F_v^*(s)}{2j}=\sum_{p=1}^{q}\frac{(-1)^n\left(v_p\,g+u_p\,h\right)}{(a+c)^2+(b+d)^2}, \tag{A10}$$

where

$$g=\left(a^2+b^2\right)-\left(c^2+d^2\right), \qquad h=2\left(bc-ad\right). \tag{A11}$$

When n becomes large,

$$F_n\to\sum_{p=1}^{q}(-1)^n\left(-\frac{C_p\,t}{n\pi}\right)\frac{\varepsilon_r\cos\theta-\sqrt{\varepsilon_r-\sin^2\theta}}{\varepsilon_r\cos\theta+\sqrt{\varepsilon_r-\sin^2\theta}}.$$

Thus, the signs of F_n alternate, and furthermore, $|F_{n+1}|<|F_n|$ but $|F_{n+1}|\to|F_n|$, viz., $F_v(s)$ satisfies the two conditions a) and b) described in Section 2.

REFERENCES

[1] A. Sommerfeld, "Über die Fortpflanzung des Lichtes in dispergierenden Medien," *Ann. Phys.*, vol. 44, pp. 177-202, 1914.

[2] J. A. Stratton, *Electromagnetic Theory*. New York: McGraw-Hill, 1941.

[3] C. A. Balanis, *Advanced Engineering Electromagnetics*. John Wiley & Sons, 1989.

[4] D. G. Dudley, T. M. Papazoglou, and R. C. White, "On the interaction of a transient electromagnetic plane wave and a lossy half-space," *J. Appl. Phys.*, vol. 45, pp. 1171-1175, Mar. 1974.

[5] T. M. Papazoglou, "Transmission of a transient electromagnetic plane wave into a lossy half-space," *J. Appl. Phys.*, vol. 46, pp. 3333-3341, Aug. 1975.

[6] J. J. A. Klaasen, "Time-domain analysis of one-dimensional electromagnetic scattering by lossy media," Rep. FEL-90-A211, TNO Phys. Electron. Lab., The Hague, Oct. 1990.

[7] J. G. Maloney, G. S. Smith, and W. R. Scott, Jr., "Accurate computation of the radiation from simple antennas using the finite-difference time-domain method," *IEEE Trans. Antennas Propagat.*, vol. 38, pp. 1059-1068, July 1990.

[8] R. Luebbers, F. P. Hunsberger, K. S. Kunz, R. B. Standler and M. Schneider, "A frequency-dependent finite-difference time-domain formuation for dispersive materials," *IEEE Trans. Electromagn. Compat.*, vol. 32, pp. 222-227, Aug. 1990.

[9] J. G. Maloney and G. S. Smith, "The use of surface impedance concepts in the finite-difference time-domain method," *IEEE Trans. Antennas Propagat.*, vol. 40, pp. 38-48, Jan. 1992.

[10] P. R. Barnes and F. M. Tesche, "On the direct calculation of a transient plane wave reflected from a finitely conducting half space," *IEEE Trans. Electromagn. Compat.*, vol. 33, pp. 90-96, May 1991.

[11] H.-Y. Pao, S. L. Dvorak and D. G. Dudley, "An accuate and efficient analysis for transient plane waves obliquely incident on a conductive half space (TE case)," *IEEE Trans. Antennas Propagat.*, vol. 44, no. 7, pp. 918–924, July 1996.

[12] H.-Y. Pao, S. L. Dvorak and D. G. Dudley, "An accuate and efficient analysis for transient plane waves obliquely incident on a conductive half space (TM case)," *IEEE Trans. Antennas Propagat.*, vol. 44, no. 7, pp. 925–932, July 1996.

[13] E. J. Rothwell and J. W. Suk, "Efficient computation of the time-domain TE plane-wave reflection coefficient," *IEEE Trans. Antennas Propagat.*, vol. 51, no. 12, pp. 3283–3285, Dec. 2003.

[14] E. J. Rothwell, "Efficient computation of the time-domain TM plane-wave reflection coefficient," *IEEE Trans. Antennas Propagat.*, vol. 53, no. 10, pp. 3417–3419, Oct. 2005.

[15] M. F. Pantoja, A. G. Yarovoy, and A. R. Bretones, "On the direct computation of the time-domain plane-wave refelction coefficients," *ACES (Applied Computational Electromgnetics Society) Journal*, vol. 24, No. 3, pp. 294-299, June 2009.

[16] E. O. Schulz-Dubois, "Sommerfeld pre and postcursors in the context of waveguide transients," *IEEE Trans. Microwave Theory Tech.*, vol. MTT 18, no. 8, pp. 455-460, 1970.

[17] L. B. Felsen and N. Marcuvitz, *Raiation and Scattering of Waves*. Englewood Cliff, NJ: Pretice-Hall, 1973.

[18] R. E. Collin, *Field Theory of Guided Waves*, 2nd ed. New York: IEEE Press, 1991.

[19] M. Cerrillo, "Transient phenomena in waveguides," *MIT Res. Lab. Electron. Tech. Rep.*, vol. 33, 1948.

[20] C. M. Knop, "Pulsed electromagnetic wave propagation in dispersive media," *IEEE Trans. Antennas Propagat.*, vol. AP-12, pp. 494-496, 1964.

[21] J. R. Wait and K. P. Spies, "On the theory of transient wave propagation in a dispersive medium," *Appl. Sci. Res.*, vol. 16, pp. 455-465, 1966.

[22] L. E. Vogler, "An exact solution for waveform distortion of arbitrary signals in ideal waveguides," *Radio. Sci.*, vol. 5, no. 12, pp.1469-1474, 1970.

[23] Y. V. Vaisleib and S. P. Gan, "Propagation of radio pulses in a regular single mode waveguide," *Telecom. Rad. Eng.*, vol. 31/32, no. 7, pp. 101-107, 1977.

[24] M. M. Agrest and M. S. Maksimov, *Theory of Incomplete Cylindrical Functions and Their Applications*. Berlin: Springer-Verlag, 1971.

[25] A. H. Mohammadian, "Time dependent Dyadic Green's functions for rectangular and circular waveguides," *IEEE Trans. Antennas Propagat.*, vol. AP-36, no. 3, pp. 369-375, 1988.

[26] S. L. Dvorak, "Exact closed-form expressions for transient fields in homogeneously filled waveguides," *IEEE Trans. Microwave Theory Tech.*, vol. 42, no. 11, pp. 2164-2170, 1994.

[27] S. L. Dvorak and D. G. Dudley, "Propagation of ultra-wide-band electromagnetic pulses through dispersive media," *IEEE Trans. Electromagn. Compat.*, vol. 37, pp. 192-200, May 1995.

[28] S. L. Dvorak, R. W. Ziolkowski and D. G. Dudley, "Ultra-wideband electromagnetic pulse propagation in a homogeneous cold plasma," *Radio. Sci.*, vol. 32, no. 1, pp. 239-250, Jan.-Feb. 1997.

[29] K. E. Oughstun and G. C. Sherman, "Propagation of electromagnetic pulses in a linear dispersive medium with aborption (the Lorentz medium)," *J. Opt. Soc. Am., Series B*, vol. 5, pp. 817-849, 1988.

[30] K. E. Oughstun and G. C. Sherman, "Uniform asymptotic description of electromagnetic pulse propagation in a linear dispersive medium with aborption (the Lorentz medium)," *J. Opt. Soc. Am., Series A*, vol. 6, pp. 1394-1420, 1989.

[31] K. E. Oughstun and G. C. Sherman, "Uniform asymptotic description of ultrashort rectangular optical pulse propagation in a linear, causally dispersive medium," *Phys. Rev. A*, vol. 41, pp. 6090-6113, 1990.

[32] K. E. Oughstun and G. C. Sherman, *Electromagnetic Pulsepropagation in Casual Dielectrics*, Berlin: Springer-Verlag, 1994.

[33] K. G. Gray, "The reflected impulse response of a Lorentz medium," *Proc. IEEE*, vol. 68, pp. 408-409, 1980.

[34] B. V. Stanic, D. R. Milanovic, and J. M. Cvetic, "Pulse reflection from a lossy Lorentz medium half-space (TM polarization)," *J. Phys. D: Appl. Phys.*, vol. 24, pp. 1245-1249, 1991.

[35] S. M. Cossmann, E. J. Rothwell, and L. C. Kempel, "Transient reflection of TE-polarized plane waves from a Lorentz-medium half-space," *J. Opt. Soc. Am., Series A*, vol. 23, no. 9, pp. 2320-2323, September 2006.

[36] S. M. Cossmann, E. J. Rothwell, and L. C. Kempel, "Transient reflection of TM-polarized plane waves from a Lorentz-medium half-space," *J. Opt. Soc. Am., Series A*, vol. 24, no. 3, pp. 882-887, March 2007.

[37] P. Debye, *Polar Molecules*. New York: Dover Publications, 1945.

[38] P. Kosmas, C. M. Rappaport, and E. Bishop, "Modeling with the FDTD method for microwave breast cancer detection," *IEEE Trans. Microwave Theory Tech.*, vol. 52, no. 8, suppl. 2, pp. 1890-1897, August 2004.

[39] B. Oswald, D. Erni, H. R. Benedickter, W. Bächtold, and H. Flühler, "Dielectric properties of natural materials," *Proc. IEEE Antennas and Propagation Society International Symposium*, vol. 4, pp. 2002-2005, 1998.

[40] K. G. Ong, W. R. Dreschel, and C. A. Grimes, Detection of human respiration using square-wave modulated electromagnetic impulses," *Microwave Optical Technol. Lett.*, vol. 36, pp. 339- 349, 2003.

[41] A. Ogunsola, U. Reggiani, and L. Sandrolini, "Modelling shielding properties of concrete," *Proc. 17th International Symposium on Electromagnetic Compatibility*, Zurich, Switzerland, pp. 34–37, Feb. 27–March 3, 2006.

[42] J. M. Zhang, et al., "Reconstruction of the parameters of Debye and Lorentzian dispersive media using a genetic algorithm," *Proc. IEEE Electromagnetic Compatibility International Symposium*, Atlanta, Georgia, USA, pp. 898–903, June 21–26, 2003.

[43] J. Guerra and J. Eiras, "High frequency dielectric relaxation in Lanthanum modified $PbTiO_3$ ferroelectric ceramics," *Material Res.*, vol. 7, pp. 325–328, 2004.

[44] R. Piesiewicz, et al., "Terahertz characterisation of building materials," *Electron. Lett.*, vol. 41, pp. 1002-1004, 2005.

[45] S. B. Jones, R. W. Mace, and D. Or, A time domain reflectometry coaxial cell for manipulation and monitoring of water content and electrical conductivity in variably saturated porous media," *Vadose Zone J.*, vol. 4, pp. 977-982, 2005.

[46] E. J. Rothwell, "Plane-wave impulse response of a Debye half space," *Electromagnetics*, vol. 27, no. 4, pp. 195–206, May 2007.

[47] K. S. Cole and R. H. Cole, "Dispersion and absorption in dielectrics," *J. Chemical Phys.*, vol. 9, no. 4, pp.341–351, Apr. 1941.

[48] J. W. Suk and E. J. Rothwell, "Transient analysis of TE-plane wave reflection from a layered medium," *J. Electromagn. Wave Appl.*, vol. 16, No. 2, pp. 281-297, 2002.

[49] J. W. Suk and E. J. Rothwell, "Transient analysis of TM-plane wave reflection from a layered medium," *J. Electromagn. Wave Appl.*, vol. 16, No. 9, pp. 1195-1208, 2002.

[50] J. C. Oh, E. J. Rothwell and D. P. Nyquist, "Natural resonance representation of the transient field reflected by a conductor-backed lossy layer," *J. Electromagn. Wave Appl.*, vol. 17, No. 5, pp. 673-694, 2003.

[51] J. C. Oh, E. J. Rothwell, B. T. Perry and M. J. Havrilla, "Natural resonance representation of the transient field reflected by a conductor-backed layer of Debye material," *J. Electromagn. Wave Appl.*, vol. 18, No. 5, pp. 571-589, 2004.

[52] B. T. Perry and E. J. Rothwell, "Calculation of the transient plane-wave reflection from an N-layer medium by the method of subregions," *IEEE Trans. Antennas Propagat.*, vol. AP-55, no. 11, pp. 3293-3299, Nov. 2007.

[53] P. G. Petropoulos, "Analysis of exponential time-differencing for FDTD in lossy dielectrics," *IEEE Trans. Antennas Propagat.*, vol. AP-45, no. 6, pp. 1054-1057, June 1997.

[54] Q. Chen, M. Katsurai and P. H. Aoyagi, "An FDTD formulation for dispersive media using a current density," *IEEE Trans. Antennas Propagat.*, vol. AP-46, no. 10, pp. 1739-1746, Oct. 1998.

[55] T. Wuren, T. Takai, M. Fuji and I. Sakagami, "Effective 2-Debye-pole FDTD model of electromagnetic interaction between whole human body and UWB radiation," *IEEE Microwave and Wireless Component Letters*, vol. 17, no. 7, pp 483-485, July 2007.

[56] M. R. Tofighi, "FDTD modeling of biological tissues Cole–Cole dispersion for 0.5-30 GHz using relaxation time distribution samples—novel and improved implementations," *IEEE Trans. Microwave Theory Tech.*, vol. 57, no. 10, pp. 2588-2596, Oct. 2009.

[57] F. L. Teixeira, "Time-domain finite difference and finite-element methods for Maxwell equations in complex media," *IEEE Trans. Antennas Propagat.*, vol. AP-56, no. 8, pp. 2150-2166, August 2008.

[58] S. L. Dvorak and E. F. Kuester, "Numerical computation of the incomplete Lipschitz-Hankel integral $Je_0(a,z)$," *J. Comput. Phys.*, vol. 87, no. 2, pp. 301-327, Apr. 1990.

[59] I. S. Gradshteyn and I. M. Ryzhik, *Tables of Integrals, Series, and Products*. New York: Academic, 1994.

[60] M. Abramowitz and I. Stegun, *Handbook of Mathematical Functions*, New York: Dover, 1965.

[61] P. Wyns, D. P. Foty, and K. E. Oughstun, "Numerical analysis of the precursor fields in linear dispersive pulse propagation," *J. Opt. Soc. Am., Series A*, vol. 6, pp. 1421-1429, 1989.

[62] B. Davies, *Integral Transforms and Their Applications*, 3rd ed., Chapter 19, pp. 327-355, New York: Springer, 2002.

[63] T. J. Bromwich, *An Introduction to the Theory of Infinite Series*, 2nd ed., Chapter III, pp. 53-66, London, U. K.: Macmillan, 1926.

[64] R. M. Simon, M. T. Stroot, and G. H. Weiss, "Numerical inversion of Laplace transforms with applications to percentage labeled mitoses experiments," *Computers and Biomedical Research*, vol. 5, pp. 596-607, 1972.

[65] T. Hosono, "Numerical inversion of Laplace transform," *Trans. Inst. Elec. Eng. Japan*, vol. 99, no. 5, pp. 43-49, Oct. 1979.

[66] T. Hosono, "Numerical inversion of Laplace transform and some applications to wave optics," *Radio Sci.*, vol. 16, no. 6, pp. 1015–1019, Nov.–Dec. 1981.

[67] W. R. LePage, *Complex Variables and the Laplace Transform for Engineers*, pp. 157-162, New York: McGraw-Hill, 1961.

[68] S. He and S. Ström, "Time-domain propagating modes in a finitely conducting half-space and calculation of the transient reflection," *IEEE Trans. Electromagn. Compat.*, vol. 37, no. 2, pp. 277-282, May 1995.

[69] Q. Zeng and G. Y. Delisle, "Characterization of a transient wave reflected from a lossy half space using numerical inversion of Laplace transform," *Antem 2004/URSI: 10th International Symposium on Antenna Technology and Applied Electromagnetics and URSI Conference*, pp. 87-90, Ottawa, ON, July 20-23, 2004.

[70] Q. Zeng and G. Y. Delisle, "Time-domain analysis for electromagnetic pulses reflected from a conductive half space," in *Proceedings of 2006 IEEE Canadian Conference on Electrical and Computer Engineering (CCECE2006)*, pp. 92-95, Ottawa, Ontario, Canada, May 7-10, 2006.

[71] F. B. Hildebrand, *Introduction to Numerical Analysis*, pp. 457–462, New York: Dover, 1974.

[72] C. W. Chuang and D. L. Moffatt, "Natural resonances of radar targets via Prony's method and target discrimination," *IEEE Trans. Aerospace and Electronic Systems*, vol. AES-12, no. 5, pp. 583-589, Sept. 1976.

[73] R. C. Qiu, "A generalized time domain multipath channel and its application in ultra-wideband (UWB) wireless optimum receiver design–Part II: Physics-based system analysis," *IEEE Trans. Wireless Comm.*, vol. 3, no. 6, 2312–2324, Nov. 2004.

[74] A. Muqaibel, A. Safaai-Jazi, A. Bayram, A. M. Attiya and S.M. Riad, "Ultrawideband through-the–wall propagation," *IEE Proc.-Microw. Antennas Propag.*, vol. 152, no. 6, pp. 581-588, Dec. 2005.

[75] Z. Chen, R. Yao and Z. Guo, "The characteristics of UWB signal transmitting through lossy dielectric slab," *IEEE Radio and Wireles Conference 2004*, pp. 134-138, Atlanta, GA, USA, Sept. 19–22, 2004.

[76] P. Yeh, *Optical Waves in Layered Media*, pp. 66 and pp. 86–88, New York, NY: John Wiley & Sons, 1988.

[77] E. J. Rothwell and M. J. Cloud, *Electromagnetics*, Chapter 4, pp. 189-348, Boca Raton, FL: CRC Press, 2001.

[78] C. A. Brau, *Modern Problems in Classical Electrodynamics*, Chapter 7, pp. 318- 376, New York, NY: Oxford University Press, 2004.

[79] Q. Zeng and G. Y. Delisle, "Path loss model for ultra wideband signal propagation," *ANTEM / URSI 2006: 12th International Symposium on Antenna Technology and Applied Electromagnetics [ANTEM] and Canadian Radio Sciences [URSI/CNC]*, pp. 415-419, Montreal, Quebec, Canada, July 16-19, 2006.

[80] M. Ghavami, L. B. Michael and R. Kohno, *Ultra Wideband Signal and Systems in Communcation Engineering*, Section 4.3, pp. 110-121, Chichester, England; Hoboken, NJ: John Wiley & Sons, 2004.

[81] M. Ho and F.-S. Lai, "Effects of medium conductivity on electromagnetic pulse propagation onto dielectric half space: One-dimensional simulation using characteristic-based method," *J. Electromagn. Wave Appl.*, vol. 21, No. 13, pp. 1773-1785, 2007.

[82] J. W. Suk, "Transient analysis of plane-wave scattering in a layered medium," Ph.D. dissertation, Michigna State University, East Lansing, MI, December 2000.

[83] Q. Zeng and G. Y. Delisle, "Time domain analysis of ultra wideband pulse reflection from a lossy interface," *International URSI Commission B – Electromagnetic Theory Symposium (EMTS 2007)*, Ottawa, Ontario, Canada, July 26 – 28, 2007.

[84] Q. Zeng and G. Y. Delisle, "Characterization for ultra wideband pulses transmitting through a lossy dielectric slab," *2006 IEEE International Conference on Ultra-Wideband (ICUWB 2006)*, pp.213-218, Waltham, Massachusetts, USA, September 24-27, 2006.

[85] J.-Z. Bao, M. L. Swicord, and C. C. Dawes, "Microwave dielectric characterization of binary mixtures of water, methanol and ethanol," J. Chem. Phys., vol. 104, pp. 4441-4450, 1996.

[86] Q. Zeng and G. Y. Delisle, "Time domain analysis of electromagnetic pulse propagating in plasma," in *Proceedings of 2008 IEEE International Symposium on Antennas and Propagation and USNC/URSI National Radio Science Meeting*, San Diego, California, USA, July 5-12, 2008.

[87] Q. Zeng and G. Y. Delisle, "Waveform parameter estimation and dispersive material characterization", in *Proceedings of the 25th Progress In Electromagnetics Research Symposium (PIERS 2009)*, Beijing, China, pp. 169-175, March 23 – 27, 2009.

[88] Q. Zeng and G. Y. Delisle, "Waveform parameter estimation and material characterization," *PIERS Online*, Vol. 5, No. 3, pp. 241-247, 2009.

[89] Q. Zeng and G. Y. Delisle, "Transient analysis of electromagnetic wave reflection from a stratified medium," in *Proceedings of 2010 Asia-Pacific Symposium on Electromagnetic Compatibility (2010 APEMC)*, Beijing, China, pp. 892-895, April 12 – 16, 2010.

[90] S. Ohnuki, Y. Kitaoka, and S. Kishimoto, "Analysis of transient electromagnetic scattering from arbitrary objects," accepted by *2010 Asia-Pacific Symposium on Electromagnetic Compatibility (2010 APEMC)*, Beijing, China, April 12 – 16, 2010.